Department of AERONAUTICS and ASTRONAUTICS
STANFORD UNIVERSITY

WILLIAM B. GEVARTER

ATTITUDE CONTROL OF A FLEXIBLE, SPINNING, TOROIDAL MANNED SPACE STATION

NOVEMBER 1965

This work was performed in association with research sponsored by the National Aeronautics and Space Administration under Research Grant NsG 133-61

SUDAER NO. 250

Department of Aeronautics and Astronautics
Stanford University
Stanford, California

ATTITUDE CONTROL OF A FLEXIBLE, SPINNING, TOROIDAL MANNED SPACE STATION

by

William B. Gevarter

SUDAER No. 250
November 1965

This work was performed in association with research sponsored by the National Aeronautics and Space Administration under Research Grant NsG 133-61

ABSTRACT

This study has considered a continuous attitude-control system for controlling the direction of the spin axis of a flexible, spinning, toroidal manned space station. The basic objective was to find locations within the space station for the control actuators (forces or moments) and attitude sensors such that the space station is stable and the excitation of vibration by the control system is at a minimum. When flexure is considered, these locations are of the utmost importance since they determine the coupling of the flexural motions with the rigid-body motion to be controlled.

For small flexural motions, the equations of motion can be linearized and stability determined from an examination of the system characteristic roots as the control parameters are varied. Unfortunately, for flexible systems with control, determination of these roots is very difficult and therefore computer solutions are generally utilized. As a result, the fundamental relationships between sensor and actuator locations and flexural mode response in a vehicle with automatic control have not heretofore been explicitly treated.

The approach used for this problem was first to indicate the basic form of the equations of motion of flexible vehicles with linear feedback control, and their associated characteristic equations. The characteristic roots were then determined by expanding them about their normalized flexural modal poles. The resulting expressions yielded general relationships which the locations of the sensors and actuators, designed for control of the rigid motions of a flexible vehicle, must satisfy in order for the flexible motions to be stable as well. This approach was applied to (1) vehicles whose control axes are not coupled, such as conventional beamlike vehicles, and (2) the more complex case of vehicles whose control axes are coupled via flexure, which includes unconventional platelike vehicles such as the toroid studied in this report.

The flexural frequencies and mode shapes of the spinning space station were determined analytically. Then the rigid-body equations of angular motion about axes in the plane of the toroid were transformed into a

single vector equation in the body-fixed frame, and a suitable two-axis linear feedback control system was chosen.

Applying the general stability relations to the spinning space station made it possible to observe the influence of the locations of the control actuators and sensors on station stability. The results thus obtained were verified using a computer program. For a control system using simple rate and position feedback, and employing a pair of actuators about each of the orthogonal control axes, it was determined that:

1. There is no location for a single sensor package (e.g., star tracker and derived rate) that will yield stability of the flexural modes for control gains appropriate to the rigid-body mode.

2. The desirable solution is to use a control sensor for each control axis, and place it with one of its corresponding actuators. For this solution, the control axes are uncoupled, only the odd modes of vibration are excited, and the system is stable. Further reduction in excitation of the flexural modes can be achieved by employing lead-lag rate networks or filtered rate in place of pure rate.

3. When the above solution is employed, certain latitude may be tolerated in the location of sensors and in the mismatch of control forces with acceptable stability.

CONTENTS

NOMENCLATURE

a_n	μ_n/q_n, the factor converting the n^{th}-mode generalized coordinate to the quantity sensed by the feedback instrument--defined by Eq. (2.10)
c	defined by Eq. (4.29)
d	defined by Eq. (4.30)
$f_i(\gamma)$	force per unit angle in the i^{th} direction
$\check{f}_i(\gamma)$	equivalent force per unit angle in the i^{th} direction--defined by Eqs. (B2.28) - (B2.30)
g	acceleration of gravity; parameter defined in Eq. (9.8)
h	ratio of the y-axis to the x-axis control gains
j	square root of -1
k	K_p/p_i^2, defined by Eq. (3.5)
k'	K_v/p_i, defined by Eq. (3.4)
k_o	K_p/p_o^2, defined by Eq. (D.2)
k_o'	K_v/p_o, defined by Eq. (D.3)
k_+'	$(K_v/p_3)(1 + \alpha_{63})$, defined by Eq. (6.17)
k_-'	$(K_v/p_3)(1 + \alpha_{73})$
$\check{m}$	$[m(\gamma)R^3]/EI$, defined by Eq. (B2.27)
$m(\gamma)$	mass per unit angle of the station rim
p	vibrational frequency
p_n	n^{th}-mode natural frequency

TABLES

ILLUSTRATIONS

$q_n(t)$	n^{th}-mode generalized coordinate
r_n	p_n/p_i, defined by Eq. (3.3)
r_{on}	p_n/p_o, defined by Eq. (D.4)
$\bar{r}$	the undeflected vector position of the mass particle with respect to the vehicle center of mass
$\Delta\bar{r}$	vector deflection of a flexible vehicle with respect to a rigid-body reference frame
s	Laplace operator
s_{n1}, s_{n2}	conjugate complex roots associated with the n^{th} mode; defined by Eqs. (3.25) and (3.26)
$\tilde{s}$	s/p_i, defined by Eq. (3.2)
$\tilde{s}_i$	$s_i/p_i = \epsilon + j(1+\delta)$, normalized system characteristic root (in the upper half plane) associated with the i^{th} mode; defined by Eq. (3.6)
t	time
u_n	Q_n/Q_c, the factor converting the rigid-mode control Q_c to the n^{th}-mode generalized forcing function Q_n--defined by Eq. (2.9)
w	defined by Eq. (4.31)
$\bar{w}_n(\bar{r})$	n^{th}-mode eigenvector
x,y,z	body-fixed axes defined by Fig. 7
$z(\gamma,t)$	out-of-plane deflection defined by Fig. 7
A	mass moment of inertia of the station about a diameter
B'	defined by Eq. (7.3)

B_n	ratio of twist to deflection for the n^{th} mode--defined by Eq. (5.1)
C	moment of inertia about the station spin axis
E_{x_n}, E_{y_n}	defined by Eqs. (4.1) and (4.2)
EI	bending rigidity (Young's modulus multiplied by the area moment of inertia), used in Eq. (B2.10)
F	force
F_n	n^{th}-mode generalized force
ΔF_i	force imbalance defined by Eqs. (5.24) and (5.25)
G	matrix defined by Eq. (4.15)
G_+, G_-	defined by Eq. (4.13)
$G_{xx}, G_{xy}, G_{yx}, G_{yy}$	components of G defined by Eqs. (4.6) through (4.9)
G(s)	defined by Eq. (2.12)
I	area moment of inertia
K	gain matrix defined by Eq. (4.4)
K_p	position gain
K_v	velocity gain
M	moment; mass of station
ΔM_i	moment imbalance defined by Eqs. (5.26) and (5.27)
$M_i'(\gamma)$	rate of change with respect to γ of the moments in the i^{th} direction
M_n	n^{th}-mode generalized mass defined by Eq. (A.31)

Q	rigid-mode forcing function
Q_n	F_n/M_n, n^{th}-mode forcing function, defined by Eq. (1.2)
R	centroidal radius of the rim of the station (defined in Fig. 7); distance from the force to the center of mass of the vehicle (see Fig. 2)
U	defined by Eq. (3.33)
V_n	n^{th}-mode potential energy
X,Y,Z	inertial axes defined by Fig. 7
$\alpha_{xx},\alpha_{xy},\alpha_{yx},\alpha_{yy}$	functions of sensor and control locations--defined by Eqs. (4.15) - (4.18)
$\alpha_{1_n}^2$	$-\left(a_{xx_n} a_{yy_n} - a_{xy_n} a_{yx_n}\right)$, defined by Eq. (6.7)
α_{2_n}	$a_{xx_n}[-(-1)^{(n-1)/2}] + a_{yy_n}$, defined by Eq. (6.5)
α_{5_n}	$\left\{\left(\alpha_{2_n}\right)^2 + [-(-1)^{(n-1)/2}]4\alpha_{1_n}^2\right\}$, defined by Eq. (6.6)
α_{6_n}	$-(R/2)\left(\alpha_{5_n} + \alpha_{2_n}\right)$, defined by Eq. (6.11)
α_{7_n}	$(R/2)\left(\alpha_{5_n} - \alpha_{2_n}\right)$, defined by Eq. (6.12)
$\beta(\gamma,t)$	twist about the centroidal line of the cross sections--defined by Fig. 7
β_n	n^{th}-mode slope at the sensor (Fig. 2)
γ	central angle of position along the rim (Fig. 7)
γ,γ'	location of x and y sensors, defined by Eqs. (5.16) through (5.19)

δ	imaginary portion of the departure of $\tilde{s}_i$ from the normalized i^{th}-mode pole
ϵ	real portion of $\tilde{s}_i$
ζ	equivalent viscous damping
ζ_n	n^{th}-mode equivalent viscous damping
ζ_{3_+}	$\zeta_3/(1 + \alpha_{63})$, defined by Eq. (6.18)
θ, ϕ, ψ	Euler angles relating body-fixed axes to inertial axes, defined by Fig. 7
μ	a rigid-body motion, used in Eq. (2.4)
μ	$(\phi + j\theta)e^{j\psi}$, the small vector angle between the rigid-mode spin axis and the inertial reference
μI_p	torsional stiffness of the cross section about its centroidal axis, utilized in Eq. (B2.10)
σ	Poisson's ratio
τ_o, τ_1	time constants of rate network defined by Eq. (3.16)
ω	frequency along the imaginary axis in the s plane
$\omega_x, \omega_y, \omega_z$	components of angular velocity in the rigid-body frame
Δp_n	precessional velocity of the n^{th} in-plane inextensible mode, defined by Eq. (B3.8)
Ω	spin speed, nominal value of $\dot{\psi}$
$\Omega_{3_+}^2$	$\left(1 + \alpha_{63} r_o^2\right)/(1 + \alpha_{63})$, defined by Eq. (6.19)

Superscripts

•	derivative with respect to time
T	transpose of a vector

Subscripts

b	body fixed
c	control
co	rigid-mode parameter with control
n,m,i	integers; n^{th}, m^{th}, and i^{th} modes of vibration
ns	n^{th} sine mode of vibration
nc	n^{th} cosine mode of vibration
o	rigid-mode parameter without control
s	sensed
x	component along x axis
y	component along y axis
z	component along z axis
D	disturbance
F	flexure
R	rigid mode
ref	reference control input

ADDITIONAL NOMENCLATURE FOR APPENDIXES

$\hat{q}$	q/R, defined by Eq. (D.10)
u,v,w	components of deflection along x_o, y_o, z_o
x_o,y_o,z_o	local undeflected axes; x_o is radial directed inward, y_o is parallel to z. See Fig. 30.
x_b,y_b,z_b	local body-fixed axes, originally along x_o, y_o, z_o in the undeflected case
A_{nmij}	a parameter composed of u_n's and a_n's defined by Eq. (D.24)
B	a matrix defined by Eq. (D.21)
B'	a matrix defined by Eq. (D.28)
$\bar{L}$	linear vector operator defined by Eq. (A.8)
P	internal pressure of station
P	Q/p_o, defined by Eq. (D.5)
S	internal area of station cross section
T_o	$p_o\tau_o$, defined by Eq. (D.15)
T_1	$p_o\tau_1$, defined by Eq. (D.16)
V	volume
$\bar{\mathfrak{M}}$	external moment vector, per unit length s, acting on the station

α	small vector angle of the spin axis to the inertial axes--defined by Eq. (C.3)
κ,κ'	components of curvature about x_b, y_b
κ_o,κ'_o	initial components of curvature about x_o, y_o
ρ	mass density
τ	$p_o t$, defined by Eq. (D.1)
τ	twist about z_b
τ_o	initial twist about z_o
$\bar{\omega}$	the angular velocity of the rigid body
$\bar{\Phi}$	the small vector rotation of the body axes over the arc length ds
$\bar{\Psi}$	the small vector angle defined by Eq. (B1.2) which specifies the rotation of the deflected local body-fixed axes b to the undeflected local axes o

ACKNOWLEDGMENT

I wish to thank my advisor, Professor Robert H. Cannon, Jr., for his suggestion of this problem and for his guidance in its pursuit. I also wish to thank Professor John V. Breakwell for many stimulating discussions during the course of the research. I am also indebted to Professors Benjamin O. Lange and James M. Kelley and to Dr. Dale R. Ingwerson for their help and encouragement on various aspects of the problem. The assistance provided under NASA Research Contract NsG 133-61 for the computational time and for preparation of this report is gratefully acknowledged.

I. INTRODUCTION

This study has investigated a continuous attitude-control system for controlling the direction of the spin axis of a flexible, spinning, toroidal manned space station. The specific objective was to find locations within the manned space station for the control actuators (forces or moments) and sensors such that the spacecraft is stable and the excitation of vibration by the control system is at a minimum.

If the manned space station were rigid, the locations of the sensors and actuators would be unimportant. When flexure is considered, however, these locations are of the utmost importance because they determine the coupling of the flexural motions to the rigid-body motion to be controlled. This coupling can lead to instability, an effect which has been observed on missiles, boosters, and other space vehicles.

The conventional approach to this flexible vehicle problem is to select a control law for the rigid-body mode, choose a convenient location for the actuators and sensors, and then analyze the system to determine if it is stable and has a satisfactory response to expected inputs. This analysis is often difficult and it is common to employ computers in its solution.

If the calculated stability or response is unsatisfactory, new locations for the sensors (or for the actuators) may be tried, the use of multiple sensors may be explored, or the control law may be modified to include fixed or variable compensation. The compensation may consist of circuits to modify the phase or magnitude of the system transfer function at unsatisfactory roots associated with particular flexible modes, or it may consist of filters to reduce the effect of the control feedback at the frequencies of the unwanted flexural modes.

Variable compensation is usually adaptive in nature, adjusting the frequencies of the compensatory circuits to match undesirable frequencies actually observed during operation, or changing gains to modify the observed response so that it will approximate more nearly the desired response. An excellent discussion of compensation techniques, particularly adaptive ones, for alleviating control problems that result from flexure is presented in Ref. 1.

A somewhat different approach was employed recently by Schaefer [Ref. 2]. Instead of starting with a control law for the rigid-body mode, he used sufficient sensors to be able to determine all the "states" of the system, including those of the important flexural modes. Then, by means of a computer, a control was determined that would drive all the states from the initial observed state to the desired final state in an optimum or near-optimum fashion.

The approach used in this study is, first, to identify the basic nature of flexible-vehicle control problems and indicate how these problems can be treated analytically--to an acceptable degree of approximation--for the case of a system designed for the control of the rigid mode. This step results in general relationships that the locations of the sensors and actuators (designed for control of the rigid motion) must satisfy if the flexible motions as well as the rigid-body motions are to be stable. These relationships are then applied to the spinning space station to determine locations of the actuators and sensors such that the system is stable and the flexible modes are minimally excited.

A. HISTORICAL BACKGROUND

The stability problem associated with the attitude control of a flexible, spinning, toroidal manned space station is an example of a wider class of problems: the stability and control of flexible vehicles. Unfortunately, no comprehensive history of the overall flexible-vehicle problem has been found in the literature and for this reason an attempt has been made here to fill this need.

1. Stability and Control of Flexible Vehicles

In order to appreciate fully the history of flexible-vehicle stability analysis, it was considered desirable to classify the basic ways that flexibility can affect vehicle stability. The resulting six classifications, and a brief discussion on pertinent references, are presented in Section 1.b. The equations of flexible vehicles, which are derived in Appendix A, are summarized below.

a. Equations of Flexible Vehicles

In Appendix A it is shown that for small vehicle deflections the equations of rigid-body motion appear uncoupled from the flexural motions except when angular deflection produces a significant change in the direction of an applied force. It is shown further that when the deflection $\Delta\bar{r}(\bar{r},t)$ is expanded in N of its modal components

$$\Delta\bar{r}(\bar{r},t) = \sum_{n=1}^{N} q_n(t)\ \bar{w}_n(\bar{r}) \tag{1.1}$$

and if, in addition, the vehicle is not spinning, or if it is spinning and the deflection is along the direction of the spin vector or is due to pure torsion about the spin axis, then the equations for the modal generalized coordinates appear as

$$\ddot{q}_n + 2\zeta_n p_n \dot{q}_n + p_n^2 q_n = \frac{F_n(t)}{M_n} \triangleq Q_n(t) \qquad (n = 1 \text{ to } N) \tag{1.2}$$

where

$\bar{r}$ = the undeflected vector position of the mass particle with respect to the vehicle center of mass

ζ_n = n^{th}-mode equivalent viscous damping ratio approximating structural damping

p_n = natural frequency of the n^{th} mode

F_n = n^{th}-mode generalized force

M_n = n^{th}-mode generalized mass

From the above it is evident that the rigid-body motions and the modal flexural motions are uncoupled from one another except through the forces (or moments).

b. Dynamic Coupling

Dynamic coupling takes two basic forms: (1) the elements (or equations) appear in tandem such that the motion of the first element excites the second but the motion of the second element has a negligible effect on the first, or (2) the motion of the individual elements interact with each other (i.e., feedback is present) and instability is possible.

There are several basic ways in which the modal equations, Eqs. (1.2), may become "feedback coupled" and instability may occur. A somewhat arbitrary classification of these possible couplings is given below--based on the principal physical phenomena involved.

1. Type 1, Change in Applied Forces Due to Modal Deflection. Deflection of a mode may cause the applied forces to change their direction (and/or their magnitude), which in turn changes the generalized forces of the other modes.

2. Type 2, Deflection Picked Up by the Control Sensor. A control system using one or more feedback sensors is employed to control the rigid-body mode. However, these sensors also sense deflection, which causes the control system to modify the forces acting upon the rigid-body and flexural modes. In active control systems of flexural vehicles (e.g., automatic control systems for missiles, aircraft, trains, satellites, space boosters, etc.), this is the principal type of coupling and for that reason it has been singled out as the coupling of primary concern in this study.

3. Type 3, Only Rigid Mode Picked Up by the Control Sensor. A control system is employed to control a rigid-body motion or the motion of one of several flexurally connected rigid bodies in series. The feedback sensor is so placed that only the desired rigid-body motion is sensed. Although the other modes are excited by the control forces, lack of feedback through the control system usually makes this a "tandem" situation, for which flexibility seldom induces instability.

4. Type 4, Modal Coupling Due to Damping. If the modal damping (e.g., damping due to aerodynamic forces) is not everywhere proportional to the mode shape, then the modal orthogonality conditions do not apply and the modes therefore have velocity coupling. This coupling, without other types of feedback, does not generally lead to instability.

5. Type 5, Coupling with Massive Elements. If there are massive elements (such as hinged engines or sloshing fuel) connected to the vehicle but free to move relative to it, then it is possible that the combined system of massive elements plus vehicle bending modes will be unstable.

6. Type 6, Instability of a Single Mode Through Force Coupling. In addition to the coupling between modes that may lead to instability, a single mode of deflection may become unstable by so affecting the magnitude and/or phase of the applied forces that either oscillatory or nonoscillatory divergence occurs, such as in aerodynamic flutter or angle-of-attack divergence of an airplane wing.

The effect of flexibility on the stability and control of vehicles first became important in connection with the study of aircraft. Instabilities of types 1, 3, 4, 5, and 6 underwent a considerable amount of investigation leading to the development of a field of study called "aeroelasticity." References 3 and 4 cover this field in detail.

With the advent of aircraft autopilots, instabilities of type 2 also became a consideration [Ref. 5]; however, the interaction of flexibility and the automatic control of vehicles did not achieve major importance until the advent of very flexible missiles, such as the Atlas, which led to the detailed study of the problem as indicated in Refs. 6 through 11.

The need to consider all types of possible instabilities in missiles led to very complex sets of equations requiring the use of computer solutions. However, Refs. 12, 13, and 14 explain how the root locus method may be employed to obtain solutions to simplified equations, providing greater insight into the problem than the computer solution does. Recently, Wang [Ref. 15] has been able to find sufficient conditions for stability of a simplified flexible vehicle using Lyapunov's Direct Method, although he remarks on the difficulty of finding a suitable Lyapunov function in the more general case.

The continuing problem of the type 2 instability in missiles and space boosters has resulted recently in the exploration of adaptive control techniques for its suppression, as indicated in Refs. 1 and 16 through 20.

With the recent consideration of spinning manned spacecraft of large dimensions, the effect of flexibility on the stability and control of these vehicles has also been given special attention, particularly because of the large size and low allowable structural weight characteristic of such vehicles. Reference 21 presents a study of the effects of

flexibility of the cable on the stability and controllability of a spinning space station consisting of a manned capsule counterbalanced by the last rocket stage on the end of a cable. This is basically a type 3 stability problem. Tai and Loh [Ref. 22] analyzed a similar configuration for its response to gravity gradient excitation. These investigators also analyzed the free vibration of an elastic space station of a Y-configuration [Ref. 23]. In Ref. 24, Hopper examines the response of large flexible rotating space stations during docking maneuvers.

The type 1 stability problem associated with the interaction of adjacent in-plane flexural modes during "spin up" has been considered by Freuh and Miller [Ref. 25] for a variety of manned-space-station configurations, including a torous configuration. Having solved for the flexural modes on a computer, they develop approximate analytical results for the amount of structural damping necessary for stability and indicate that this type of instability is negligible for a structural damping ratio greater than 0.01. Freuh and Miller also verified their results experimentally for a cross-shaped configuration, as reported in Ref. 26.

It is pointed out that none of the above references on spinning space stations deals with the problem which is of concern here--the active control of attitude where placement of the sensors and control forces is the basic consideration in determining the stability of the flexible modes.

The fundamental considerations between sensor placement and flexural modal response in a vehicle with automatic control were, in general, masked in the past by the complexity of the general flexible missile and aircraft control problem. References 27 and 28 partially recognized these considerations but offered no closed-form analytical solutions so that the effect on stability could not be clearly discerned. These relationships are explored in Chapter III, in which approximate closed-form analytic solutions are developed to determine the system's characteristic roots, to furnish stability criteria, and to provide an indication of the real-time response.

For the problem under consideration, in addition to the coupling that takes place through the control system between the rigid mode to be controlled and the flexible modes, it is also found that the vehicle axes around which it is desired to exercise control are coupled through the control system by flexibility. Reference 29 stresses the difficulty of trying to analyze control systems with multiple inputs by conventional control analysis techniques, therefore the solutions developed in Chapter III for control about a single vehicle axis are extended in Chapter IV to include control about multiple axes. The validity of these approximate formulas was checked by computer solutions.

2. The Toroidal Space Station

The wheel-shaped configuration for a spinning manned space station was popularized by Von Braun [Ref. 30], over 13 years ago. In 1962 Berglund and Weber examined this configuration in more detail [Ref. 31]. The equations of motion for any of this general class of wheel-shaped configurations, with or without spokes and a hub, can be obtained by the matrix methods of Ref. 32, and the mode shapes and real-time response can be obtained using a digital computer. In order to indicate the basic nature of such vehicle systems, a uniform toroid, or ring, was chosen so that analytical solutions could be obtained. Unfortunately, as pointed out by Lang [Ref. 33], "forced-motion solutions for vibrating rings have been given very little consideration." Therefore it was necessary to return to Love [Ref. 34], a basic reference, and extend his derivation in a somewhat modified form to fit the problem. Further complication was introduced by the spin of the ring. Again, no reference could be found on analytic solutions for spinning rings, though some work has been done on spinning membranes with holes [Ref. 35], spinning disks [Refs. 36, 37], and rotating thin-walled circular cylinders [Ref. 38]. However, it was possible to modify our equations of motion and their solutions to include spin.

3. Control Systems for Spinning Vehicles

Considerable work has been done in the last few years on synthesizing control systems for spinning vehicles, as is indicated by Refs. 45-58.

The control system suggested by Lange [Ref. 39] was found to be well suited to the problem at hand, and therefore was adapted for the spinning, toroidal manned space station.

B. ORGANIZATION OF MATERIAL

The general form of the linearized equations of motion of flexible vehicles* is given in Chapter II. For equations of this type a reasonable initial choice of control is proportional position and rate feedback. Based on this choice of control, the system transfer function and characteristic equation are developed in terms of the flexural coupling parameters u_n and a_n for the force and sensor locations. The difficulties of using the conventional analytic methods for determining the system stability and characteristic roots are discussed.

An approximate approach to finding the system characteristic roots, which is much simpler, is developed in Chapter III for vehicles with uncoupled control axes. It is based on the expansion of the characteristic roots about the normalized modal poles. Using these roots, an indication of the real-time response and frequency response of the system is also derived. Extensions of this approach to more complex control systems are indicated. A physical interpretation of the results is given and the effect of the sensor and force locations on system stability is illustrated for a simple beamlike vehicle.

In Chapter IV the system transfer function and characteristic equation are derived for flexible vehicles having coupled control axes (e.g., platelike vehicles). A transformation of the controlled variables is indicated which results in factoring of the system characteristic equation. The solution of such factored characteristic equations by the root locus or Nyquist method is discussed. Because of the difficulties of finding the system roots by conventional methods, the root expansion approach of Chapter III is extended to obtain system roots and stability criteria for vehicles having coupled control axes.

In Chapter V a mathematical model of a spinning manned space station is formulated, the equations of motion are developed, and the ranges of values of the modal frequencies are derived. A conventional rate- and

*These equations are for vehicles of arbitrary shapes, including beamlike as well as toroidal.

position-feedback control system is postulated employing a star tracker as a sensor. This results in a two-axis control system of the type discussed in Chapter IV, the axes being coupled due to flexure. The flexural coupling parameters a_n and u_n are given as a function of the sensor and control-force locations.

The stability of the station, for balanced pairs of control forces and various sensor locations, is investigated in Chapter VI for the first excited flexible mode $(n = 3)$, using the analytical techniques derived earlier. In Chapter VII the stability of the higher modes and the effects of unbalanced control forces or moments are considered. The results thus obtained were verified using a computer program.

Chapter VIII presents a summary of the work done, and general conclusions, for any flexible vehicle employing a linear control system. It also gives recommended locations for the forces and sensors for the spinning space station.

A detailed derivation yielding the basic form of the equations of motion of flexible vehicles is included in Appendix A. The equations of motion of the spinning space station are developed in Appendix B. Appendix C presents the synthesis of a linear control system for the spinning space station and the effects of flexibility on the output of the feedback sensor. Appendix D summarizes the system equations, and puts them in a form suitable for digital computer evaluation.

C. CONTRIBUTIONS OF THIS RESEARCH

The principal contributions of the present investigation are summarized as follows:

1. Development of the basic form of the equations of motion of flexible vehicles, from which the equations of forced motion of spinning pressurized toroids and the determination of their natural frequencies can be deduced.
2. Formulation of a general method of approach, and derivation of simple formulas, for quickly estimating the stability, roots, and real-time response of flexible vehicles employing multiaxis linear control systems.
3. A general solution to the problem of where to place the sensors, control forces, and moments for stability of a flexible, spinning, toroidal manned space station.

4. The physical interpretation of the effect of flexibility on a control system, which can be used as a guide to the design or study of the control of flexible vehicles.

5. Discovery that the Coriolis forces induce precession, relative to the spinning toroid, of the natural in-plane inextensible vibrations.

II. EQUATIONS OF MOTION OF CONTROLLED FLEXIBLE VEHICLES

The basic form of the equations of motion of uncontrolled flexible vehicles of arbitrary shape is presented in detail in Appendix A and summarized in Section A below.

In Section B we derive the system transfer function and characteristic equation for a linear control system, in terms of the force- and sensor-location coupling parameters u_n and a_n, and discuss their study by conventional techniques.

A. EQUATIONS OF MOTION WITHOUT CONTROL

Because they impose no external forces, natural vibrations of a vehicle do not change the following:

1. The position of the system mass center.
2. The linear momentum of the system.
3. The angular momentum of the system.

Thus if the vehicle deflection $\Delta\bar{r}$ at location $\bar{r}$ is expanded in terms of N normal modes as

$$\Delta\bar{r}(\bar{r},t) = \sum_{n=1}^{N} q_n(t)\ \bar{w}_n(\bar{r}) \tag{2.1}$$

we find that, for a flexible vehicle, we can express the equations of rigid-body motion as uncoupled from the equations of vibration. For nonspinning vehicles, or for spinning vehicles whose deflection is in the direction of the spin vector or is purely torsional deflection about the spin axis, the equations of vibration (making use of the orthogonality conditions of the normal modes) appear in linearized form as

$$\ddot{q}_n + 2\zeta_n p_n \dot{q}_n + p_n^2 q_n = \frac{F_n}{M_n} \triangleq Q_n \tag{2.2}$$

where p_n^2 is the square of the n^{th} natural frequency of vibration

$$p_n^2 = \frac{V_n}{2q_n^2 M_n} \tag{2.3}$$

and V_n is the potential energy associated with the n^{th} mode.

B. EQUATIONS OF MOTION WITH CONTROL

The equation of motion of a rigid-body motion μ often appears as

$$\ddot{\mu} + 2\zeta_o p_o \dot{\mu} + p_o^2 \mu = Q_c + Q_D \tag{2.4}$$

where

p_o = rigid-mode natural frequency

ζ_o = rigid-mode damping ratio without control

Q_D = disturbance forcing function

To control this rigid-body motion, a control function of the following form is usually chosen:

$$Q_c = -K_v \frac{d}{dt}(\mu - \mu_{ref}) - K_p(\mu - \mu_{ref}) \tag{2.5}$$

Substituting Eq. (2.5) into Eq. (2.4) yields

$$\ddot{\mu} + 2\zeta_{co} p_{co} \dot{\mu} + p_{co}^2 \mu = Q_D = \left(K_v \frac{d}{dt} + K_p\right)\mu_{ref} \tag{2.6}$$

where

$$p_{co} = \left(p_o^2 + K_p\right)^{1/2} \tag{2.7}$$

and for ζ_o negligible compared to the damping furnished by the controller,

$$\zeta_{co} = \frac{K_v}{2p_{co}} \tag{2.8}$$

(Ref. 40 indicates that desirable values of ζ_{co} are 0.7 to 0.8).

Thus when flexible behavior is included, the controlled-system dynamics may be represented as shown in Fig. 1, if the control axes are uncoupled. In the figure, u_n represents the factor converting the rigid-body control Q_c to the n^{th} mode generalized forcing function, Q_n:

$$u_n = \frac{Q_n}{Q_c} \tag{2.9}$$

and a_n represents the factor converting the n^{th} generalized coordinate to the quantity sensed by the feedback sensor (or sensors):

$$a_n = \frac{\mu_n}{q_n} \tag{2.10}$$

The factors u_n and a_n are determined in sign and magnitude by the location of the control force and sensor, respectively, with respect to the n^{th} mode shape.

The system transfer function is given by

$$\frac{\mu_s(s)}{\mu_{ref}(s)} = \frac{(K_v s + K_p)\, G(s)}{1 + (K_v s + K_p)\, G(s)} \tag{2.11}$$

where, considering the first N flexural modes,

$$G(s) = \sum_{n=0}^{N} \frac{u_n a_n}{s^2 + 2\zeta_n p_n s + p_n^2} \tag{2.12}$$

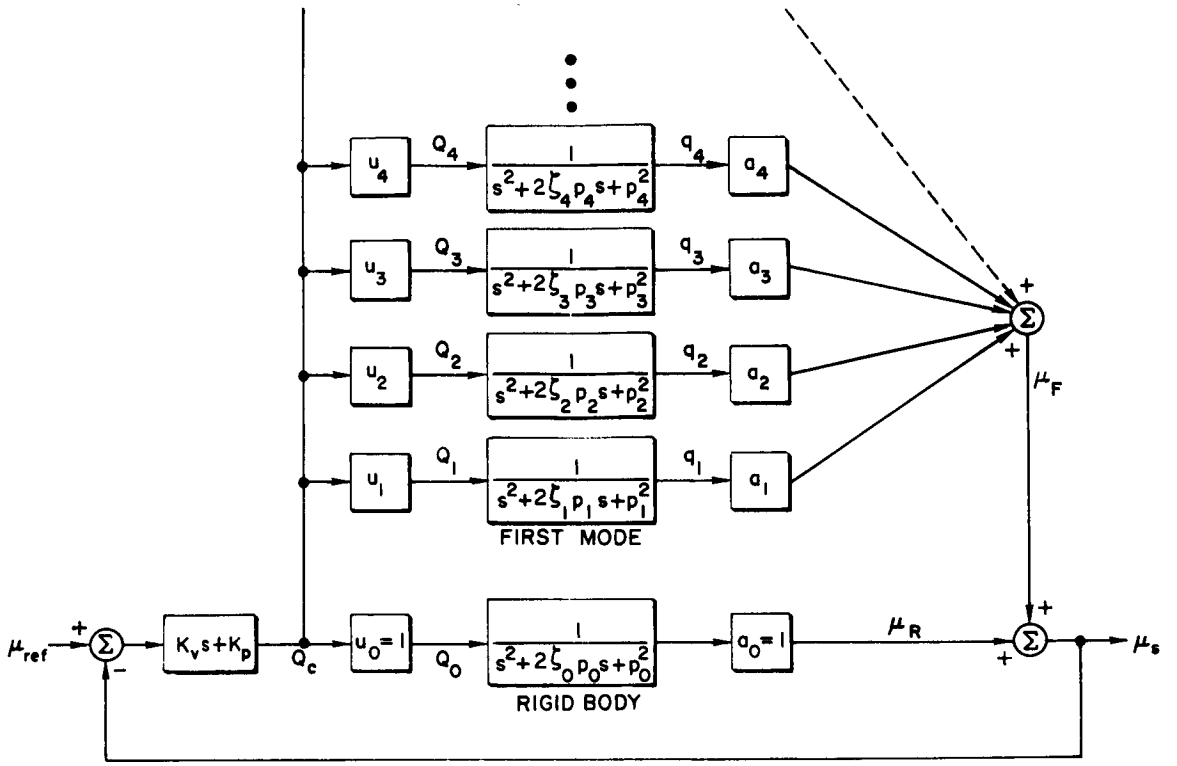

35564

FIG. 1. BLOCK DIAGRAM REPRESENTATION OF ONE AXIS OF A FLEXIBLE VEHICLE EMPLOYING A LINEAR-FEEDBACK CONTROL SYSTEM WITH UNCOUPLED AXES.

The characteristic equation is

$$1 + (K_v s + K_p)\, G(s) = 0 \tag{2.13}$$

which can also be written as

$$[1 + K_p G(s)] \left[1 + \frac{K_v s\, G(s)}{1 + K_p G(s)}\right] = 0 \tag{2.14}$$

The roots of this equation can be found, in principle, by using a double root-locus plot: first plotting the locus of roots with respect to K_p and then, for K_p fixed, plotting the locus of roots with respect to K_v. However, the zeros of $G(s)$ are not readily available, so that the solution of a quartic is required when two flexible modes are included

(e.g., see Fig. 20 on p. 80) the order of the equation rising by two for each additional mode. The effort can be halved if damping is neglected in finding the zeros; but the overall effort is still considerable if we include the higher modes.

Because of the difficulty involved in determining the system stability and characteristic roots by conventional analytical and graphical methods, we devote the next two chapters to developing simple formulas for determining the stability and estimating the system characteristic roots of flexible vehicles employing linear feedback control systems that have coupled as well as uncoupled control axes.

III. A GENERAL METHOD FOR DETERMINING STABILITY AND ESTIMATING REAL-TIME RESPONSE FOR SYSTEMS WITH UNCOUPLED AXES*

In this chapter a general method is developed for determining the stability, finding the system characteristic roots, and providing an indication of the real-time response of flexible vehicles employing linear feedback control, whose control axes can be considered uncoupled. The approach is to expand the characteristic roots about their normalized modal poles.

In Section A we develop a stability criterion and estimate the roots for small gains. This development is extended in Section B to include more complex control systems. Sections C and D provide an indication of the real-time response of the system and a physical interpretation of the results. The effects of sensor and control locations on system stability for a simple vehicle are illustrated in Section E. The previous results are extended in Section F to include an estimate of the system roots for large gains.

A. STABILITY AND CHARACTERISTIC ROOTS FOR SMALL EFFECTIVE GAINS

A much simpler approach than the conventional root-locus method for studying stability is to expand the characteristic roots about the normalized modal poles. Observe that in Eq. (2.13), if we neglect the small structural damping ratio ζ_n, there are no roots on the imaginary axis, except for $K_v = 0$ and $K_v = \infty$, so that the loci associated with K_v never cross the imaginary axis. Thus if a root starts off into the left half plane, it will remain stable for all gains, whereas if it starts off into the right half plane, it will always be unstable. Small structural damping displaces the root locus to the left but does not change the relative character of the results. Therefore, to determine if a locus associated with the i^{th} mode is stable, it is necessary only to determine its behavior in the vicinity of the i^{th}-mode pole. This is the customary problem of determining departure directions for the loci.

*e.g., beamlike vehicles.

To normalize the i^{th}-mode pole, the numerator and denominator of each term of $G(s)$ in Eq. (2.13) are divided by p_i^2 to obtain

$$1 + (k'\tilde{s} + k) \sum_{n=0}^{N} \frac{u_n a_n}{\tilde{s}^2 + 2\zeta_n r_n \tilde{s} + r_n^2} = 0 \tag{3.1}$$

where

$$\tilde{s} \triangleq s/p_i \tag{3.2}$$

$$r_n \triangleq p_n/p_i \tag{3.3}$$

$$k' \triangleq K_v/p_i = \text{effective velocity gain for the } i^{th} \text{ mode} \tag{3.4}$$

$$k \triangleq K_p/p_i^2 = \text{effective position gain for the } i^{th} \text{ mode} \tag{3.5}$$

For small gains the root near the i^{th}-mode upper pole can be expressed as

$$\tilde{s} = \epsilon + j(1+\delta) \tag{3.6}$$

where

$$\epsilon^2, \delta^2 \ll 1 \tag{3.7}$$

Substituting Eq. (3.6) into Eq. (3.1), and making use of inequality (3.7) and the relations

$$|\zeta_n \epsilon|, \ |\zeta_n \delta|, \ |k'\delta|, \ |k'\epsilon|, \ |k\delta|, \ |k\epsilon|, \ |k\zeta_n|, \ |k'\zeta_n| \ll 1 \tag{3.8}$$

and

$$\epsilon^2, \delta^2 \ll \left| \frac{1 - r_n^2}{2} \right|^2 \qquad n \neq i, m \tag{3.9}$$

we obtain

$$[-\delta + j(\zeta_i + \epsilon)]^2 + [-\delta + j(\zeta_i + \epsilon)]\left[\left(\frac{1 - r_m^2}{2}\right) + \left(\frac{k'j + k}{2}\right)(u_m a_m + u_i a_i)\right]$$

$$+ \frac{(k'j + k)}{2} u_i a_i \left(\frac{1 - r_m^2}{2}\right) = 0 \qquad (3.10)$$

where m is the mode whose natural frequency is closest to that of the i^{th} mode. By solving Eq. (3.10) for $[-\delta + j(\zeta_i + \epsilon)]$, and then equating real and imaginary parts, we may obtain the roots near the i^{th} and m^{th} modal poles. Equation (3.10) is useful for estimating the roots when two natural frequencies are close together, or when the first-mode natural frequency is close to that of the rigid mode.

In the more common case (which is treated in special detail here) the modal frequencies are well separated so that

$$\epsilon^2, \delta^2 \ll \left|\frac{1 - r_m^2}{2}\right|^2 \qquad (3.11)$$

and Eq. (3.10) yields the relative departure of the upper i^{th}-mode root from its pole as

$$\epsilon = -k' \frac{u_i a_i}{2} - \zeta_i \qquad (3.12)$$

$$\delta = k \frac{u_i a_i}{2} \qquad (3.13)$$

For k fixed, it is evident from Eq. (3.12) that the roots always leave the imaginary axis at 0° or 180° as k' is increased. Therefore for stability of the i^{th} mode without structural damping, it is only necessary that

$$\boxed{\text{sgn } u_i = \text{sgn } a_i} \tag{3.14}$$

If for given locations of the actuator and sensor, Eq. (3.14) is true for all modes, then the entire system will be stable. In order for this stability to occur in a vehicle that can be characterized by a beam, it will be necessary when employing a control force to place the sensor and actuator at such locations as the beginning or the end of the mode shapes,* where the signs of the slope and deflection are normally the same for all modes.

The effective gains k' and k decrease rapidly with mode number [as is evident from Eqs. (3.4) and (3.5)]; therefore, for the case where $|u_n a_n|$ does not increase with mode number, Eqs. (3.12) and (3.13) will yield a good approximation to the higher modal roots. It should also be observed that for this case the damping of the higher modal roots with control will be determined primarily by structural damping, and therefore the very high frequency modes will not be troublesome with normal structural damping.

Equations (3.12) and (3.13) may also be used to approximate the first modal root, their validity depending on how well the assumptions are satisfied (particularly the separation of the frequency of the first mode from the rigid-body mode).

Using Eqs. (2.8) and (3.4) we can also express ϵ in terms of the rigid-mode damping ratio with control, as:

$$\epsilon = - \frac{\zeta_{co}}{p_i} \left(p_o^2 + K_p \right)^{1/2} u_i a_i - \zeta_i \tag{3.15}$$

*For a uniform toroid, the beginnings of the mode shapes are determined by the axes chosen for control.

B. USE OF A RATE NETWORK

If a lead-lag rate network is employed in place of rate, Eq. (2.13) appears in the modified form:

$$1 + \left[K_v \frac{s + (1/\tau_o)}{s + (1/\tau_1)} + K_p\right] G(s) = 0 \tag{3.16}$$

Proceeding as before, for the poles well separated, we obtain

$$\epsilon = -k' \frac{u_i a_i}{2} \left\{\frac{\tau_1[1 - (\tau_1/\tau_o)]}{1 + \tau_1^2 p_i^2}\right\} - \zeta_i \tag{3.17}$$

$$\delta = \left\{\frac{k + k'\tau_1^2 p_i \left[1 + \left(\tau_o \tau_1 p_i^2\right)^{-1}\right]}{1 + \tau_1^2 p_i^2}\right\} \frac{u_i a_i}{2} \tag{3.18}$$

When the lead-lag network is designed so as not to alter the rigid-mode roots from their pure rate values, we have that

$$\tau_1^2\left(p_o^2 + K_p\right) \ll 1 \ll \tau_o^2\left(p_o^2 + K_p\right) \tag{3.19}$$

and k' can be written in terms of the rigid-mode damping ratio with control as:

$$k' = \frac{K_v}{p_i} = 2\zeta_{co} \frac{r_o}{\tau_1} \sqrt{1 + k} \tag{3.20}$$

Using Eqs. (3.19) and (3.20), Eqs. (3.17) and (3.18) can be rewritten as

$$\epsilon = - \frac{\zeta_{co} r_o \sqrt{1 + k}}{1 + \tau_1^2 p_i^2} u_i a_i - \zeta_i \tag{3.21}$$

$$\delta = \left\{ \frac{k}{2} + \frac{\zeta_{co}\tau_1 p_o \sqrt{1+k}}{1 + \tau_1^2 p_i^2} \left[1 + \left(\tau_o \tau_1 p_i^2 \right)^{-1} \right] \right\} u_i a_i \qquad (3.22)$$

It can be observed from Eq. (3.16) that, neglecting damping, no root locus crosses the imaginary axis, so that the criterion for stability is still that of Eq. (3.14). It can also be observed from Eqs. (3.21) and (3.22) that the higher mode root departures are greatly reduced from the pure rate case.

From Eqs. (3.21) and (3.22), it is found that with k fixed and k' varied the angle of departure Φ of the i^{th}-mode locus from its pole is

$$\Phi = \tan^{-1}\left[\frac{\delta - (k/2)u_i a_i}{\epsilon + \zeta_i} \right]$$

$$= \tan^{-1}\left\{ \frac{\left[\tau_1 p_i + (1/\tau_o p_i)^{-1} \right] \text{sgn}\,(u_i a_i)}{-\text{sgn}\,(u_i a_i)} \right\} \qquad (3.23)$$

As expected, this angle is simply the angle obtained with pure rate, modified by the angle change produced by using the rate network instead of pure rate.

A similar perturbation analysis can be carried out for additional poles and zeros in series with the controller transfer function (as might be provided by an actuator). Again the angle of departure from the i^{th}-mode pole (with k fixed) will simply be that obtained with pure rate feedback alone (determined by the $\text{sgn}\, u_i a_i$), then shifted in angle to account for the phase change at the pole due to the additional poles and zeros. For the cases where the higher mode roots stay relatively close to their poles, the angle of departure is usually all that is required to determine their stability.

C. REAL-TIME RESPONSE

1. Response to a Unit-Step Input

In terms of the characteristic roots of the system, Eq. (2.11) can be written as

$$\frac{\mu_s(s)}{\mu_{ref}(s)} = \frac{(K_v s + K_p)\, G(s) \left[\prod_{n=0}^{N} \left(s^2 + 2\zeta_n p_n s + p_n^2\right)\right]}{\prod_{n=0}^{N} (s - s_{n1})(s - s_{n2})} \tag{3.24}$$

where the conjugate complex roots associated with the n^{th} mode are

$$s_{n1} = [\epsilon_n + j(1 + \delta_n)]p_n \tag{3.25}$$

$$s_{n2} = [\epsilon_n - j(1 + \delta_n)]p_n \tag{3.26}$$

Taking the inverse Laplace transform of Eq. (3.24) and using inequalities (3.7) and (3.8) gives the contribution of the i^{th} mode to the response to a step input* as

$$\mu_i(t) \approx \left| \frac{k' u_i a_i \left[1 + (k/k')^2\right]^{1/2}}{1 + \delta_i + 2 \sum_{n=i}^{N} \delta_n} \right| \cdot \left[\exp\ (\epsilon_i p_i t)\right] \cos\left[p_i(1 + \delta_i)t + \tan^{-1}(-k'/-k)\right] \tag{3.27}$$

*A step input might be applied to produce a vehicle constant attitude.

Using Eqs. (3.12) and (3.13) for ϵ and δ, for $k = 0$, Eq. (3.27) reduces to:

$$\mu_i(t) \approx \frac{K_v}{p_i} |u_i a_i| \left\{ \exp \left[- \left(K_v \frac{u_i a_i}{2} + \zeta_i p_i \right) t \right] \right\} \sin p_i t \qquad (3.28)$$

It is observed that, for the same $u_i a_i$ for all modes, the amplitude of the response of the higher modes to a step input diminishes rapidly as the natural frequency of the mode increases. For ζ_i approximately constant with i, the time constant of decay rapidly decreases as the natural frequency of the mode increases so that for the higher modes the time constant associated with ζ_i will usually dominate compared to the time constant associated with the control.

2. Frequency Response to a Reference Input

The steady-state frequency response of the stable system can be obtained by setting $s = j\omega$ in Eq. (2.11), where, for the i^{th} mode at resonance and the modal frequencies well separated,

$$(K_v j\omega + K_p)\, G(j\omega) \approx \left(- \frac{K_p}{\omega^2} \sum_{n=0}^{i-1} u_n a_n + \frac{K_v}{\omega} \frac{u_i a_i}{2\zeta_i} + \sum_{n=i+1}^{N} \frac{K_p}{p_n^2} u_n a_n \right)$$

$$-j \left(\frac{K_v}{\omega} \sum_{n=0}^{i-1} u_n a_n + \frac{K_p}{\omega^2} \frac{u_i a_i}{2\zeta_i} - \sum_{n=i+1}^{N} \frac{K_v \omega}{p_n^2} u_n a_n \right) \qquad (3.29)$$

Observe that for the frequencies above resonance the excitation is small and can be ignored when $|u_n a_n|$ does not increase with mode number.

D. PHYSICAL INTERPRETATION

In deriving the general approach it was observed that, for ϵ and δ small compared to the separation of frequencies, the characteristic roots of the system associated with the i^{th} mode were relatively

independent of the other modes. Therefore, referring to Fig. 1, for the purpose of deriving the i^{th}-mode roots we can consider the system to be just the i^{th} mode of flexure with the feedback loop around it.

Physically this can be interpreted as follows. If the i^{th} mode is excited, then it will respond at its loop resonant frequency. If ϵ is small compared to the frequency separation, then the i^{th} mode will be relatively undamped and have a high Q (amplification ratio) at this frequency compared to the other modes (δ must also be small compared to the frequency separation to maintain the frequency separation large compared to ϵ). Thus the i^{th} mode passes its loop resonant frequency very readily compared to the other modes, so that they can be considered to be effectively blocked off.

If another frequency is close to the i^{th} frequency compared to ϵ, δ, or ζ, then it will have a sufficiently high response at the i^{th}-mode loop frequency so that it must be considered. In that case we have a quadratic expression determining the ϵ and δ, as in Eq. (3.10).

For the case where the frequencies are well separated each mode must be stabilized independently. As there is only one controller, an undesired sign reversal must be avoided in the loop. Therefore for a system with simple rate and position feedback, the sign of u_n must be the same as the sign of a_n.

If, besides rate and position feedback, there are additional leads or lags in series with the gain, the following observations can be made:

If these leads or lags have time constants that are small compared to the period of the rigid-mode loop, then they have very little effect upon it. However, as we consider the higher modes, it is found that a point may be reached where the control is applied too early or too late so that it tends to aid the deflection rather than retard it, which in turn leads to instability for an otherwise stable mode or, conversely, perhaps leads to stability for an otherwise unstable mode.

E. THE $u_n a_n$ RELATIONSHIPS FOR ATTITUDE CONTROL OF A SIMPLE BEAMLIKE FLEXIBLE VEHICLE

The relationship of u_n and a_n to the positions of the forces and sensors along the mode shape can be illustrated by considering a simple

position- and rate-feedback attitude control system for a flexible rocket, missile, or satellite employing a lateral force F at the aft end for attitude control. For such a simplified vehicle the $u_n a_n$ relationships shown in Fig. 2 apply.

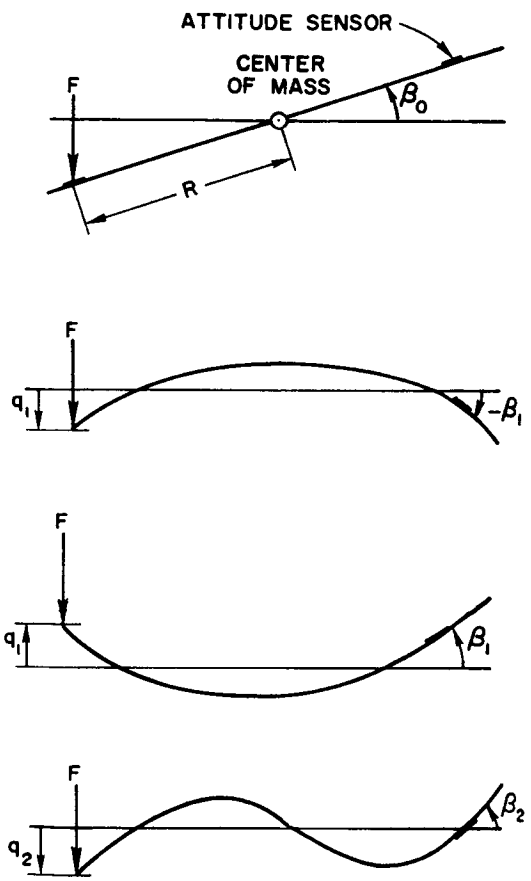

a. $u_o = 1, \quad a_o = 1$

b. $u_1 > 0, \quad a_1 < 0$

c. $u_1 < 0, \quad a_1 > 0$

d. $u_2 > 0, \quad a_2 < 0$

$$Q_c = \frac{FR}{\left[\begin{array}{l}\text{mass moment of inertia} \\ \text{about the center of mass}\end{array}\right]}$$

$$u_n = Q_n/Q_c$$

$$a_n = \beta_n/q_n$$

FIG. 2. THE u_n AND a_n RELATIONS FOR ATTITUDE CONTROL OF A SIMPLIFIED FLEXIBLE ROCKET.

Comparing the first mode in Fig. 2b to the rigid-body mode in Fig. 2a, it is found that $u_1 > 0$, but for the sensor location shown the sensor reads a negative angle for a positive q_1, so that $a_1 < 0$. Thus we have a sign reversal as we go around the first-mode loop. If the first-mode shape were normalized instead so that q_1 is positive upward, as shown in Fig. 2c, then the sensor would read a positive angle for a positive q_1, so that $a_1 > 0$; but observe that then $u_1 < 0$. It is apparent that, as the way we normalize a mode shape is arbitrary, stability depends only upon the sign of the product $a_i u_i$, not upon the signs of the terms themselves.

From Fig 2d, we observe that the second mode is stable, even though the first mode is unstable. It is readily apparent that to insure that all the modes are stable (no sign reversal in any modal loop), we need only place the control force and the sensor together at either end of the vehicle, for at the beginnings and ends of mode shapes the signs of the slopes and deflections are the same for all modes.

Observe from Fig. 3 that simply putting the control force and sensor together at an arbitrary location does not insure that the sign of $u_n a_n$

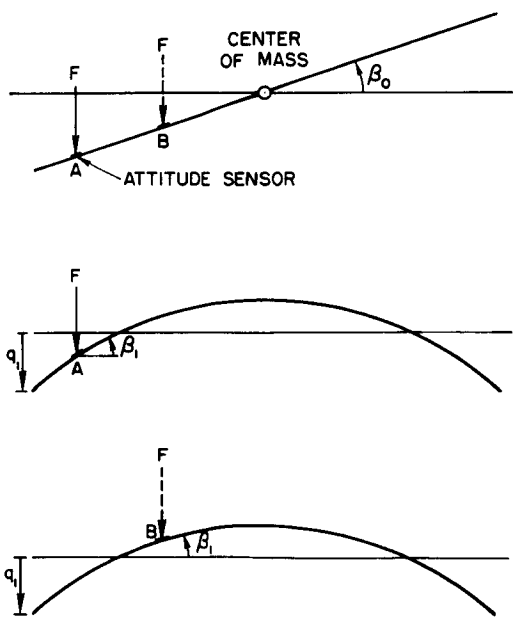

a. $u_o = 1$, $a_o = 1$

b. $u_1 > 0$, $a_1 > 0$

c. $u_1 < 0$, $a_1 > 0$

35566

FIG. 3. THE u_n and a_n RELATIONS FOR A SIMPLIFIED VEHICLE ATTITUDE CONTROL SYSTEM WITH THE CONTROL FORCE AND SENSOR AT A SINGLE LOCATION, AS A FUNCTION OF THAT LOCATION.

will be positive. Thus position A yields $u_1 a_1 > 0$, whereas position B yields $u_1 a_1 < 0$. Therefore with a control system employing simple position and rate feedback, the first mode would be unstable for position B, and stable for position A.

F. ROOTS FOR LARGE GAINS

When the poles are well separated (as indicated in Fig. 20, p. 80), inequality (3.7) may also be applicable for large gains. For this case we obtain, from Eq. (3.1), for

$$\left| \frac{2[\delta - j(\epsilon + \zeta_n r_n)]\ [-\delta + j(\epsilon + \zeta_i)]}{1 - r_n^2} \right| \ll 1 \qquad (n \neq i) \qquad (3.30)$$

that

$$\epsilon = \frac{-k' \frac{u_i a_i}{2} \left(1 + k \frac{u_i a_i}{2}\right) - \zeta_i \left[(1 - kU)^2 + k'^2 U \left(U + \frac{u_i a_i}{2}\right)\right]}{(1 - kU)^2 + k'^2 \left(U + \frac{u_i a_i}{2}\right)^2} \qquad (3.31)$$

$$\delta = \frac{k \frac{u_i a_i}{2} (1 - kU) - k'^2 \frac{u_i a_i}{2} \left(U + \frac{u_i a_i}{2}\right) - \zeta_i k' \frac{u_i a_i}{2} (1 - kU)}{(1 - kU)^2 + k'^2 \left(U + \frac{u_i a_i}{2}\right)^2} \qquad (3.32)$$

where

$$U = \sum_{\substack{n=0 \\ n \neq i}}^{N} \frac{u_n a_n}{1 - r_n^2} \qquad (3.33)$$

When the zero is close enough to the pole so that inequality (3.7) holds (e.g., when the mode is excited very little), the relative departure of the upper i^{th}-mode zero of $G(s)/[1+K_p G(s)]$ from the i^{th}-mode pole is given by

$$\lim_{k' \to \infty} \epsilon = \frac{-\zeta_i U}{U + \frac{u_i a_i}{2}} \tag{3.34}$$

$$\lim_{k' \to \infty} \delta = \frac{-\frac{u_i a_i}{2}}{U + \frac{u_i a_i}{2}} \tag{3.35}$$

Observe from Eq. (3.35) that inequality (3.7) would not hold for very large values of k' if U had not been included.

IV. FLEXIBLE VEHICLES WITH COUPLED TWO-AXIS LINEAR-FEEDBACK CONTROL SYSTEMS*

In this chapter the results of the previous chapters are extended to encompass flexible vehicles whose control axes are coupled via the control system. These vehicles include unconventional platelike vehicles, such as the toroid studied in this report.

In Section A we develop the system transfer function and characteristic equation for such a vehicle, and indicate how the characteristic equation may be factored. The conventional techniques of solution of these factored characteristic equations, including the difficulties involved, are then discussed.

In Section B, the simpler root expansion approach of Chapter III is extended to obtain the system roots, for small gains, for vehicles having coupled control axes. Section C considers the roots and stability criteria of the first excited flexible mode for large values of gain.

A. CHARACTERISTIC EQUATION

Employing similar nomenclature and using similar arguments to those of Chapter II, we can usually represent a flexible vehicle employing a coupled two-axis linear-feedback control system by the diagram shown in Fig. 4. The u's, a^T's, q's and Q_x and Q_y shown on the figure are $(N+1) \times 1$ vectors and the rest of the quantities are scalars, except $1/E_x$ and $1/E_y$ which are defined as

$$\frac{1}{E_x} = \begin{bmatrix} \frac{1}{E_{x_o}} & & 0 \\ & \ddots & \\ 0 & & \frac{1}{E_{x_N}} \end{bmatrix} = \begin{bmatrix} \frac{1}{s^2 + 2\zeta_{s_o} p_{x_o} s + p_{x_o}^2} & & 0 \\ & \ddots & \\ 0 & & \frac{1}{s^2 + 2\zeta_{x_N} p_{x_N} s + p_{x_N}^2} \end{bmatrix} \tag{4.1}$$

*e.g., platelike vehicles.

$$\frac{1}{E_y} = \begin{bmatrix} \frac{1}{E_{y_o}} & & 0 \\ & \ddots & \\ 0 & & \frac{1}{E_{y_N}} \end{bmatrix} = \begin{bmatrix} \frac{1}{s^2 + 2\zeta_{y_o} p_{y_o} s + p_{y_o}^2} & & 0 \\ & \ddots & \\ 0 & & \frac{1}{s^2 + 2\zeta_{y_N} p_{y_N} s + p_{y_N}^2} \end{bmatrix} \tag{4.2}$$

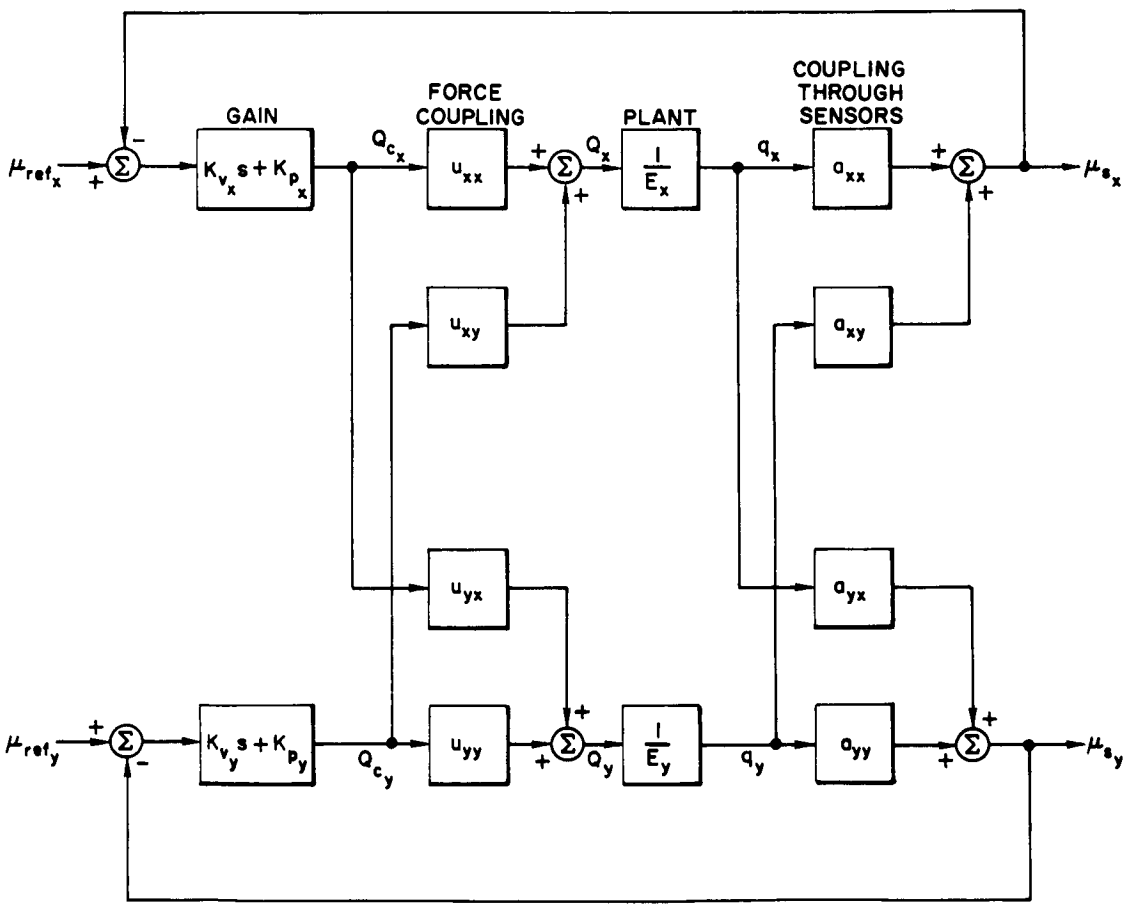

35567

FIG. 4. A MATRIX BLOCK DIAGRAM OF A FLEXIBLE VEHICLE WITH COUPLED TWO-AXIS LINEAR-FEEDBACK CONTROL.

Using Fig. 4 we find the sensed output vector as

$$\mu_s \triangleq \begin{Bmatrix} \mu_{s_x} \\ \mu_{s_y} \end{Bmatrix} = GK\mu_{ref}(I + GK)^{-1} \tag{4.3}$$

where

$$K \triangleq \begin{bmatrix} \left(K_{v_x} s + K_{p_x}\right) & 0 \\ 0 & \left(K_{v_y} s + K_{p_y}\right) \end{bmatrix} \tag{4.4}$$

$$G \triangleq \begin{bmatrix} G_{xx} & G_{xy} \\ G_{yx} & G_{yy} \end{bmatrix} \tag{4.5}$$

and where

$$G_{xx} = \sum_{n=0}^{N} \left(\frac{a_{xx_n} u_{xx_n}}{E_{x_n}} + \frac{a_{xy_n} u_{yx_n}}{E_{y_n}} \right) \tag{4.6}$$

$$G_{xy} = \sum_{n=0}^{N} \left(\frac{a_{xx_n} u_{xy_n}}{E_{x_n}} + \frac{a_{xy_n} u_{yy_n}}{E_{y_n}} \right) \tag{4.7}$$

$$G_{yx} = \sum_{n=0}^{N} \left(\frac{a_{yx_n} u_{xx_n}}{E_{x_n}} + \frac{a_{yy_n} u_{yx_n}}{E_{y_n}} \right) \tag{4.8}$$

$$G_{yy} = \sum_{n=0}^{N} \left(\frac{a_{yx_n} u_{xy_n}}{E_{x_n}} + \frac{a_{yy_n} u_{yy_n}}{E_{y_n}} \right) \tag{4.9}$$

Observe that, using these definitions, Fig. 5 is the concise matrix equivalent of Fig. 4.

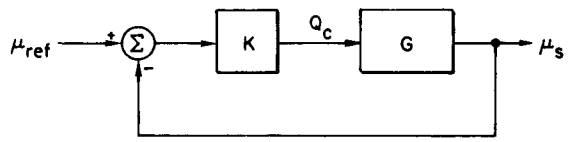

FIG. 5. CONCISE MATRIX BLOCK DIAGRAM EQUIVALENT OF FIG. 4.

35568

From Eq. (4.3), using the definitions of Eqs. (4.4) and (4.5), the characteristic equation of the system is

$$1 + \left(K_{v_x} s + K_{p_x}\right)G_{xx} + \left(K_{v_y} s + K_{p_y}\right)G_{yy}$$

$$+ \left(K_{v_x} s + K_{p_x}\right)\left(K_{v_y} s + K_{p_y}\right)\left(G_{xx}G_{yy} - G_{xy}G_{yx}\right) = 0 \qquad (4.10)$$

If the gains for the two axes are linearly related so that

$$\left(K_{v_y} s + K_{p_y}\right) = h\left(K_{v_x} s + K_{p_x}\right) \triangleq h(K_v s + K_p) \qquad (4.11)$$

we may readily factor Eq. (4.10) into

$$\left[1 + K_p G_+(s)\right]\left[1 + K_p G_-(s)\right]\left[1 + \frac{K_v s G_+(s)}{1 + K_p G_+(s)}\right]\left[1 + \frac{K_v s G_-(s)}{1 + K_p G_-(s)}\right] = 0 \qquad (4.12)$$

where

$$G_\pm(s) = \frac{2h\left(G_{xx}G_{yy} - G_{xy}G_{yx}\right)}{\left(G_{xx} + hG_{yy}\right) \pm \sqrt{\left(G_{xx} - hG_{yy}\right)^2 + 4hG_{xy}G_{yx}}} \qquad (4.13)$$

Though formidable, when the characteristics and gains of the two axes are equal, and the axes are uncoupled when flexure is neglected, this expression can be handled by conventional root locus (or Nyquist) techniques if we consider the rigid-body mode and only the first excited flexible mode. However, due to the radical in the denominator of $G_{\pm}(s)$, we will not always have 0° or 180° root loci.

Because of the difficulty of employing conventional analytical techniques, in the next section we shall extend the general approach of Chapter III to include vehicles whose control axes are coupled via the control system.

B. A GENERAL METHOD FOR ESTIMATING THE STABILITY AND CHARACTERISTIC ROOTS OF FLEXIBLE VEHICLES HAVING COUPLED CONTROL AXES

For the coupled system, the characteristic equation no longer has the simple form of Eq. (2.13), and it therefore cannot be stated that the root loci do not cross the imaginary axis, making the simple stability theorem of Chapter III unavailable to us. We can, however, still use the stability theorem for each of the factored portions of Eq. (4.12) if, neglecting structural damping, the radical in Eq. (4.13) is always real when evaluated on the imaginary axis.

More generally, we can obtain linear expansions of the system roots about their normalized modal poles; and for those modes for which inequalities (3.7) - (3.9) are satisfied, these expansions will yield good approximations to the actual roots, so that when their angle of initial departure due to k' is well away from 90° or 270°, we can determine stability from the sign of ϵ as in the uncoupled case.

If we make the assumption, that for each control axis, the departure of the modal roots from their poles is small relative to the separation of the modal frequencies, then using a procedure similar to that used in Chapter III, together with the assumptions and definitions of that chapter, we obtain the following approximations to the modal roots.

Case I: The m^{th} y-axis natural frequency is approximately equal to the i^{th} x-axis natural frequency.

For this case the characteristic equation reduces to:

$$\left[-\delta + j\left(\zeta_{x_i} + \epsilon\right)\right]^2 + \left[-\delta + j\left(\zeta_{x_i} + \epsilon\right)\right]\left[(k'_x j + k_x)\alpha_{xx} + (k'_y j + k_y)\alpha_{yy}\right] + (k'_x j + k_x)(k'_y j + k_y)\left(\alpha_{xx}\alpha_{yy} - \alpha_{xy}\alpha_{yx}\right) = 0 \qquad (4.14)$$

where we have defined

$$\alpha_{xx} \triangleq \frac{a_{xx_i} u_{xx_i}}{2} + \frac{a_{xy_m} u_{yx_m}}{2} \qquad (4.15)$$

$$\alpha_{xy} \triangleq \frac{a_{xx_i} u_{xy_i}}{2} + \frac{a_{xy_m} u_{yy_m}}{2} \qquad (4.16)$$

$$\alpha_{yx} \triangleq \frac{a_{yx_i} u_{xx_i}}{2} + \frac{a_{yy_m} u_{yx_m}}{2} \qquad (4.17)$$

$$\alpha_{yy} \triangleq \frac{a_{yx_i} u_{xy_i}}{2} + \frac{a_{yy_m} u_{yy_m}}{2} \qquad (4.18)$$

Thus from Eq. (4.14), we may solve for the relative departures of the characteristic roots near the i^{th} x pole and the m^{th} y pole from

$$\left[-\delta + j\left(\zeta_{x_i} + \epsilon\right)\right] = -\frac{1}{2}\left[(k'_x j + k_x)\alpha_{xx} + (k'_y j + k_y)\alpha_{yy}\right] \pm \frac{1}{2}\sqrt{\left[(k'_x j + k_x)\alpha_{xx} + (k'_y j + k_y)\alpha_{yy}\right]^2 - 4(k'_x j + k_x)(k'_y j + k_y)(\alpha_{xx}\alpha_{yy} - \alpha_{xy}\alpha_{yx})} \qquad (4.19)$$

If the gains are linearly related as in Eq. (4.11), then Eq. (4.23) yields

For the radical real,

$$\epsilon = \frac{k'}{2}\left[-(\alpha_{xx} + h\alpha_{yy}) \pm \sqrt{(\alpha_{xx} - h\alpha_{yy})^2 + 4h\alpha_{xy}\alpha_{yx}}\right] - \zeta_{x_i} \qquad (4.20)$$

$$\delta = -\frac{k}{2}\left[-(\alpha_{xx} + h\alpha_{yy}) \pm \sqrt{(\alpha_{xx} - h\alpha_{yy})^2 + 4h\alpha_{xy}\alpha_{yx}}\right] \qquad (4.21)$$

For the radical imaginary

$$\epsilon = -\frac{k'}{2}(\alpha_{xx} + h\alpha_{yy}) \pm \frac{k}{2}\left|\sqrt{(\alpha_{xx} - h\alpha_{yy})^2 + 4h\alpha_{xy}\alpha_{yx}}\right| - \zeta_{x_i} \qquad (4.22)$$

$$\delta = \frac{k}{2}(\alpha_{xx} + h\alpha_{yy}) \pm \frac{k'}{2}\left|\sqrt{(\alpha_{xx} - h\alpha_{yy})^2 + 4h\alpha_{xy}\alpha_{yx}}\right| \qquad (4.23)$$

If we have transfer functions in series with the gains, similar perturbation procedures are applicable.

Case II: The separation between p_{x_i} and the closest y frequency, p_{y_m}, is large compared to the i^{th} x-root departure from its pole.

For this case the relative departure from the i^{th} x pole is given as

$$\delta = k_x \frac{u_{xx_i} a_{xx_i}}{2} + k_y \frac{u_{xy_i} a_{yx_i}}{2} \qquad (4.24)$$

$$\epsilon = -\left(k'_x \frac{u_{xx_i} a_{xx_i}}{2} + k'_y \frac{u_{xy_i} a_{yx_i}}{2}\right) - \zeta_{x_i} \qquad (4.25)$$

By comparing these equations with Eqs. (3.12) and (3.13), we see immediately the effect of coupling when the frequencies of the two axes are different.

By interchanging x and y, Eqs. (4.24) and (4.25) can of course be used to find the root near the y-axis i^{th} pole for this case.

C. ROOTS OF THE FIRST EXCITED FLEXIBLE MODE FOR LARGE GAINS

For the reasons given in Chapter III, the first excited mode is usually most critical from the stability viewpoint, so that it is important to consider it for large gains. We shall consider the case for which the two axes are identical, the modal frequencies are well separated, the rigid modes are uncoupled, and

$$\epsilon^2, \delta^2 \ll 1 \tag{4.26}$$

$$\epsilon^2, \delta^2 \ll \left| \frac{1 - r_n^2}{2} \right|^2 \qquad n \neq 0,1 \tag{4.27}$$

$$\left| \frac{2[\delta - j(\epsilon + \zeta_o r_o)][-\delta + j(\epsilon + \zeta_1)]}{1 - r_o^2} \right| \ll \sup\left(\left| \frac{u_{xx_1} a_{xx_1}}{2} \right| , \left| \frac{u_{yy_1} a_{yy_1}}{2} \right| \right) \tag{4.28}$$

with no assumptions being made on the size of the gains.

Defining

$$c \triangleq -\frac{1}{2} (\alpha_{xx} + \alpha_{yy}) \tag{4.29}$$

$$d \triangleq \frac{1}{2} \sqrt{(\alpha_{xx} - \alpha_{yy})^2 + 4\alpha_{xy}\alpha_{yx}} \tag{4.30}$$

$$w \triangleq \frac{1}{1 - r_o^2} \tag{4.31}$$

we obtain from Eq. (4.10) the relative root departures from the upper pole of the first excited flexural mode, as

d real

$$\epsilon = \frac{k'(c \pm d)[1 - (c \pm d)k] - \zeta_1\left\{k'^2 w[w - (c \pm d)] + (1 - wk)^2\right\}}{(1 - wk)^2 + k'^2[w - (c \pm d)]^2} \tag{4.32}$$

$$\delta = \frac{-k(c \pm d)(1 - wk) + k'^2(c \pm d)[w - (c \pm d)] + \zeta_1\left\{k'(c \pm d)(1 - wk)\right\}}{(1 - wk)^2 + k'^2[w - (c \pm d)]^2} \tag{4.33}$$

d imaginary

$$\epsilon = \frac{k'[c \mp k'w|d| - k(c^2 + |d|^2)] \pm k|d|(1 - wk)}{(1 - wk \mp k'|d|)^2 + k'^2(w - c)^2}$$

$$- \frac{\zeta_1\left\{(1 - wk)^2 + k'^2 w(w - c) \mp k'|d|(1 - wk)\right\}}{(1 - wk \mp k'|d|)^2 + k'^2(w - c)^2} \tag{4.34}$$

$$\delta = \frac{-kc(1 - wk) \pm k'|d| + k'^2[c(w - c) - |d|^2]}{(1 - wk \mp k'|d|)^2 + k'^2(w - c)^2}$$

$$+ \frac{\zeta_1 k'\left\{c(1 - wk) \mp k'w|d|\right\}}{(1 - wk \mp k'|d|)^2 + k'^2(w - c)^2} \tag{4.35}$$

For $k = 0$, comparing Eqs. (4.20) and (4.32) we observe that for d real the stability criterion neglecting structural damping is independent of gain, being

$$c < -d \tag{4.36}$$

However, comparing Eqs. (4.22) and (4.34), we observe that for d imaginary and $k = 0$, and neglecting structural damping, the stability criterion changes with gain, being

$$c < -k'w|d| \tag{4.37}$$

Using the definitions for w, c, and d from Eqs. (4.29) through (4.31), stable locations for the sensors, for a specific force configuration, may be determined.

The simple stability criteria and the formulas for estimating the system roots associated with the flexible modes, developed in these last two chapters, will be utilized in the remainder of this study as a basis for initially determining the placement of the control actuators and sensors for the spinning space station. The results obtained in this fashion will then be checked using a computer program to solve the "complete" characteristic equation.

Before this can be done, it is first necessary to postulate a model for the spinning space station, determine its natural frequencies and mode shapes, and develop formulas for the flexural coupling parameters u_n and a_n. These topics will be treated in the following chapter.

V. EQUATIONS OF MOTION FOR THE CONTROLLED SPINNING SPACE STATION

In this chapter we postulate a model for a spinning manned space station and review the development of the equations of motion, the details of which are given in Appendix B. The range of values of the modal frequencies and damping ratios is indicated. Finally a conventional rate and position feedback control system is postulated, and the appropriate flexural coupling parameters u_n and a_n are indicated. A detailed consideration of the control system is given in Appendix C.

A. MATHEMATICAL MODEL AND EQUATIONS OF MOTION: UNCONTROLLED STATION

Loret [Ref. 41] indicates that to prevent orientation (canal) sickness in a spinning manned space station, it is desirable to keep the spin speed below 4 rpm, which indicates that station cabin radii of 60 ft or more are required to obtain the equivalent gravitational level of one-fourth of an earth g, or greater, required for satisfactory walking.

Two desirable configurations for spinning manned space stations are the wheel-shaped configurations of Fig. 6 [Ref. 31]. Inasmuch as the spokes are only a means of access to the hub (despun for docking and zero g experiments), they are smaller in diameter and of lighter weight and structure than the main compartment on the rim. Thus, during out-of-plane

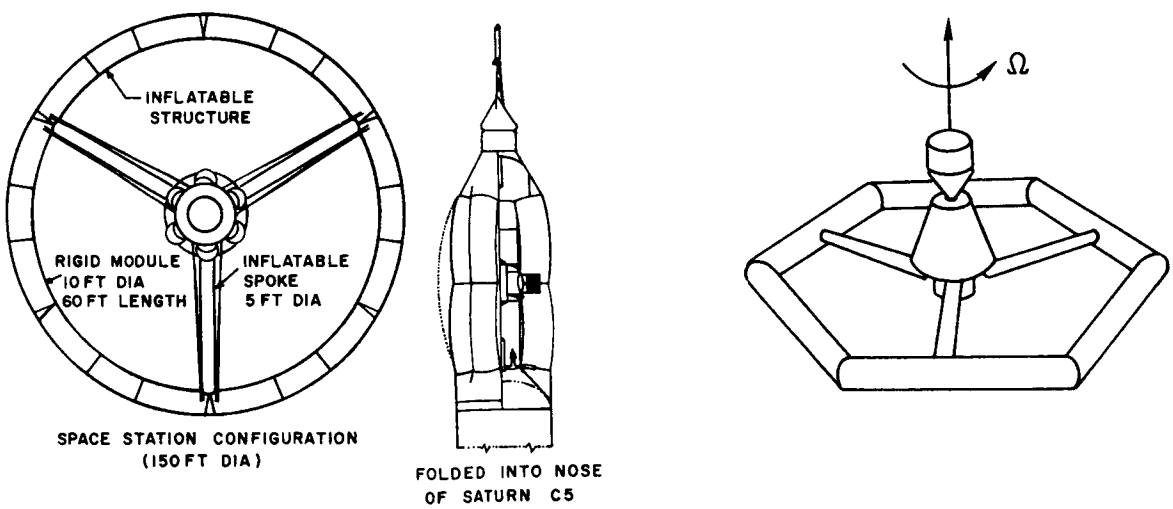

FIG. 6. SELF-ERECTING WHEEL-SHAPED SPACE STATIONS PROPOSED BY BERGLUND AND WEBER [REF. 31].

flexural motions, they tend to act as isolation between the hub and the rim, especially for the higher frequency flexural modes. Therefore as a first approximation to stations of the types represented by Fig. 6, we can consider the station to be represented, for our purposes of analysis of the out-of-plane motion, by a uniform toroid or ring which is the rim of the station.

For numerical purposes, when we wish to illustrate our results by example, we will consider a station having a mean rim radius of 85 ft, a spin speed of 3 rpm, and a symmetrical cross section about 10 ft in diameter for the rim. Such a station would provide a g level of about one-third g.

Because of their dimensions, the toroids being considered behave during vibration essentially as rings. Love [Ref. 34] shows that for a nonspinning, unpressurized ring, the linearized motion divides itself conveniently into sets of uncoupled motions: motion out of the plane of the ring and motion in the plane of the ring. The primary linear effects of pressurization and spin are to produce an equilibrium tension in the ring and to induce Coriolis forces during in-plane motion.

The tension due to pressure simply retards buckling of the cross section, while the tension due to spin produces restoring forces during deflection, resulting in higher frequencies of vibration. The Coriolis forces during free in-plane inextensible vibrations cause the "standing" vibration to precess relative to the ring, as indicated by Eq. (B3.20).

As neither effect produces coupling of the in-plane and out-of-plane motions, these motions are also decoupled for our case. In attempting to control the motion of the spin axis, we excite or sense only the out-of-plane motion (to first order). Therefore for the rest of this study we shall consider only the out-of-plane motion due to flexure. This flexure can be represented by the linear deflection $z(\gamma,t)$ and the twist $\beta(\gamma,t)$ of the centroidal line of the ring as indicated in Fig. 7.

Love shows that for a uniform ring the mode shapes of free vibrations are sines and cosines of $n\gamma$, where n is an integer, for continuity. For the n^{th} mode of free vibration, the twist is proportional to the deflection and can be obtained from Love as

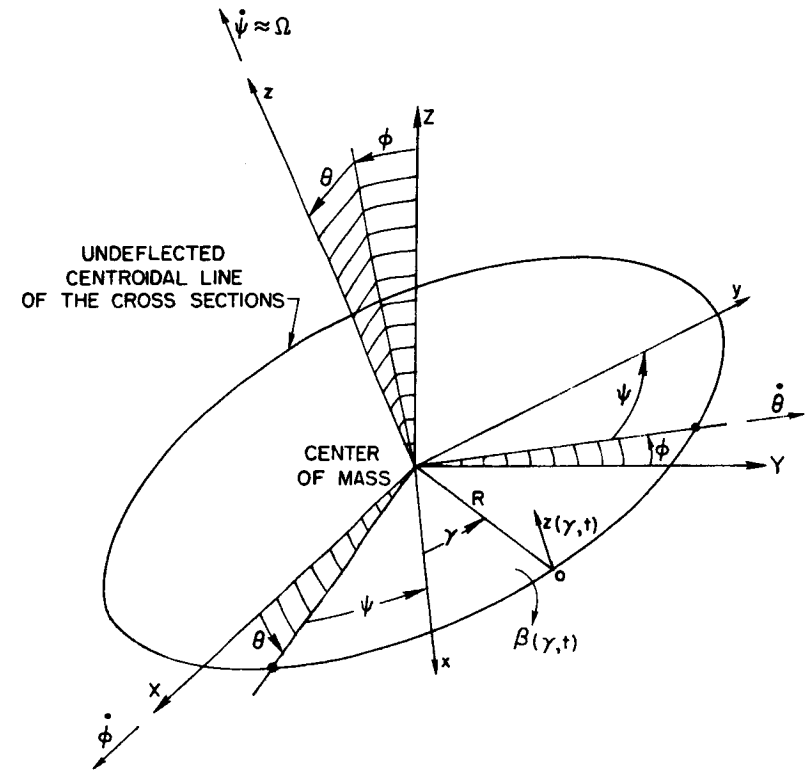

FIG. 7. BASIC GEOMETRY OF A SPINNING TOROID.

$$B_n \triangleq \frac{\beta_n}{z_n} = -\frac{1}{n^2} \frac{\left(1 + \frac{\mu I_p}{EI}\right)}{\left(1 + \frac{\mu I_p}{EI} n^2\right)} \tag{5.1}$$

where $\mu I_p/EI$ (defined in Appendix B) is the ratio of the torsional rigidity to the bending rigidity of the cross section. B_n and the mode shapes are unchanged when spin and pressurization are included.

To study the forced vibration we use the following modal expansions for flexure:

$$z(\gamma,t) = \sum_{n=2}^{N} q_{ns}(t) \sin n\gamma + \sum_{n=2}^{N} q_{nc}(t) \cos n\gamma \triangleq \sum_{n=2}^{N} z_n \tag{5.2}$$

$$\beta(\gamma,t) = \sum_{n=2}^{N} B_n q_{ns}(t) \sin n\gamma + \sum_{n=2}^{N} B_n q_{nc}(t) \cos n\gamma = \sum_{n=2}^{N} \beta_n \qquad (5.3)$$

which, upon following the equations-of-equilibrium approach of Love, yield the vibration equations:*

$$\ddot{q}_{ns} + 2\zeta_n p_n \dot{q}_{ns} + p_n^2 q_{ns} = \frac{2}{M} \int_0^{2\pi} \check{f}_z(\gamma) \sin n\gamma \, d\gamma \triangleq Q_{ns} \qquad (n \geq 2) \qquad (5.4)$$

$$\ddot{q}_{nc} + 2\zeta_n p_n \dot{q}_{nc} + p_n^2 q_{nc} = \frac{2}{M} \int_0^{2\pi} \check{f}_z(\gamma) \cos n\gamma \, d\gamma \triangleq Q_{nc} \qquad (n \geq 2) \qquad (5.5)$$

where

$$\int_0^{2\pi} \check{f}_z \sin n\gamma \, d\gamma = \int_0^{2\pi} f_z \sin n\gamma \, d\gamma + \int_0^{2\pi} \frac{M'_x}{R} (n \cos n\gamma \cos \gamma + \sin n\gamma \sin \gamma) \, d\gamma$$

$$+ \int_0^{2\pi} \frac{M'_y}{R} (n \cos n\gamma \sin \gamma - \sin n\gamma \cos \gamma) \, d\gamma \qquad (5.6)$$

$$\int_0^{2\pi} \check{f}_z \cos n\gamma \, d\gamma = \int_0^{2\pi} f_z \cos n\gamma \, d\gamma + \int_0^{2\pi} \frac{M'_x}{R} (-n \sin n\gamma \cos \gamma + \cos n\gamma \sin \gamma) \, d\gamma$$

$$+ \int_0^{2\pi} \frac{M'_y}{R} (-n \sin n\gamma \sin \gamma - \cos n\gamma \cos \gamma) \, d\gamma \qquad (5.7)$$

For isotropic structural material and a symmetric cross section,

$$p_n^2 = \frac{n^2(n^2 - 1)^2}{\check{m}(n^2 + 1 + \sigma)} + n^2\Omega^2 \qquad (5.8)$$

*We are concerned only with $n \geq 2$, for $n = 0$ corresponds to rigid-body translation and $n = 1$ corresponds to rigid-body rotation about a station diameter.

and

$$B_n = -\frac{1}{R}\,\frac{(2+\sigma)}{\left[1+\frac{(1+\sigma)}{n^2}\right]} \tag{5.9}$$

where the first term of the frequency equation is the same as that given in Love and the second term results from including the potential energy (during out-of-plane deflection) which is due to the centrifugal tension.

If, for our space station example, we consider the ratio of structural weight to gross weight of the station to be on the order of one-tenth, and consider a range of structural materials, we find that we can approximate the limits of the square of the ratios of frequency to spin speed as

$$\boxed{n^4 \leqq \frac{p_n^2}{\Omega^2} \leqq 50\ n^4} \qquad (n \geqq 2) \tag{5.10}$$

where the higher frequencies correspond to the higher stiffness-to-weight-ratio structural materials. We also obtain approximately the same range by considering allowable elongations due to the tension resulting from centrifugal and pressure forces.

We shall consider the structural equivalent viscous damping ratio ζ_n to be the same for all frequencies and to have the range

$$\boxed{0.02 \leqq \zeta_n \leqq 0.2} \tag{5.11}$$

with the lower values corresponding to the stiffer materials.

Equations (5.10) and (5.11) are the fundamental equations on which we base our numerical results.

If we observe that, for small motions of the spin axis from its inertial reference, the small vector angle between the rigid-mode spin axis and the inertial reference, as seen in the body-fixed frame, is given by

$$\mu \triangleq (\phi + j\theta)e^{-j\psi} \triangleq \mu_x + j\mu_y \tag{5.12}$$

then, as indicated by Lange [Ref. 39], we can write the vector equation for the motion of the spin axis as

$$\ddot{\mu} + \Omega^2 \mu = \frac{M_x + jM_y}{A} \triangleq Q \tag{5.13}$$

B. EQUATIONS WITH CONTROL

By applying conventional position- and rate-feedback control

$$Q_c = -K_v \frac{d}{dt}(\mu - \mu_{ref}) - K_p(\mu - \mu_{ref}) \tag{5.14}$$

to Eq. (5.13), the resulting system diagram is the same as that shown in Fig. 4.

The angle μ may be directly measured by a star tracker, with rate being derived from it, or rate may be obtained using body-mounted rate gyros, if we observe from the Coriolis law that

$$\dot{\mu} = (\omega_x + j\omega_y) - j\Omega\mu \tag{5.15}$$

Since the two methods are equivalent, even when we consider flexure, we shall assume henceforth that rate is derived from the star-tracker angle μ. Because of the μ term in Eq. (5.13), it is only necessary to employ $\dot{\mu}$ feedback to obtain asymptotic stability.

The a_n's can be determined by observing that the body-mounted star tracker senses twist, β, and $\partial z/R\partial\gamma$ which is the slope of the deflection, as well as sensing the actual difference of the spin axis from the inertial reference. Thus

$$a_{xx_n}(\gamma) = \frac{n \cos n\gamma}{R} \cos\gamma - (B_n \sin n\gamma) \sin\gamma \tag{5.16}$$

$$a_{xy_n}(\gamma) = -\frac{n \sin n\gamma}{R} \cos\gamma - (B_n \cos n\gamma) \sin\gamma \tag{5.17}$$

$$a_{yx_n}(\gamma') = \frac{n \cos n\gamma'}{R} \sin \gamma' + (B_n \sin n\gamma') \cos \gamma' \qquad (5.18)$$

$$a_{yy_n}(\gamma') = -\frac{n \sin n\gamma'}{R} \sin \gamma' + (B_n \cos n\gamma') \cos \gamma' \qquad (5.19)$$

where γ is the location of the x-axis sensor and γ' is the location of the y-axis sensor. The x axis corresponds to the sine modes; the y axis to the cosine modes.

The u_n's are a function of the locations at which the control forces or moments are placed. If we use control forces, the standard approach is to use two orthogonal pairs, one for each axis, as shown in Fig. 8.

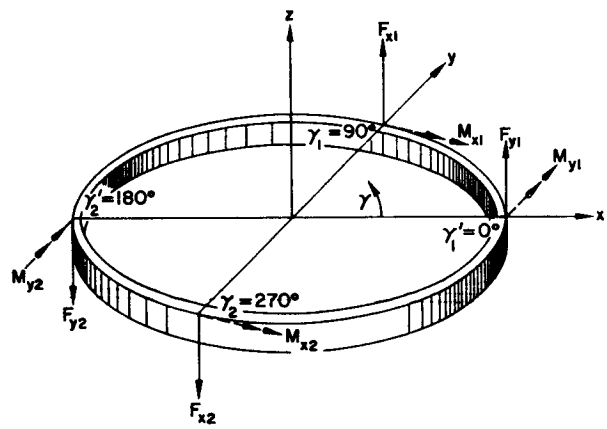

35571

FIG. 8. LOCATION OF SENSORS AND CONTROL FORCES OR MOMENTS.

Using Eqs. (5.6), (5.7), and (5.13) in Eq. (2.9), we find that

$$u_{xx_n} = \begin{cases} R(-1)^{(n-1)/2} & (n \text{ odd}, \quad n > 2) \\ 0 & (n \text{ even}) \end{cases} \qquad (5.20)$$

$$u_{xy_n} = \begin{cases} 0 & (n \text{ odd}) \\ 0 & (n \text{ even}) \end{cases} \qquad (5.21)$$

$$u_{yx_n} = \begin{cases} 0 & (n \text{ odd}) \\ R\Delta F_x(-1)^{n/2} & (n \text{ even}) \end{cases} \qquad (5.22)$$

$$u_{yy_n} = \begin{cases} -R & (n \text{ odd}, \quad n > 2) \\ -R\Delta F_y & (n \text{ even}) \end{cases} \tag{5.23}$$

where we have defined the fractional force in imbalances ΔF_y and ΔF_x as:

$$\Delta F_y \triangleq \frac{F_{y_1} - F_{y_2}}{F_{y_1} + F_{y_2}} \tag{5.24}$$

$$\Delta F_x \triangleq \frac{F_{x_1} - F_{x_2}}{F_{x_1} + F_{x_2}} \tag{5.25}$$

We find that we have the same equations for the u_n's if, as shown in Fig. 8, we employ control moments (assuming that their gyroscopic coupling is negligible) rather than control forces at the same locations and if we replace the fractional force imbalances, ΔF_y and ΔF_x, by the fractional moment imbalances

$$\Delta M_y \triangleq \frac{M_{y_1} - M_{y_2}}{M_{y_1} + M_{y_2}} \tag{5.26}$$

$$\Delta M_x \triangleq \frac{M_{x_1} - M_{x_2}}{M_{x_1} + M_{x_2}} \tag{5.27}$$

Observe from Eqs. (5.20) - (5.23) that for balanced forces (or moments) only the odd modes $(n = 3, 5, 7, \ldots)$ are excited.

If we use only a single control moment for each axis, and these are placed together at a single location (e.g., a single control moment device), so that one produces a moment about a radial axis (x) and the other about a tangential axis, then all the modes are excited and the associated u_n's are:

$$u_{xx_n} = nR \tag{5.28}$$

$$u_{xy_n} = 0 \tag{5.29}$$

$$u_{yx_n} = 0 \tag{5.30}$$

$$u_{yy_n} = -R \tag{5.31}$$

It is apparent from the above that the control axes are not coupled via the control actuators.

In the next two chapters, we utilize the formulas and relations, developed in these last three chapters, to determine the effects of various placements and conditions of the control forces and sensors on the excitation and stability of the spinning space station.

VI. STABILITY OF THE FIRST EXCITED FLEXIBLE MODE OF CONTROLLED SPINNING SPACE STATION FOR BALANCED CONTROL FORCES (OR MOMENTS)

In this chapter we investigate the stability of the toroidal station as a function of sensor location, considering only the first excited flexible mode $(n = 3)$, for the case of balanced control forces. The basic parameter relationships required for the study are derived in Section A. In Section B the root-locus approach is explored for our case, and in Section C numerical values for the sensor location parameters are obtained for our space station example. In Section D we establish stability criteria based on the modal root expansion approach. The system stability is explored in Section E and F using a single sensor and two sensors respectively. The final two sections contain a summary of the important results obtained from our analysis and a comparison of the results obtained from the formulas with computer solutions.

A. BASIC PARAMETER RELATIONSHIPS

As indicated in the previous chapters, the first excited mode is usually the most critical when considering stability because of the reduction of the effective gains, k' and k, with increasing mode number. For balanced control forces (or moments), the lowest excited bending mode is $n = 3$. We shall initially investigate the stability of this mode for $K_p = 0$, since (as indicated in the last chapter) only k' is required for asymptotic stability for the rigid mode.

Using Eqs. (5.20) - (5.23) in Eqs. (4.15) - (4.18), we obtain for balanced control forces,

$$\alpha_{xx} = -\frac{R}{2} a_{xx_n} \left[-(-1)^{(n-1)/2}\right] \tag{6.1}$$

$$\alpha_{xy} = -\frac{R}{2} a_{xy_n} \tag{6.2}$$

$$\alpha_{yx} = -\frac{R}{2} a_{yx_n} \left[-(-1)^{(n-1)/2}\right] \tag{6.3}$$

$$\alpha_{yy} = -\frac{R}{2} a_{yy_n} \tag{6.4}$$

Substituting Eqs. (6.1) - (6.4) into Eqs. (4.28) and (4.29) we obtain

$$c = \frac{R}{4}\left\{a_{xx_n}\left[-(-1)^{(n-1)/2}\right] + a_{yy_n}\right\} \triangleq \frac{R}{4}\alpha_{2_n} \tag{6.5}$$

$$d = \frac{R}{4}\sqrt{\alpha_{2_n}^2 + \left[-(-1)^{(n-1)/2}\right]4\alpha_{1_n}^2} \triangleq \frac{R}{4}\alpha_{5_n} \tag{6.6}$$

where

$$\alpha_{1_n}^2 \triangleq a_{xy_n} a_{yx_n} - a_{xx_n} a_{yy_n} \tag{6.7}$$

For $n = 3$ these reduce to

$$c = \frac{R}{4}\left[a_{xx_3} + a_{yy_3}\right] = \frac{R}{4}\alpha_{23} \tag{6.8}$$

$$d = \frac{R}{4}\sqrt{\alpha_{23}^2 + 4\alpha_{13}^2} = \frac{R}{4}\alpha_{53} \tag{6.9}$$

in which the α's are simply a function of the sensor locations.

B. ROOT LOCUS APPROACH

Considering just the first excited flexible mode $(n = 3)$, we can write Eq. (4.13) in the form

$$G_{\pm}(s) = \frac{E_3 + 2E_o(-c \pm d)}{E_o E_3} \tag{6.10}$$

Defining

$$\alpha_{6_n} \triangleq -\frac{R}{2}\left(\alpha_{5_n} + \alpha_{2_n}\right) \tag{6.11}$$

$$\alpha_{7_n} \triangleq \frac{R}{2}\left(\alpha_{5_n} - \alpha_{2_n}\right) \tag{6.12}$$

Eq. (6.10) can be written as

$$G_+(s) = \frac{E_3 + \alpha_{63}E_o}{E_o E_3} \tag{6.13}$$

$$G_-(s) = \frac{E_3 + \alpha_{73}E_o}{E_o E_3} \tag{6.14}$$

The factored characteristic equation, Eq. (4.12), can be written for $K_p = 0$ as

$$[1 + K_v s G_+(s)]\,[1 + K_v s G_-(s)] = 0 \tag{6.15}$$

As both portions have the same form, it is only necessary to treat the + portion, if we note that the - portion is obtained simply by replacing α_{63} by α_{73}.

Using the expressions for E_o and E_3 from Eqs. (4.1) and (4.2) in Eq. (6.13), we obtain

$$K_v s G_+(s) = K_v s \left[\frac{s^2(1 + \alpha_{63}) + 2\zeta_3 p_3 s + \left(p_3^2 + \alpha_{63}\Omega^2\right)}{(s^2 + \Omega^2)\left(s^2 + 2\zeta_3 p_3 s + p_3^2\right)}\right] \tag{6.16}$$

Dividing numerator and denominator by p_3^4 and defining

$$k'_+ = \frac{K_v}{p_3}(1 + \alpha_{63}) \tag{6.17}$$

$$\zeta_{3_+} = \frac{\zeta_3}{1 + \alpha_{63}} \tag{6.18}$$

$$\Omega^2_{3_+} \triangleq \frac{1 + \alpha_{63} r_o^2}{1 + \alpha_{63}} \tag{6.19}$$

we can write Eq. (6.16) as

$$K_v s G_+(s) = k'_+ \tilde{G}_+(\tilde{s}) \tag{6.20}$$

where

$$\tilde{G}_+(\tilde{s}) \triangleq \frac{\tilde{s}\left(\tilde{s}^2 + 2\zeta_{3_+}\tilde{s} + \Omega^2_{3_+}\right)}{\left(\tilde{s}^2 + r_o^2\right)\left(\tilde{s}^2 + 2\zeta_3\tilde{s} + 1\right)} \tag{6.21}$$

and where

$$r_o^2 \triangleq \left(\frac{\Omega}{p_3}\right)^2 \ll 1 \tag{6.22}$$

$$\tilde{s} \triangleq \frac{s}{p_3} \tag{6.23}$$

For

$$\zeta_3^2 \ll 1 \tag{6.24}$$

Eq. (6.21) can be written (for α_{53} real) in factored form as

$$\tilde{G}_+(\tilde{s}) = \frac{\tilde{s}\left[\tilde{s} - \left(-\zeta_{3_+} + j|\Omega_{3_+}|\right)\right]\left[\tilde{s} - \left(-\zeta_{3_+} - j|\Omega_{3_+}|\right)\right]}{(\tilde{s} - jr_o)(\tilde{s} + jr_o)[\tilde{s} - (-\zeta_3 + j)][\tilde{s} - (-\zeta_3 - j)]} \tag{6.25}$$

Using Eq. (6.25), we can determine stability of the system from the roots of

$$1 + k'_+ \tilde{G}_+(\tilde{s}) = 0 \tag{6.26}$$

and

$$1 + k'_- \tilde{G}_-(\tilde{s}) = 0 \tag{6.27}$$

which we obtain from Eq. (6.26) by replacing α_{63} by α_{73}.

Typical root loci for α_{53} real are given in Figs. 9-11. These loci have the expected feature that stability is determined by the location of the flexural-mode zeros.

It will be observed from Eq. (6.25), that for Ω_{3_+} complex (i.e., α_{53} imaginary), the zeros are no longer symmetric about the real axis, and we no longer have 0° or 180° root loci. For these cases the form

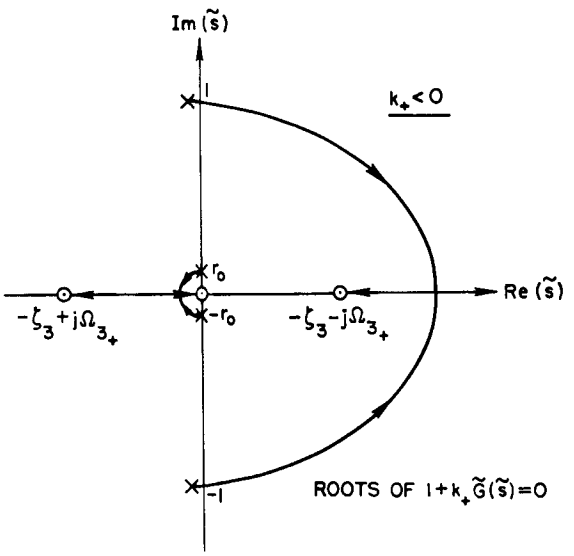

35572

FIG. 9. TYPICAL ROOT LOCUS FOR $\left(-1/r_o^2 < \alpha_{63} < -1\right) \equiv \left(0 > \Omega_{3_+}^2\right)$.

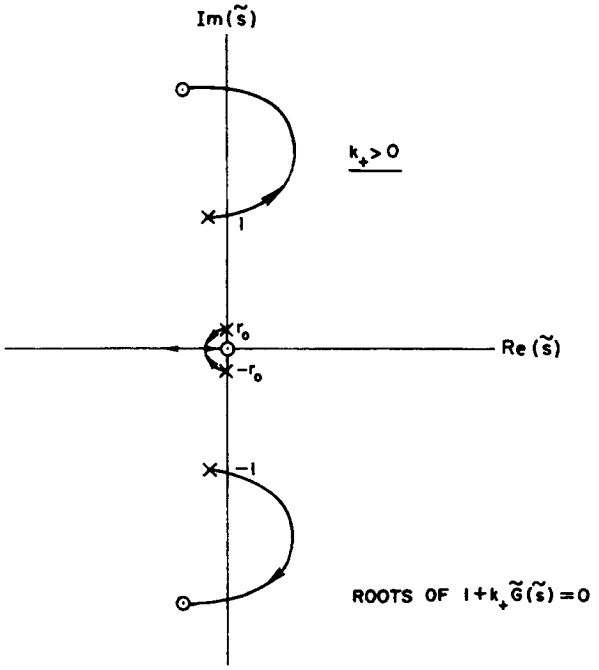

35573

FIG. 10. TYPICAL ROOT LOCUS FOR $\left(-1 < \alpha_{63} < 0\right) \equiv \left(\infty > \Omega^2_{3_+} > 1\right)$.

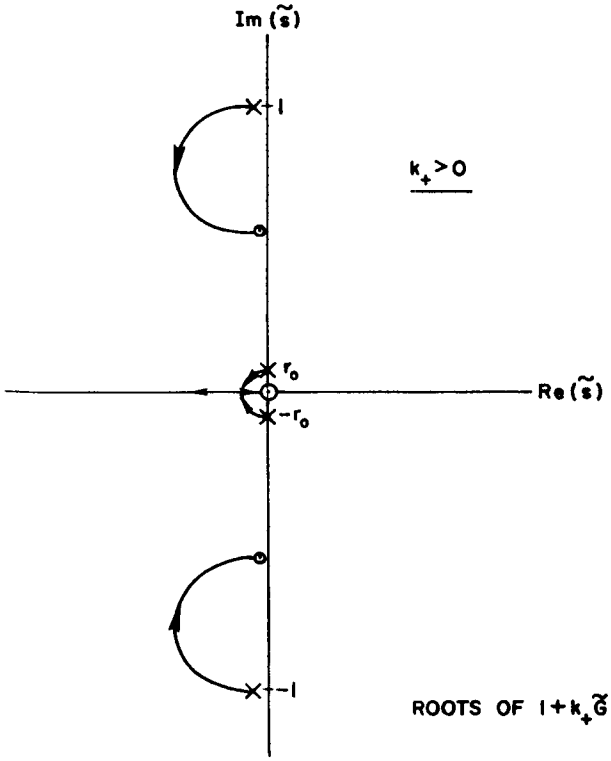

35574

FIG. 11. TYPICAL ROOT LOCUS FOR $\left(0 < \alpha_{63} \lesssim 9\right) \equiv \left(1 > \Omega^2_{3_+} \gtrsim 0.1\right)$.

of the locus is dependent on the values of α_{23} and α_{53}. (An example of a 239° root locus plot is given in Fig. 15 on page 67.) The - characteristic equation would yield the conjugate-complex root locus, which is the image of the + characteristic equation about the real axis.

Plotting the loci for various values of the parameters and finding the roots for specific gains by the root locus technique is tedious and not too illuminating. Having seen the basic form that the loci take, we find it more instructive and far simpler to turn to the root expansion formulas. However, specific cases will be illustrated by root locus sketches.

C. VALUES OF THE PARAMETERS

Employing trigonometry, we can also write Eqs. (5.16) - (5.19) for the sensor coupling parameters a_n as

$$2a_{xx_n}(\gamma) = \left(\frac{n}{R} - B_n\right) \cos \gamma(n-1) + \left(\frac{n}{R} + B_n\right) \cos \gamma(n+1) \qquad (6.28)$$

$$2a_{xy_n}(\gamma) = -\left(\frac{n}{R} - B_n\right) \sin \gamma(n-1) - \left(\frac{n}{R} + B_n\right) \sin \gamma(n+1) \qquad (6.29)$$

$$2a_{yx_n}(\gamma') = -\left(\frac{n}{R} - B_n\right) \sin \gamma'(n-1) + \left(\frac{n}{R} + B_n\right) \sin \gamma'(n+1) \qquad (6.30)$$

$$2a_{yy_n}(\gamma') = -\left(\frac{n}{R} - B_n\right) \cos \gamma'(n-1) + \left(\frac{n}{R} + B_n\right) \cos \gamma'(n+1) \qquad (6.31)$$

where γ is the location of the x-axis sensor and γ' is the location of the y-axis sensor. As an indication of the magnitude of the coefficients, we can consider a symmetric cross section of isotropic material for which we have, from Eq. (5.9),

$$B_n = -\frac{n}{R}\left[\frac{n(2+\sigma)}{1+\sigma+n^2}\right] \tag{6.32}$$

Thus, for $n = 3$ and $\sigma = 0.3$,

$$B_3 \approx -\frac{2}{R} \tag{6.33}$$

so that

$$\left(\frac{3}{R} - B_3\right) \approx \frac{5}{R} \tag{6.34}$$

$$\left(\frac{3}{R} + B_3\right) \approx \frac{1}{R} \tag{6.35}$$

D. STABILITY CRITERIA BASED ON THE MODAL ROOT EXPANSION APPROACH

For large gains the stability criteria neglecting structural damping are given by Eqs. (4.36) and (4.37) as

$$c < -d \qquad (d \text{ real}) \tag{6.36}$$

$$c < -\frac{k'}{1 - r_o^2}|d| \qquad (d \text{ imaginary}) \tag{6.37}$$

Using Eqs. (6.8), (6.9), and (6.22) reduces the above, for our case, to

$$\alpha_{23} < -\alpha_{53} \qquad (\alpha_{53} \text{ real}) \tag{6.38}$$

$$\alpha_{23} < -k'|\alpha_{53}| \qquad (\alpha_{53} \text{ imaginary}) \tag{6.39}$$

By observing from Figs. 9 and 10 that, for α_{53} real and ζ_3 small, instability occurs at small values of K_v, an estimate of the minimum

structural damping required for marginal stability ($\epsilon = 0$) can be obtained, for d real, from Eqs. (4.20), (4.29), and (4.30) as

$$\zeta_i = \frac{k'}{2}\left\{-(\alpha_{xx} + \alpha_{yy}) + \left[(\alpha_{xx} - \alpha_{yy})^2 + 4\alpha_{xy}\alpha_{yx}\right]^{1/2}\right\} \tag{6.40}$$

or

$$\zeta_i = k'(c + d) \qquad (d \text{ real}) \tag{6.41}$$

Using Eqs. (6.8) and (6.9) in Eq. (6.41) yields

$$\zeta_3 = \frac{k'R}{4}(\alpha_{23} + \alpha_{53}) \qquad (\alpha_{53} \text{ real}) \tag{6.42}$$

The minimum structural damping for stability, for α_{53} imaginary, cannot be written as simply as Eq. (6.42) because the imaginary-axis crossing may occur at large gains, even for ζ_i small. An estimate of the minimum ζ_i required for this case can be obtained from Eq. (4.37) using the criterion that

$$\zeta_i = \sup\{\zeta_i(\epsilon_+ = 0),\ \zeta_i(\epsilon_- = 0)\} \tag{6.43}$$

Thus, for our case, the minimum structural damping for marginal stability is given by

$$\zeta_3 = \sup\left\{\frac{\frac{R}{4}[k'(\alpha_{23} \mp k'|\alpha_{53}|)]}{1 + k'\left[\mp\frac{R}{4}|\alpha_{53}| + k'\left(1 - \frac{R}{4}\alpha_{23}\right)\right]}\right\} \qquad \begin{matrix}(\alpha_{53} \text{ imaginary}) \\ K_p = 0\end{matrix} \tag{6.44}$$

These expressions can also be written in terms of the rigid-mode damping ratio with control if we observe from Eqs. (2.7), (2.8), and (3.4) that

$$k' = \frac{K_v}{p_i} = \frac{2\zeta_{co}\left(p_o^2 + K_p\right)^{1/2}}{p_i} \tag{6.45}$$

so that, for our case $(K_p = 0)$,

$$k' = 2r_o\zeta_{co} \tag{6.46}$$

E. STABILITY WITH A SINGLE SENSOR

With the force (or moment) locations fixed, the system stability is dependent only on the sensor locations, as these determine the values of α_{23} and α_{53}. For a single sensor package $(\gamma' = \gamma)$, using Eqs. (6.5) (6.6), and (6.28) - (6.31), we find that

$$\alpha_{13}^2 = -\frac{3}{R} B_3 \tag{6.47}$$

$$\alpha_{23} = \left(\frac{3}{R} + B_3\right) \cos 4\gamma \tag{6.48}$$

Substituting for B_3 from Eq. (6.33) yields

$$\alpha_{13}^2 \approx \frac{6}{R^2} \tag{6.49}$$

$$\alpha_{23} \approx \frac{\cos 4\gamma}{R} \tag{6.50}$$

Using this in Eq. (6.9), we have

$$\alpha_{53} \approx \frac{1}{R} (\cos^2 4\gamma + 24)^{1/2} \approx \frac{5}{R} \tag{6.51}$$

As Eq. (6.38) can never be satisfied, we can never have stability without structural damping for a system employing a single sensor package.

Substitution of Eqs. (6.46), (6.50), and (6.51) in Eq. (6.42) gives the minimum structural damping for stability as

$$\zeta_3 = \frac{r_o\zeta_{co}}{2} [\cos 4\gamma + 5] \tag{6.52}$$

Using Eq (5.10),

$$0.016 < \frac{\Omega}{p_3} \triangleq r_o < 0.11 \tag{6.53}$$

Therefore ζ_3 required for marginal stability is roughly in the range

$$0.03\zeta_{co} < \zeta_3 < 0.3\zeta_{co} \tag{6.54}$$

Thus, for ζ_{co} in the desirable range of 0.7 - 0.8, referring to Eq. (5.11), an unusually high structural damping would be necessary to achieve a satisfactory level of stability. Consequently, a system using a single-sensor package would require a lower gain than would be desirable for the rigid system. Therefore, we shall turn our attention to separate locations for the μ_x and μ_y sensors. However, before we do, it is interesting to return to the root locus approach.

Using Eqs. (6.50) and (6.51) in Eqs. (6.11) and (6.12) we have

$$\alpha_{63} \approx -2.5 - \frac{\cos 4\gamma}{2} \tag{6.55}$$

$$\alpha_{73} \approx +2.5 - \frac{\cos 4\gamma}{2} \tag{6.56}$$

Thus the + characteristic equation is of the form shown in Fig. 9, while the - characteristic equation is of the form shown in Fig. 11.

F. TWO SENSOR PACKAGES

1. Sensors Symmetric about $\gamma = \pm 45°$

From Eq. (6.52) we observe that the minimum damping required for stability for a single sensor package occurs for

$$\gamma = 45° + m\ 90° \qquad (m \text{ an integer}) \tag{6.57}$$

Thus we might suspect that in using two sensors we should try to place them symmetrically about these locations. Further, since the actuators are 90° apart we would suspect that the sensors should be also. For generality we shall consider

$$\gamma' = \pm 90^\circ - \gamma \tag{6.58}$$

so that the sensors are symmetric about the +45° or the -45° axis.

Using Eq. (6.58) in the relations of Section C, and using Eqs. (6.7), (6.8), and (6.9) yields

$$\alpha_{23} = 2a_{xx_3} \tag{6.59}$$

$$\alpha_{53} = 2\left|a_{xy_3}\right| \tag{6.60}$$

Using Eqs. (6.28), (6.29), (6.34), and (6.35) in Eqs. (6.59) and (6.60) we have

$$R\alpha_{23} \approx 5 \cos 2\gamma + \cos 4\gamma \tag{6.61}$$

$$R\alpha_{53} \approx \left|5 \sin 2\gamma + \sin 4\gamma\right| \tag{6.62}$$

Equations (6.61) and (6.62) are plotted in Fig. 12. We observe that there are large stable regions of approximately ±28° to either side of $\gamma = \pm 90^\circ$ that satisfy the criterion of Eq. (6.38). At these locations we observe from Eqs. (6.11) and (6.12) that

$$\alpha_{63} = \alpha_{73} \approx 2 \qquad (\gamma = \pm 90^\circ) \tag{6.63}$$

yielding stable root loci of the form shown in Fig. 11. The boundary of the region corresponds to

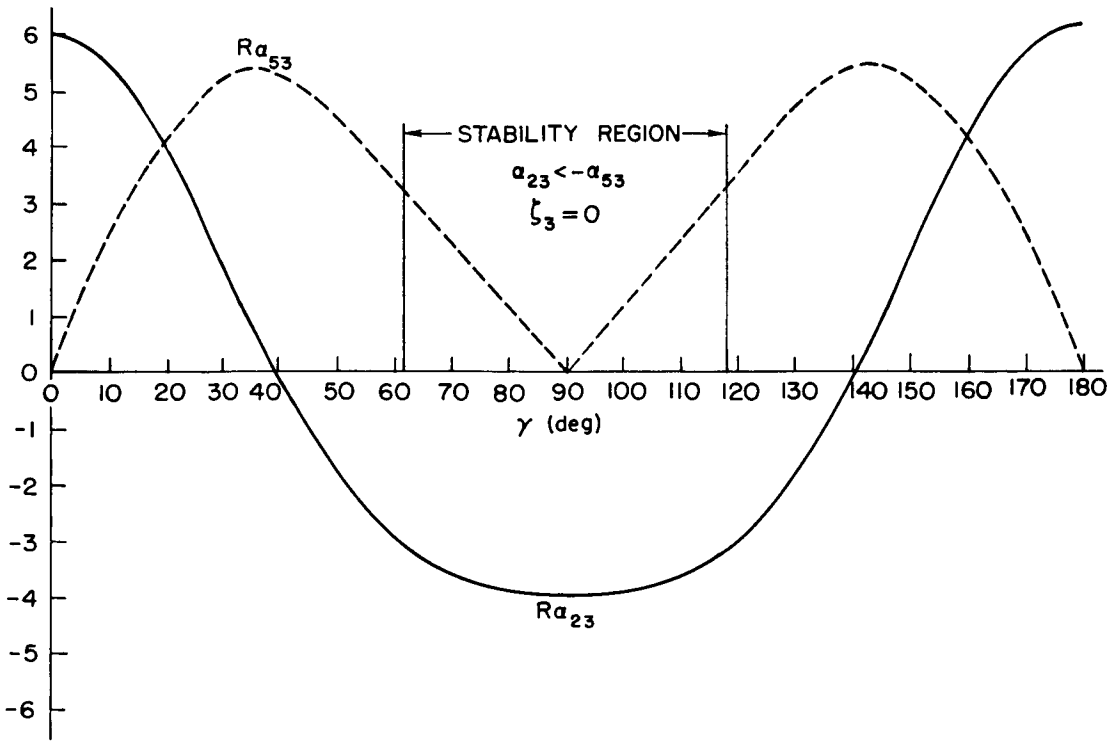

35575

FIG. 12. PARAMETERS $R\alpha_{23}$ AND $R\alpha_{53}$ AS A FUNCTION OF γ FOR $\gamma' = \pm 90^\circ - \gamma$.

$$\alpha_{63} = 0 \tag{6.64}$$

$$\alpha_{73} \approx 3 \tag{6.65}$$

which is the crossover point between (1) the case that both of the factored-characteristic-equation root loci are of the form of Fig. 11, and (2) the case where the + characteristic-equation root locus takes the form of Fig. 10.

The locations $(\gamma \pm 90^\circ)$ yielding both loci identical are equivalent to placing the μ_x sensor at either of the two points of control* of μ_x, and the μ_y sensor at $\gamma' = 0^\circ, 180^\circ$, either of the two points of control of μ_y.

*Points where the control forces are applied.

At these locations we observe from Eqs. (6.28) - (6.31) that for n odd

$$a_{xx_n}(\gamma) = -B_n(-1)^{(n-1)/2} \tag{6.66}$$

$$a_{xy_n}(\gamma) = 0 \tag{6.67}$$

$$a_{yx_n}(\gamma') = 0 \tag{6.68}$$

$$a_{yy_n}(\gamma') = B_n \tag{6.69}$$

so that for balanced control forces the two control axes of the system are uncoupled, and the only flexural motion picked up by the sensors is twist.

2. Other Sensor Locations

To explore the regions of stability further, we consider several additional cases, $\gamma' = -\gamma$ (symmetry about the origin), $\gamma' = 180° - \gamma$ (symmetry about 90°), and $\gamma' = \gamma \pm m\ 90°$ (the two sensors 90° or 180° apart). Proceeding as in Section 1, the system stability for these additional sensor locations has been determined, using the stability criteria of Section D, and is summarized as follows:

a. Sensors kept 180° apart have the same effect as a single sensor

b. Sensors 90° apart ($\gamma' = \gamma \pm 90°$) yield

$$R\alpha_{23} = 5 \cos 2\gamma + \cos 4\gamma \tag{6.70}$$

$$R\alpha_{53} = j|5 \sin 2\gamma + \sin 4\gamma| \tag{6.71}$$

These equations are identical to Eqs. (6.61) and (6.62) for the sensors symmetric about the diagonals, except that α_{53} is imaginary. Therefore an indication of the stability can be obtained from Fig. 12 as follows:

The equation for stability in this case is Eq. (6.39) rather than Eq. (6.38). Thus the stability boundary is again centered about

$$\gamma = 90°,\ 270° \tag{6.72}$$

and will stretch to somewhat less than 50° on either side, depending upon k'. For example, using Eq. (6.39), the stability boundary will stretch 45° to either side for $k' = 0.2$, and to nearly 50° for a smaller k'.

For small k's, the roots of the characteristic equation are given by Eqs. (4.22) and (4.23) as

$$\epsilon = k'c - \zeta_i \tag{6.73}$$

$$\delta = \pm k'|d| \tag{6.74}$$

which for our case becomes

$$\epsilon = \frac{k'}{4} R\alpha_{23} - \zeta_3 \tag{6.75}$$

$$\delta = \pm \frac{k'}{4} |R\alpha_{53}| \tag{6.76}$$

The angle of departure ϕ of the upper roots from their poles is given by

$$\phi \cong \tan^{-1}\left(\frac{\pm|R\alpha_{53}|}{R\alpha_{23}}\right) \tag{6.77}$$

Observe from Fig. 12 that as the sensors move away from their axes of control ($\gamma = 90°, 270°$) the root angles of departure from their poles change from their values of -180°, one departing upward, the other downward, until, for the sensors 50° away from their control axes, the root departures are both vertical. For this latter position we observe, from Eqs. (4.34) and (4.35) that for $\zeta_3 = 0$

$$\epsilon = \frac{\mp k'^2|d|}{k'^2 + (1 \mp k'|d|)^2} \tag{6.78}$$

$$\delta = \frac{\pm k'|d|(1 \mp k'|d|)}{k'^2 + (1 \mp k'|d|)^2} \tag{6.79}$$

so that one root takes off initially upward and curves into the right half plane while the other root takes off initially downward and curves into the left half plane.

For these positions of the sensors (50° away from their control axes)

$$d = \frac{R}{4}\alpha_{53} \approx 1.3j \tag{6.80}$$

$$\alpha_{63} = -2.6j = -\alpha_{73} \tag{6.81}$$

The root locus for this case is shown in Fig. 13, the solid line being for the + characteristic equation, the dotted line for the - characteristic equation.

c. Sensors symmetric about the control axes ($\gamma' = m\,180° - \gamma$, m an integer)

For this case and using Eqs. (6.5) - (6.7) we have

$$R\alpha_{23} = \cos 4\gamma \tag{6.82}$$

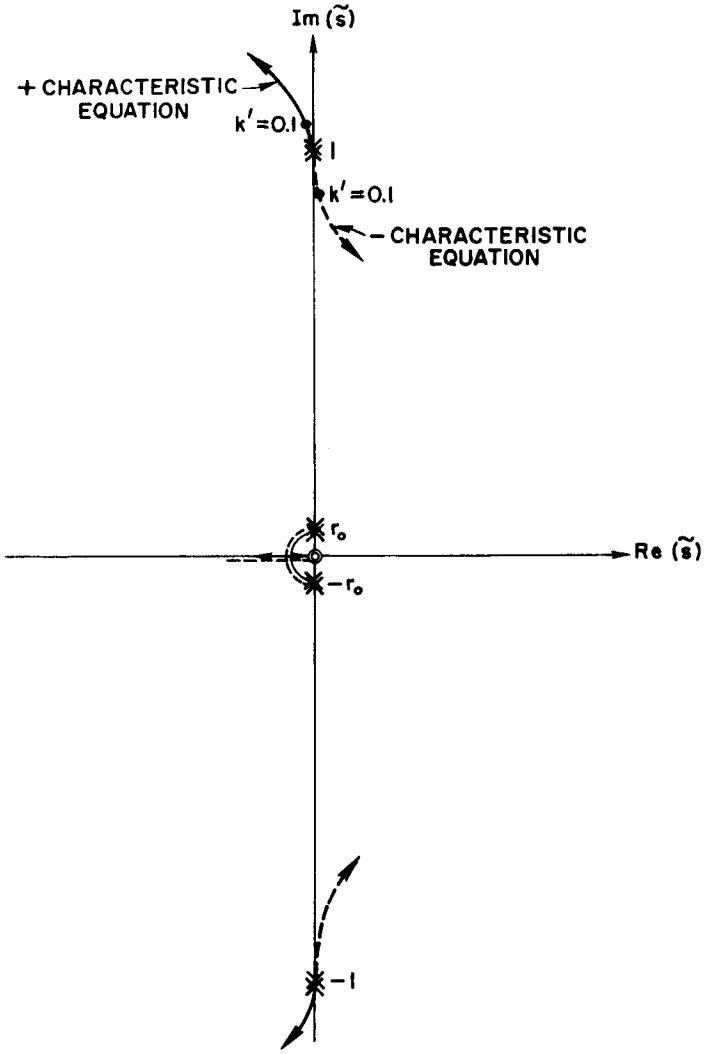

35576

FIG. 13. ROOT LOCUS ON BOUNDARIES OF STABLE REGION, $\gamma' = \gamma \pm 90°$, $\gamma = -50° \pm m\ 180°$.

and

$$R\alpha_{53} = (25 \cos 4\gamma + \sin^2 4\gamma)^{1/2} \qquad (6.83)$$

which are plotted in Fig. 14. Observe that there are regions of stability satisfying Eq. (6.39) centered about

$$\gamma = 45° + m\ 90° \qquad (m \text{ an integer}) \qquad (6.84)$$

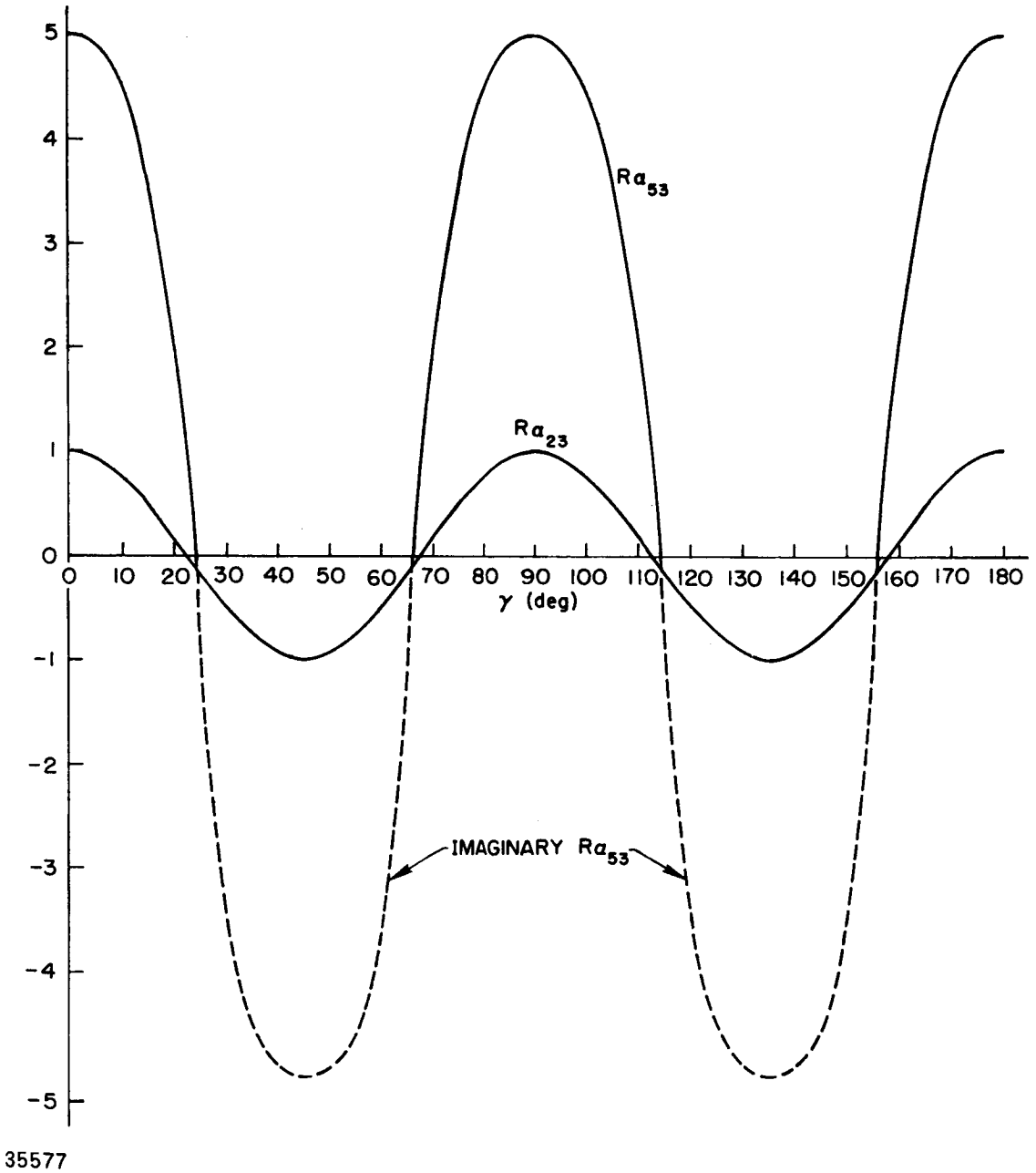

FIG. 14. PARAMETERS $R\alpha_{23}$ AND $R\alpha_{53}$ AS A FUNCTION OF γ FOR $\gamma' = m\,180° - \gamma$.

and extending about 20° to each side for

$$k' \triangleq 2r_o\zeta_{co} < 0.15 \qquad (6.85)$$

From Eq. (6.53), it is apparent that Eq. (6.85) will be satisfied for $\zeta_{co} = 0.7$, for nearly all structural materials; however it is important to determine how well damped the flexural roots are. To do this we observe the angles of initial departure from Eq. (6.77) and note that over nearly the entire stable region these angles are almost vertical, so that the roots will be poorly damped.

In the center of the region [given by Eq. (6.84)], we have

$$\alpha_{63}, \alpha_{73} = -\frac{R}{2}(\alpha_{23} \pm \alpha_{53}) = -\frac{1}{2}(1 \pm j5) \tag{6.86}$$

$$c = -\frac{1}{4} \tag{6.87}$$

$$d = \frac{5}{4} j \tag{6.88}$$

The corresponding root locus is given by Fig. 15 for the + characteristic equation. The loci for the - characteristic equation is simply the complex conjugate of Fig. 15.

Again referring to Fig. 14, there is a very narrow region in the vicinity of

$$\gamma = 45^\circ + m\ 90^\circ \pm 21^\circ \tag{6.89}$$

which satisfies the stability criterion of Eqs. (6.38) and (6.39). These points also have the advantage that since α_{63} and α_{73} are very small, the excitation of the modes by the control system is small and the roots stay essentially at the poles, with their damping being primarily structural damping. However desirable these interesting points may appear initially, they are acutely sensitive to parameter changes such as the sensors being slightly off their design location, or the vehicle being somewhat nonuniform. As these sensor locations are on the borderline of instability, they cannot be recommended and will not be pursued further.

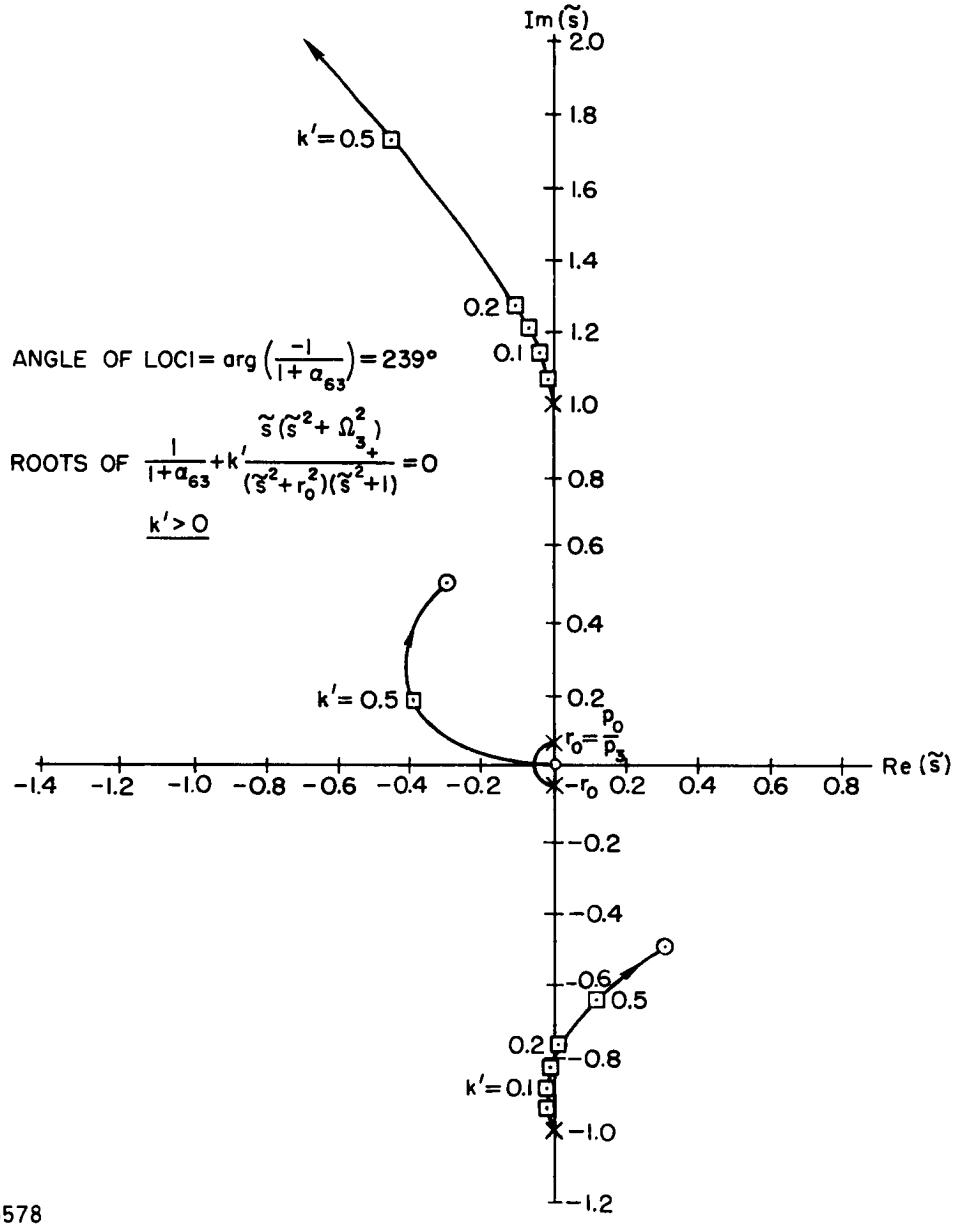

FIG. 15. ROOT LOCUS FOR $\gamma' = m\,180° - \gamma$ (γ ON A DIAGONAL).

G. CONCLUSIONS ON THE EFFECTS OF SENSOR LOCATIONS ON STABILITY

The following conclusions on sensor locations were drawn, for $K_p = 0$ and for orthogonal pairs of control forces (or moments).

1. Single Sensor Package

Without structural damping it is impossible to find a position that will stabilize the third mode (first flexible mode) using a single sensor package.

The minimum third-mode structural damping ratio ζ_3 for marginal stability is roughly in the range

$$0.03\zeta_{co} < \zeta_3 < 0.3\zeta_{co} \tag{6.90}$$

where the low portion of the range is for materials of high structural stiffness. As Eq. (6.90) requires, for $\zeta_{co} \geq 0.7$, higher values of ζ_3 than can reasonably be expected, ζ_{co} would have to be lower than the desirable range of 0.7 to 0.8 to achieve even marginal stability with a single sensor package. Therefore separate sensor locations for each control axis were investigated.

2. Two Sensors without Structural Damping

If the μ_x sensor (the sensor that controls motion about the body-fixed x axis) is placed at $\gamma = 90°$, or 270°, and the μ_y sensor is placed at $\gamma = 0°$, or 180°, the system is uncoupled and stable for all values of gain.

If the sensors are symmetrically placed about the diagonals ($\gamma = \pm 45°$), the regions of stability extend, for any value of gain, approximately 28° to each side of the above locations.

If the sensors are kept 90° apart, the stable region may extend nearly 50° to either side of the above locations, depending on the value of the gain.

If the sensors are placed symmetrically about $\gamma = 0°$ or 90°, there is a stable region of about ±20° width about the locations where the sensors are 90° apart, for rate gains of

$$K_v = 2\Omega\zeta_{co} < 0.15p_3 \tag{6.91}$$

However, this region is poorly damped for all stable values of gain. At the boundaries of this region there are very narrow stable regions for the sensor locations, where the excitation of the third mode by the control system is small and the roots stay essentially at their poles. However, these locations are acutely sensitive to vehicle parameter

changes, and because they border on an unstable region, they cannot be recommended.

Therefore, it is recommended that the μ_x sensor be placed in the vicinity of $\gamma = \pm 90^\circ$ and the μ_y sensor in the vicinity of $\gamma = 0^\circ, 180^\circ$. These locations, for which the control axes decouple, are equivalent to placing each of the sensors at one of its corresponding control forces.

H. COMPARISON OF RESULTS WITH COMPUTER SOLUTIONS

In this study we have formulated an analytical method of attacking the stability problem associated with flexible vehicle control. In this chapter we have applied our simple formulas to determine the stability of the first excited flexible mode of a spinning, toroidal space station whose control axes are coupled due to flexibility. The results obtained using these formulas have been verified using modified root locus techniques. However, as was pointed out earlier, the root locus method cannot be readily applied to the higher modes when we consider coupled control axes, leaving us only with the formulas we have derived for small gains for these modes.

To determine the effects of including the higher modes on the solution for the first excited flexible mode and to obtain an indication of the accuracy of our approximate formulas for finding the roots, we now utilize a digital computer to solve the "complete equations." In Appendix D we have put the complete equations in standard form ("state space" form). This form of the equations is suitable both for finding the system roots by digital computer routines for finding the eigenvalues of a matrix, and for obtaining the real time response by integration. These equations are the complete set of linear equations suitable for small motions, and are applicable to the entire class of flexible vehicle control problems that are considered here. The only inputs required for a particular vehicle are the values of the flexible vehicle force and sensor coupling parameters, u_n and a_n, and the natural frequencies and structural damping.

As the formulas we have been utilizing in this chapter for finding the roots are postulated on the modal natural frequencies being well separated from the rigid-mode natural frequency, compared to the root departures from their poles, we shall choose for our space station example:

$$\frac{p_n}{\Omega} = 2n^2 \qquad (n \geq 2) \tag{6.92}$$

$$\zeta_n = 0.05 \tag{6.93}$$

which, referring to Eqs. (5.10) and (5.11), corresponds to the lower frequency (or stiffness) range for the space station. These values are used in all computer solutions throughout this report. For computational economy, we shall always limit ourselves to the first three excited flexible modes in our calculations.

The formulas we have derived for computing the system roots and the root locus techniques we have used are both most complex when d is imaginary. We shall therefore choose as our example from this chapter the case where the sensors are on the diagonals (relative to the control axes) for which we have drawn the root locus in Fig. 15. The corresponding computer solution (considering three modes, $n = 3, 5, 7$) is shown for the first mode in Fig. 16. Observe that, except for the effect of damping and the fact that the roots of both the + and - characteristic equations are included on the same plot, there is negligible difference between it and Fig. 15 except at large gains where the effects of the presence of the additional two modes become important. In Fig. 17 we present a detailed plot of the first excited mode ($n = 3$) over the K_v range of interest, together with a tabulation of the computer results and those obtained for small k' from formulas (4.22) and (4.23) and for large k' from formulas (4.34) and (4.35). It is seen that there is good agreement between the results obtained by the formulas and the computer results for ζ_{co} as high as one ($k'_o = 2$), with the results obtained from the formulas for large $k's$ being particularly close to the computer results.

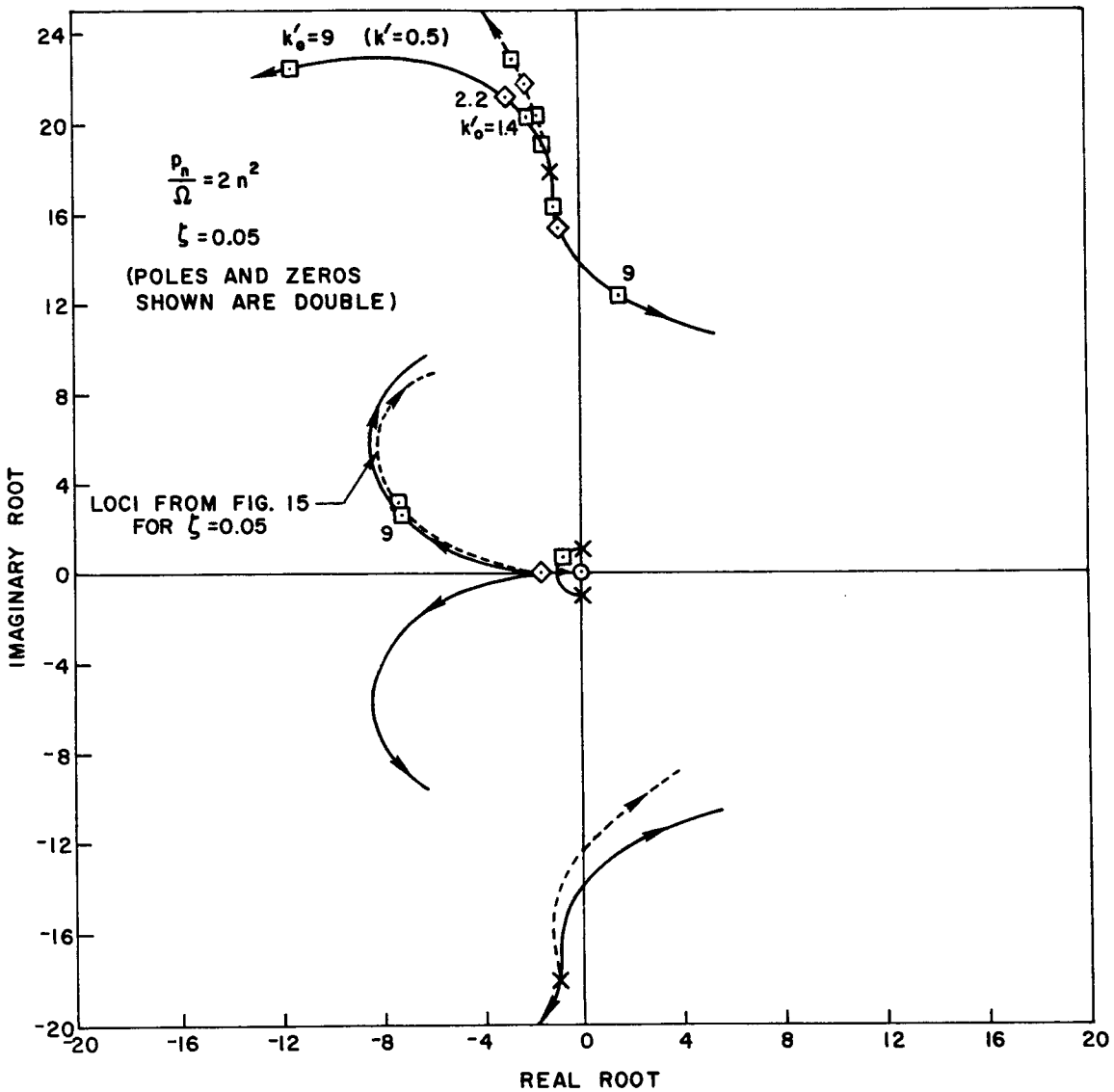

FIG. 16. COMPUTER SOLUTION FOR $\gamma' = -\gamma$, $\gamma = 45°$.

Figure 18 illustrates the roots for all three flexible modes (n = 3, 5, 7). It should be observed for this figure, and for all future root loci for coupled axes, all poles and zeros shown are double. It is particularly apparent from the figure that sensor locations on the diagonals are a poor choice, as the fifth mode goes unstable at a gain of $k'_o = 1.2$ $(\zeta_{co} = 0.6)$.

Figure 19 illustrates the effect of position feedback. This is the same case as Fig. 18 except that $k_o = K_p/\Omega^2$ is equal to 1 rather than

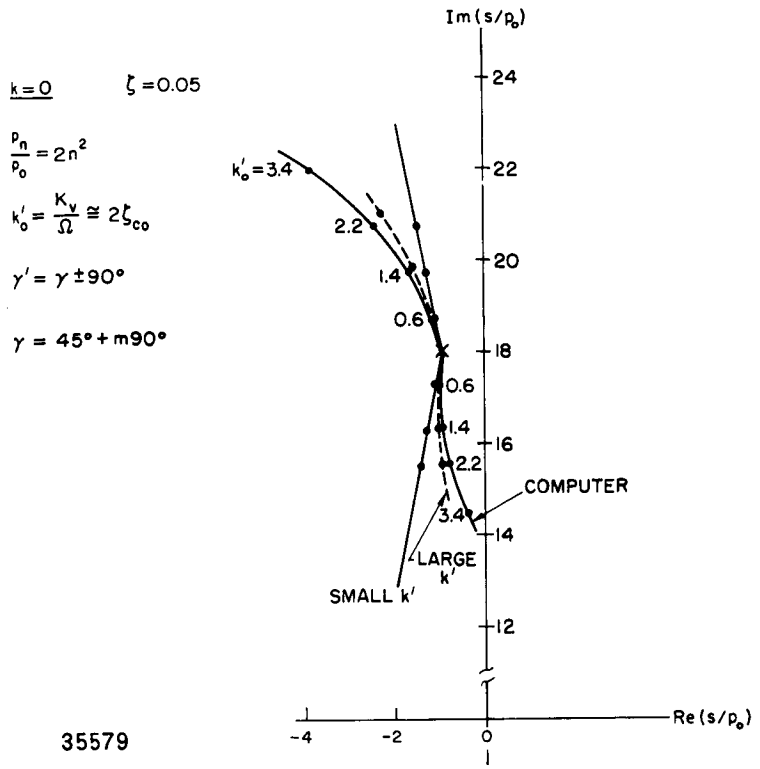

VALUES OF ROOTS

k_o'	+ Characteristic Equation			- Characteristic Equation		
	Computer	Formula		Computer	Formula	
		Small Gain	Large Gain		Small Gain	Large Gain
0	-0.90* 18.00	-0.90 18.00	-0.90 18.00	-0.90 18.00	-0.90 18.00	-0.90 18.00
0.6	-1.14 18.73	-1.05 18.75	-1.13 18.76	-0.97 17.24	-1.05 17.25	-0.98 17.27
1.4	-1.63 19.76	-1.25 19.75	-1.58 19.85	-0.93 16.33	-1.25 16.25	-1.00 16.38
2.2	-2.36 20.75	-1.45 20.75	-2.25 20.97	-0.77 15.51	-1.45 15.25	-0.94 15.59

*Upper values are for Re (s/p_o); lower, for Im (s/p_o).

FIG. 17. COMPARISON OF SOLUTIONS FOR THIRD-MODE ROOTS.

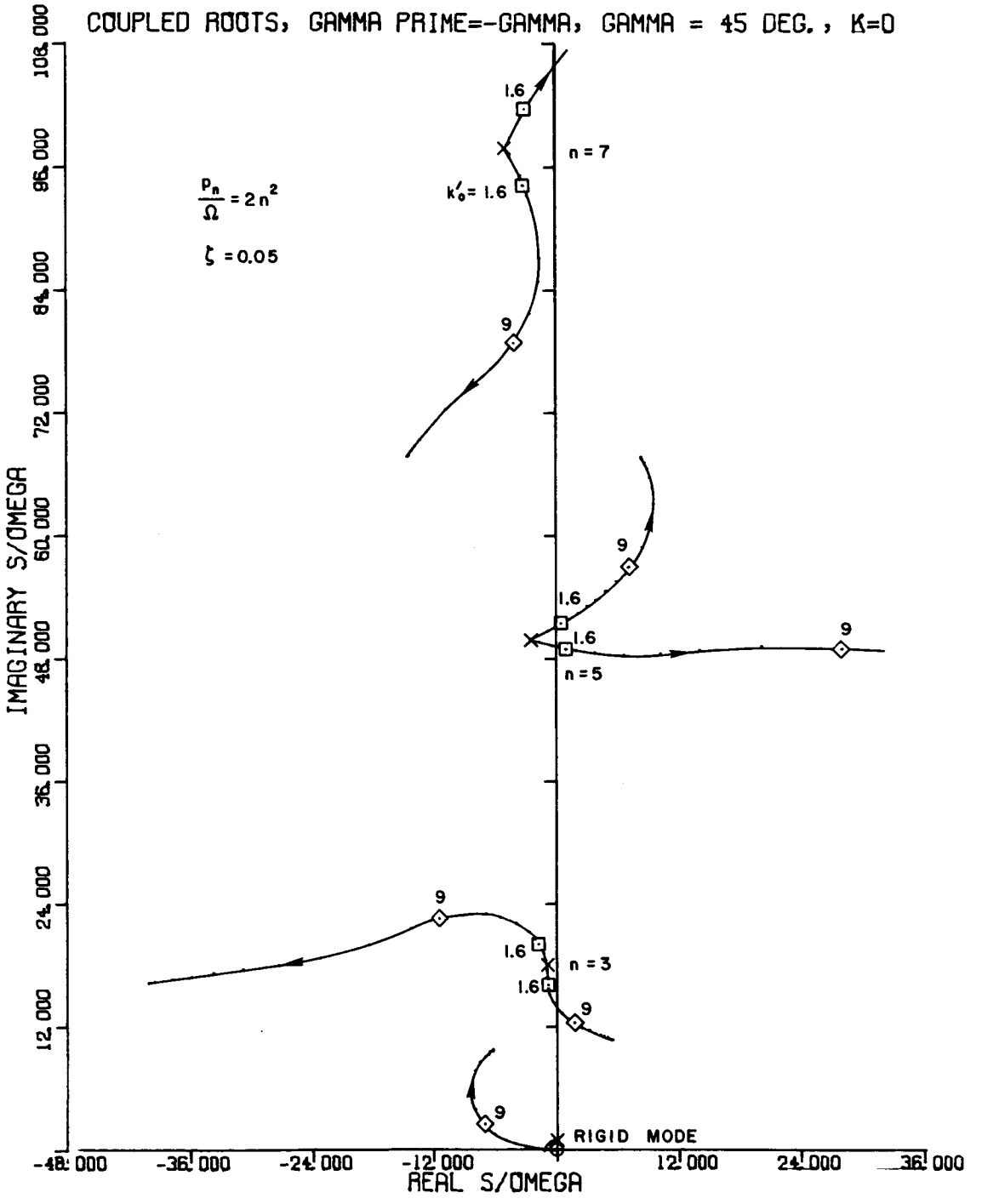

FIG. 18. ROOT LOCUS FOR COUPLED ROOTS, $\gamma' = -\gamma$, $\gamma = 45°$, $k_o = 0$.

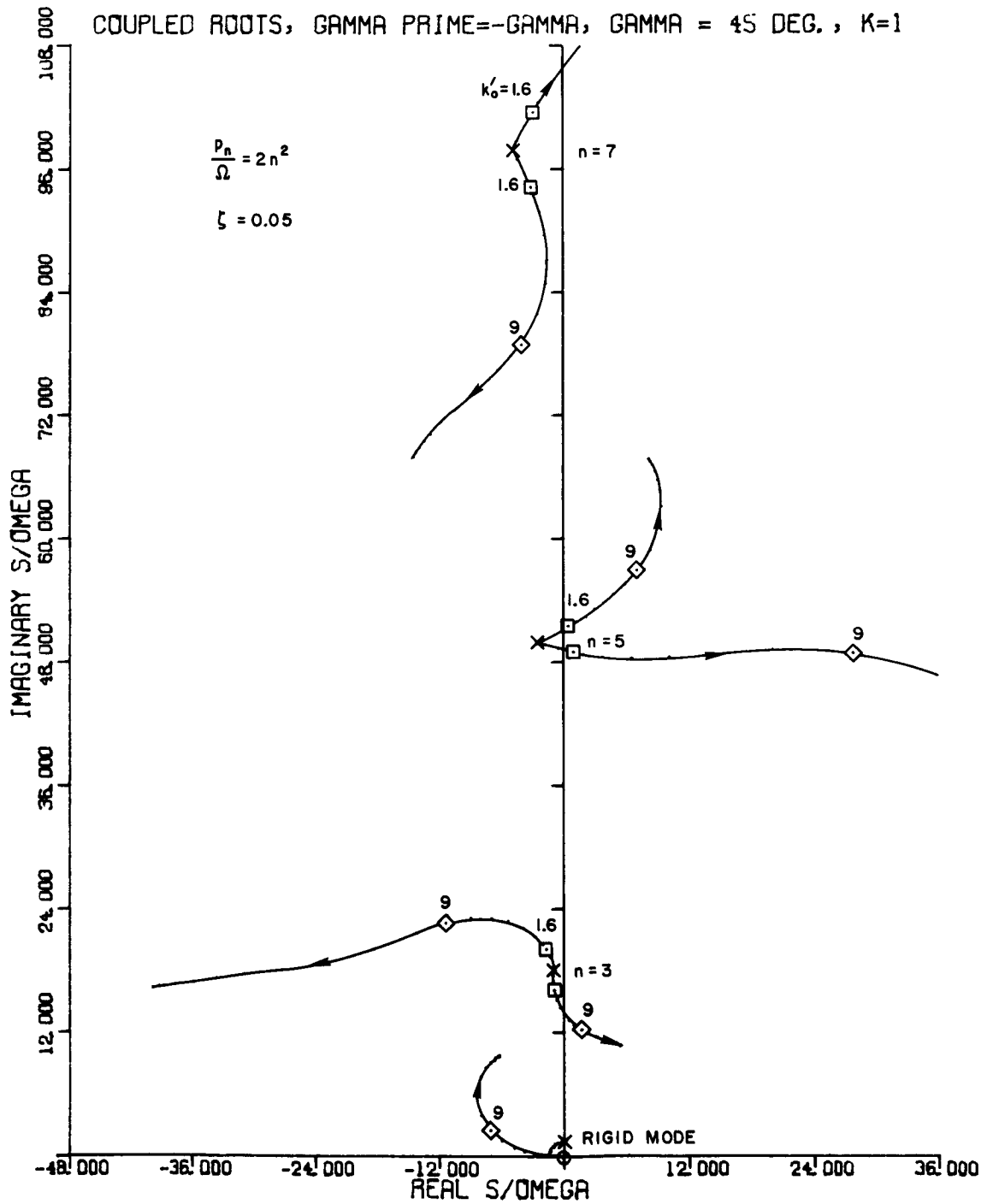

FIG. 19. ROOT LOCUS FOR COUPLED ROOTS, $\gamma' = -\gamma$, $\gamma = 45°$, $k_o = 1$.

0. There has been virtually no change in the roots associated with the flexible modes, even though the rigid-mode effective stiffness has been doubled. Table 1 provides a comparison of the values of the roots obtained from the formulas with those obtained using the computer, for $\zeta_{co} = 0.7 \quad (k'_o = 1.4)$. From the table, the small k' formulas appear adequate for determining the roots of the higher modes.

In the next chapter we explore the stability of the higher modes with the sensors at their recommended locations (at one of their points of control), and examine the sensitivity of system stability to deviations from nominal conditions.

TABLE 1. COMPARISON OF SOLUTIONS FOR THE FLEXURAL MODAL ROOTS

$\zeta_{co} = 0.7 \quad (k'_o = 1.4), \quad k_o = 1$

Solution	Third Mode		Fifth Mode		Seventh Mode	
	Root 1 + Charac. Equation	Root 2 - Charac. Equation	Root 1	Root 2	Root 1	Root 2
Computer	-1.57* 19.79	-1.00 16.32	-0.31 50.99	+0.43 49.06	-3.19 101.12	-3.30 94.64
Small k' Formula	-1.18 19.76	-1.32 16.26	+0.03 50.95	+0.002 48.98	-3.21 101.23	-3.26 94.75
Large k' Formula	-1.51 19.87	-1.06 16.38				

*Upper number represents the real part of the root in the upper half plane. The lower number represents the imaginary part of the root.

VII. STABILITY OF HIGHER MODES OF THE CONTROLLED SPINNING STATION AND THE EFFECTS OF UNBALANCED FORCES OR MOMENTS

In the first two sections of this chapter the stability of the higher modes for orthogonal pairs of balanced control forces is investigated for the sensors at both their optimum location, as determined for the third mode, and in the vicinity of the optimum locations. The effects of unbalanced control forces (or moments), for the case where the forces for the two axes are orthogonal, are determined in Section C. Then in Section D we investigate the stability for the case where the control moments for the two axes are located at the same point. The results obtained from these investigations are summarized in Section E.

A. STABILITY OF THE HIGHER MODES FOR BALANCED CONTROL FORCES WITH THE SENSORS AT THEIR CONTROL POINTS

1. Stability Using the Root-Expansion Approach

It was found in Chapter VI that, for balanced control forces, if the sensors are placed at one of their points of control, then the third mode would be stable and the axes uncoupled. Thus if the μ_x sensor is placed at $\gamma = 90°$ or $270°$, and the μ_y sensor is placed at $\gamma = 0°$ or $180°$, it can be observed from Eqs. (5.20) - (5.23) and (6.66) - (6.69) that the two axes are uncoupled and that, for both axes:

$$a_n u_n = \begin{cases} -RB_n & (n \text{ odd}) \\ 0 & (n \text{ even}) \end{cases} \tag{7.1}$$

where, from Eq. (6.32), for $\sigma = 0.3$ and a symmetric cross section,

$$RB_n = - \frac{2.3}{1 + (1.3/n^2)} \tag{7.2}$$

Using Eq. (7.2) in (7.1)

$$a_n u_n \cong 2.3 \triangleq B' \qquad (n \text{ odd}, \quad n > 2) \tag{7.3}$$

Substituting Eq. (7.3) into Eqs. (3.13) and (3.15) gives, for k' small,

$$\epsilon = -2.3\zeta_{co} r_o \sqrt{1 + \left(K_p/p_o^2\right)} - \zeta_i \tag{7.4}$$

$$\delta = 1.15 \frac{K_p}{p_i^2} \tag{7.5}$$

The roots themselves are given by

$$s = p_i[\epsilon + j(1 + \delta)]$$

$$= \left[-2.3\zeta_{co}\sqrt{p_o^2 + K_p} - \zeta_i p_i\right] + j[p_i + 1.15(K_p/p_i)] \tag{7.6}$$

Observe that the real portion of the roots due to control is approximately the same for all flexible modes. However, for ζ_i the same for all modes, the structural damping dominates for the higher modes.

From Eqs. (3.28) and (3.29), it is apparent that, as $u_i a_i$ is constant with mode number, for small gains the response of the higher modes is small and should cause very little trouble. Further reduction in the response of the flexible modes could be achieved using a rate network in place of rate, as can be observed from Eqs. (3.21) and (3.22).

2. Root Locus Approach

As the two axes are uncoupled for these sensor locations, the characteristic equation has the form of Eq. (2.13), which for $K_p = 0$ can be written as

$$1 + K_v s\, G(s) = 0 \tag{7.7}$$

where

$$G(s) = \sum_{n=0}^{N} \frac{u_n a_n}{E_n} = \sum_{n=0}^{N} \frac{u_n a_n}{s^2 + 2\zeta_n p_n s + p_n^2} \tag{7.8}$$

To find the open-loop zeros is obviously difficult if we consider many modes. Therefore we shall restrict ourselves to two flexible modes. Thus

$$G(s) = \frac{1}{E_o} + \frac{u_3 a_3}{E_3} + \frac{u_5 a_5}{E_5} = \frac{E_3 E_5 + E_o(u_3 a_3 E_5 + u_5 a_5 E_3)}{E_o E_3 E_5} \tag{7.9}$$

Substituting for $u_n a_n$ from Eq. (7.3), neglecting structural damping in the numerator, and observing from Eq. (5.10) that

$$\left(\frac{\Omega}{p_n}\right)^2 \ll 1 \qquad (n \geq 3) \tag{7.10}$$

reduces Eq. (7.9) to

$$G(s) = \frac{s^4(1 + 2B') + s^2(1 + B')\left(p_3^2 + p_5^2\right) + p_3^2 p_5^2}{E_o E_3 E_5} \tag{7.11}$$

Dividing numerator and denominator by p_5^6 and factoring the numerator, we obtain

$$G(s) \approx \frac{\dfrac{(1 + 2B')}{p_5^2}\left[\tilde{s}^2 + \dfrac{r_3^2}{(1 + B')\left(1 + r_3^2\right)}\right]\left[\tilde{s}^2 + \dfrac{(1 + B')}{(1 + 2B')}\left(1 + r_3^2\right) - \dfrac{r_3^2}{(1 + B')\left(1 + r_3^2\right)}\right]}{\left(\tilde{s}^2 + r_o^2\right)\left(\tilde{s}^2 + 2\zeta_3 r_3 \tilde{s} + r_3^2\right)\left(\tilde{s}^2 + 2\zeta_5 \tilde{s} + 1\right)} \tag{7.12}$$

Substituting for B' from Eq. (7.3), and observing from Eq. (5.10) that

$$r_3^2 = \left(\frac{p_3}{p_5}\right)^2 = \left(\frac{3}{5}\right)^4 \tag{7.13}$$

we can write Eq. (7.7) as

$$1 + k'(5.6)\,\frac{\tilde{s}(\tilde{s}^2 + 0.035)\,(\tilde{s}^2 + 0.63)}{\left(\tilde{s}^2 + r_o^2\right)\left(\tilde{s}^2 + 0.72\zeta_3\tilde{s} + 0.13\right)\left(\tilde{s}^2 + 2\zeta_5\tilde{s} + 1\right)} = 0 \tag{7.14}$$

The corresponding root locus is shown in Fig. 20.

3. Computer Results

Figure 21 presents computer results for the same case, indicating good agreement with the root locus approach. Figure 22 provides a comparison between roots computed by formulas (3.12) and (3.13) for small k', formulas (3.28) and (3.29) for large k', and the computer results. Observe the excellent agreement between all methods for values of k'_o up to 1.4 ($\zeta_{co} = 0.7$) and the excellent agreement of the large k' formulas with the computer results for values of k'_o up to 5. Figure 23 indicates the small effects of using a position feedback of $k_o = 1$ (doubling the effective stiffness of the rigid-body mode). Table 2 compares the formula results with the computer results for this case. It indicates that use of the formulas for preliminary design is very satisfactory when the conditions under which these formulas were derived are satisfied. In particular, the simple small k' formulas appear quite adequate as a "first step" design tool, and we shall utilize them in this manner in the rest of this chapter.

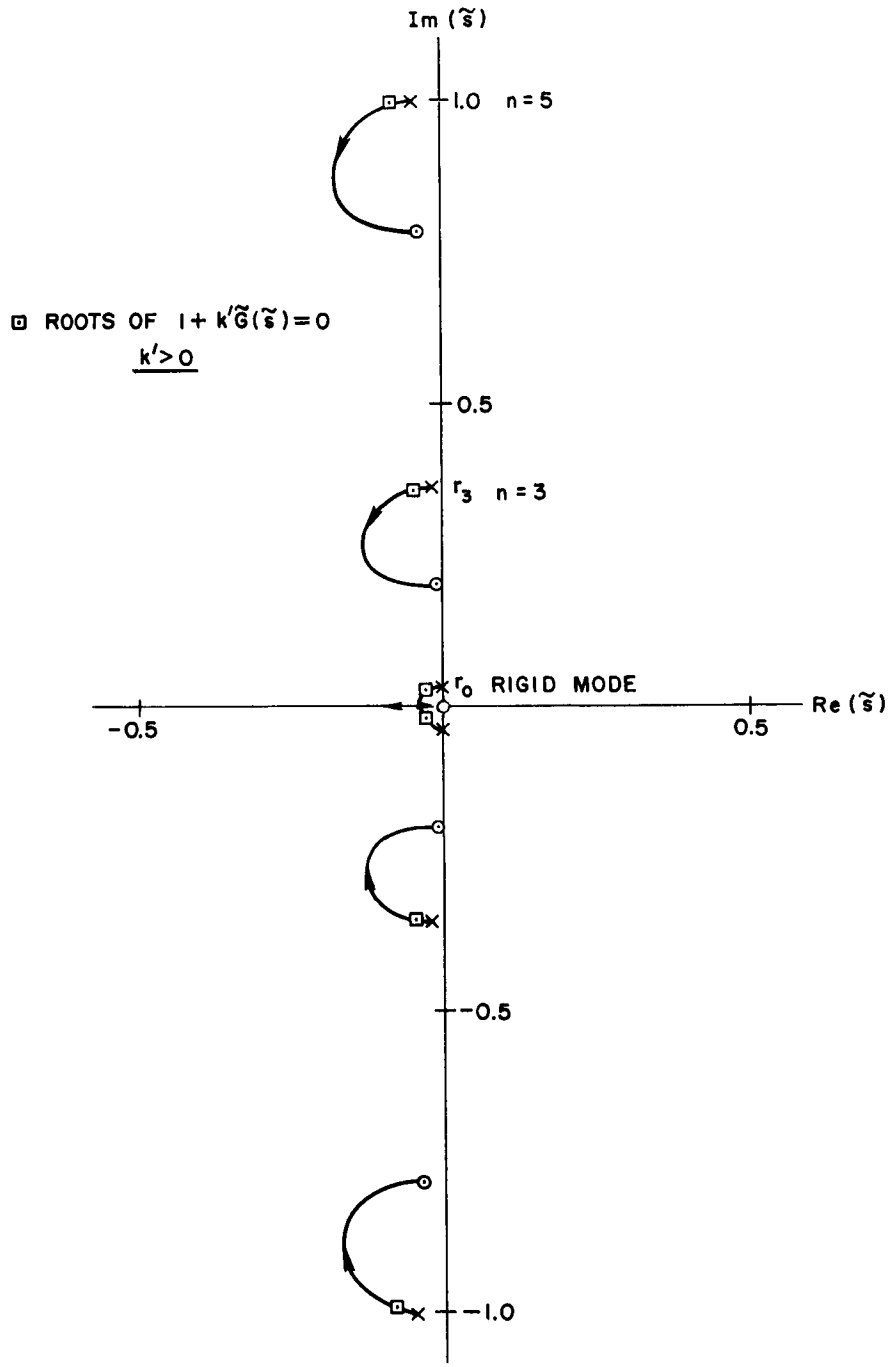

35580

FIG. 20. ROOT LOCUS CONSIDERING TWO FLEXIBLE MODES (n = 3, 5) FOR SENSORS AT THEIR POINTS OF CONTROL.

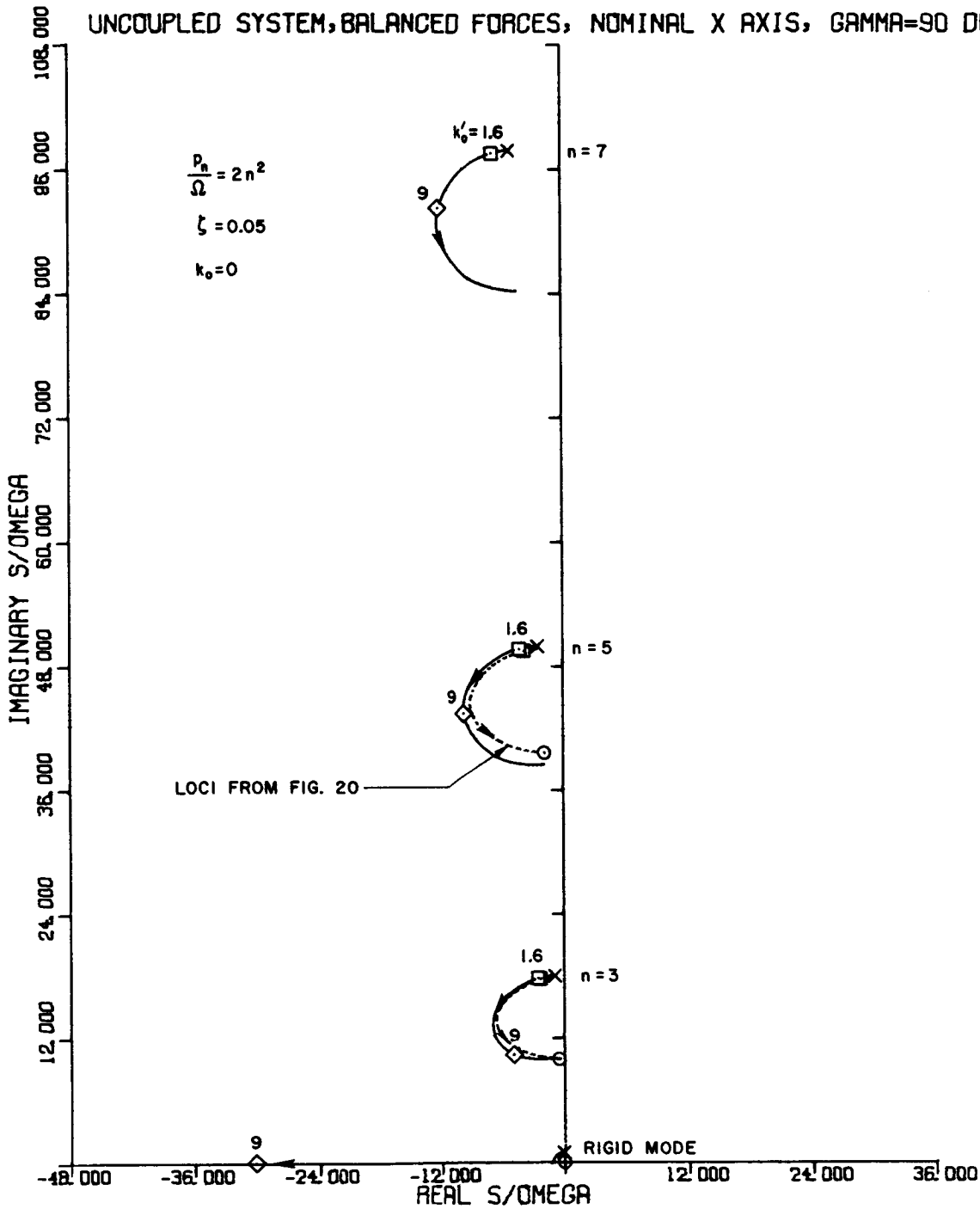

FIG. 21. ROOT LOCUS FOR UNCOUPLED SYSTEM, BALANCED FORCES, NOMINAL x AXIS, $\gamma = 90°$, $k_o = 0$.

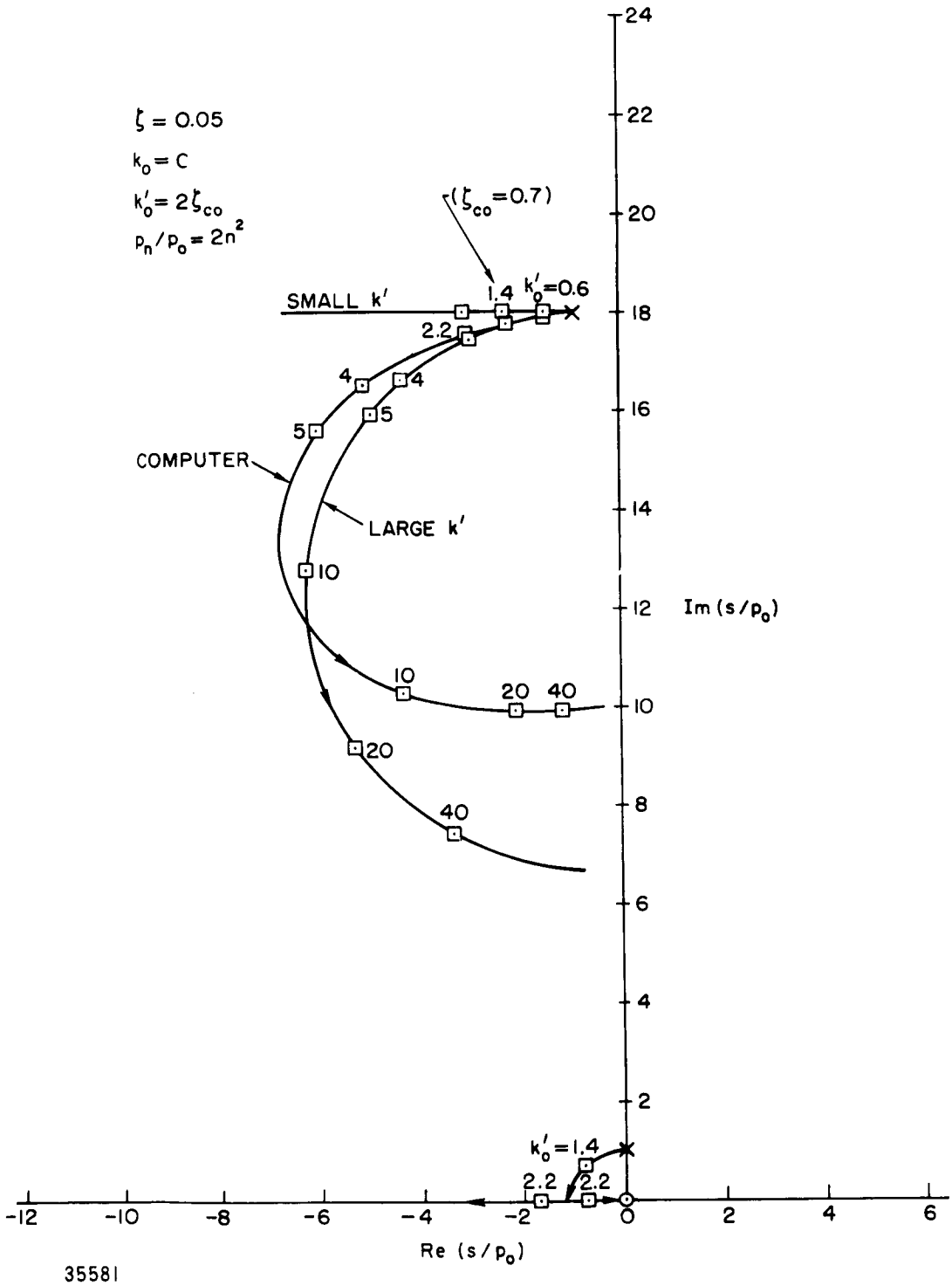

FIG. 22. COMPARISON OF RESULTS FOR n = 3.

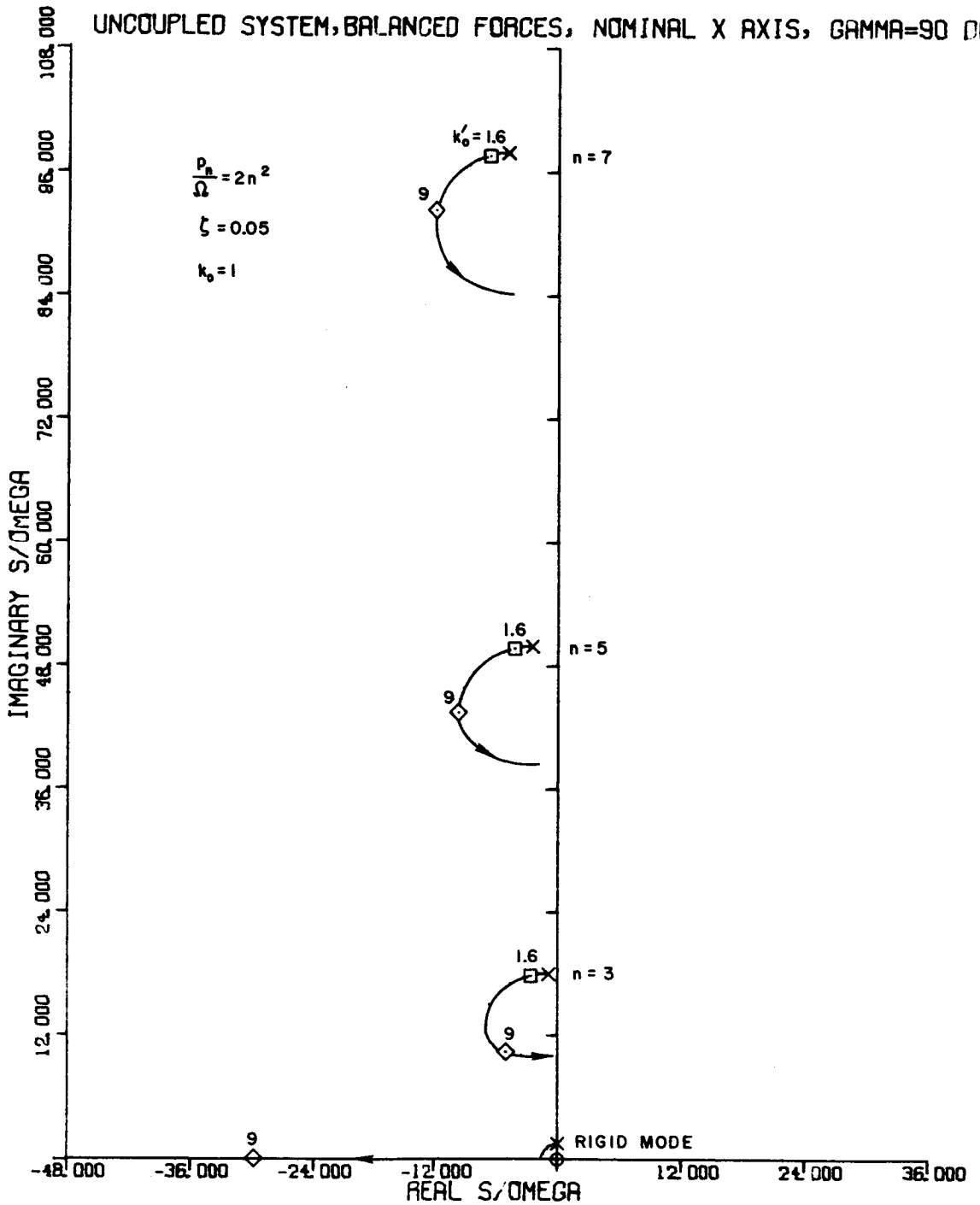

FIG. 23. ROOT LOCUS FOR UNCOUPLED SYSTEM, BALANCED FORCES, NOMINAL x AXIS, $\gamma = 90°$, $k_o = 1$.

TABLE 2. COMPARISON OF ROOTS FOR THE NOMINAL CASE

$k_o = 0$

k'_o	Rigid Mode	Third Mode			Fifth Mode			Seventh Mode		
		Computer	Small k'	Large k'	Computer	Small k'	Large k'	Computer	Small k'	Large k'
1.4	-0.70*	-2.31	-2.30	-2.28	-4.03	-4.03	-4.01	-6.46	-6.48	-6.45
	1.24	17.84	18.06	17.81	49.75	50.02	49.79	97.66	98.01	97.77
2.2	-1.12	-3.14	-3.10	-3.01	-4.90	-4.91	-4.84	-7.33	-7.38	-7.30
	0.90	17.61	18.06	17.53	49.51	50.02	49.53	97.40	98.01	97.50

*Upper number represents the real part of the root in the upper half plane. The lower number represents the imaginary part of the root.

Figure 24 indicates the effects of using a rate network instead of rate feedback for this example. Three flexible modes $(n = 3, 5, 7)$ were used, but only the roots associated with the first are shown. Values of the time constants of $\tau_o p_o = 5$ and $\tau_1 p_o = 0.5$ were used. As indicated in Section 1, and as can be seen by a comparison of Figs. 22 and 24, use of a rate network greatly reduces the distance of the root departures from the flexible-mode poles. However, for the rate-network time constants chosen, the shape of the rigid-mode locus is also affected, so that only a maximum damping ratio of 0.35 can be achieved. By using active networks, a wider ratio of lead-lag time constants can be attained, so that a rigid-mode damping ratio of 0.7 can be realized.

Table 3 provides a comparison between computer results and the use of formulas (3.17) and (3.18) for computing the flexural-mode roots when a rate network is employed. Observe the good agreement between the two methods.

B. STABILITY OF THE HIGHER MODES FOR BALANCED FORCES WITH THE SENSORS NEAR THEIR CONTROL POINTS

Chapter VI indicated that for balanced control forces the stability region of interest centered about the

$$\mu_x \quad \text{sensor at} \quad \gamma = \pm 90^\circ \tag{7.15}$$

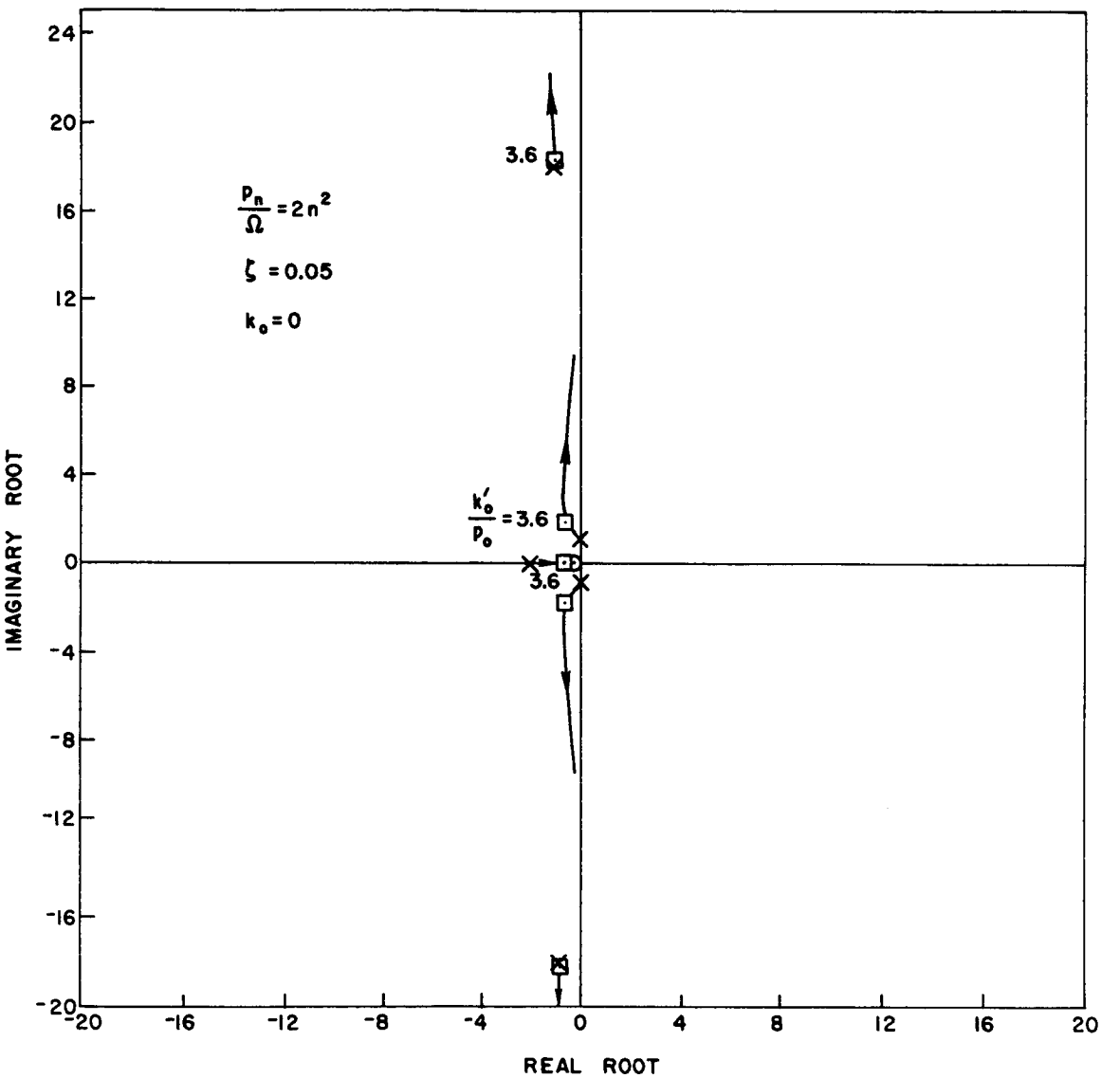

FIG. 24. ROOT LOCUS FOR UNCOUPLED SYSTEM, NOMINAL X AXIS, BALANCED FORCES, LEAD-LAG NETWORK.

TABLE 3. COMPARISON OF METHODS OF FINDING ROOTS FOR BALANCED CONTROL FORCES WITH THE SENSORS AT ONE OF THEIR POINTS OF CONTROL AND USING A RATE NETWORK

$k_o = 0,\ \tau_1 p_o = 0.5,\ \tau_o p_o = 5,\ k_o'/p_o^2 = 3.6\ (\zeta_{co} = 0.32)$

Method	Network Root	Rigid Mode	Third Mode	Fifth Mode	Seventh Mode
Computer	-0.735* 0	-0.609 1.80	-0.920 18.18	-2.503 50.02	-4.901 97.92
Formula			-0.920 18.22	-2.503 50.08	-4.901 98.04

*Upper number represents the real part of the root in the upper half plane. The lower number represents the imaginary part of the root.

and the

$$\mu_y \quad \text{sensor at} \quad \gamma' = 0^\circ \text{ or } 180^\circ \tag{7.16}$$

To investigate the stability region in this vicinity for the higher modes, let

$$\gamma = \begin{cases} 90^\circ + \Delta\gamma \\ -90^\circ + \Delta\gamma \end{cases} \tag{7.17}$$

$$\gamma' = \begin{cases} \Delta\gamma' \\ 180^\circ + \Delta\gamma' \end{cases} \tag{7.18}$$

When $|u_n a_n|$ does not increase with mode number as fast as p_n, then for the very high modes the root time constants are dominated by the structural damping, regardless of where we put the sensor, so that sensor location is unimportant. For the modes not quite that high, we shall assume the incremental angles to be small enough that

$$\sin n\Delta\gamma = n\Delta\gamma \tag{7.19}$$

$$\sin n\Delta\gamma' = n\Delta\gamma' \tag{7.20}$$

$$\cos n\Delta\gamma = \cos n\Delta\gamma' = 1 \tag{7.21}$$

Substituting Eqs. (7.19) - (7.21) into Eqs. (5.16) - (5.19), we obtain for

$$n\Delta\gamma^2 \ll 1 \tag{7.22}$$

that

$$a_{xx_n}(\gamma) = (-1)^{(n-1)/2} B_n \tag{7.23}$$

$$a_{xy_n}(\gamma) = (-1)^{(n-1)/2} n\Delta\gamma \left(\frac{1}{R} + B_n\right) \tag{7.24}$$

$$a_{yx_n}(\gamma) = n\Delta\gamma' \left(\frac{1}{R} + B_n\right) \tag{7.25}$$

$$a_{yy_n}(\gamma') = B_n \tag{7.26}$$

Substituting Eqs. (7.23) - (7.26) into Eqs. (6.5) and (6.6), we obtain

$$c = \frac{R}{2} B_n \tag{7.27}$$

$$d = \frac{n}{2} \left|1 + RB_n\right| \sqrt{-\Delta\gamma'\Delta\gamma} \tag{7.28}$$

For

$$\text{sgn}\ (\Delta\gamma') = -\text{sgn}\ (\Delta\gamma) \tag{7.29}$$

d is real, and we can substitute Eqs. (7.27) and (7.28) into Eqs. (4.20) and (4.21) to obtain

$$\delta = -\frac{k}{2}\left(RB_n \pm n\left|1 + RB_n\right|\sqrt{-\Delta\gamma'\Delta\gamma}\right) \tag{7.30}$$

$$\epsilon = \frac{k'}{2}\left(RB_n \pm n\left|1 + RB_n\right|\sqrt{-\Delta\gamma'\Delta\gamma}\right) - \zeta_n \tag{7.31}$$

For

$$\text{sgn}\ (\Delta\gamma') = \text{sgn}\ (\Delta\gamma) \tag{7.32}$$

d is imaginary, so that substituting Eqs. (7.27) and (7.28) into Eqs. (4.22) and (4.23) yields

$$\delta = -\frac{k}{2} RB_n \pm \frac{k'}{2} n\left|1 + RB_n\right|\sqrt{\Delta\gamma'\Delta\gamma} \tag{7.33}$$

$$\epsilon = +\frac{k'}{2} RB_n \pm \frac{k}{2} n\left|1 + RB_n\right|\sqrt{\Delta\gamma'\Delta\gamma} - \zeta_n \tag{7.34}$$

For a symmetrical cross section employing isotropic structural material, we have, from Eq. (7.2), that

$$RB_n \approx -2.3 \qquad (n \geq 3) \tag{7.35}$$

From Eq. (6.45) we can express k' in terms of the controlled rigid-mode damping ratio ζ_{co} as

$$k' = \frac{K_v}{p_n} = 2\frac{\Omega}{p_n}\zeta_{co}\sqrt{1 + \left(K_p/\Omega^2\right)} \tag{7.36}$$

and from Eq. (3.5), we have

$$k = \frac{K_p}{p_n^2} \tag{7.37}$$

Substituting Eqs. (7.35) - (7.37) into Eqs. (7.30), (7.31), (7.33), and (7.34), we obtain, for $\underline{-\Delta\gamma'\Delta\gamma > 0}$,

$$\boxed{\delta = \frac{K_p}{2p_n^2}\left(2.3 \mp 1.3n\sqrt{-\Delta\gamma'\Delta\gamma}\right)} \tag{7.38}$$

$$\boxed{\epsilon = -\frac{\Omega}{p_n}\zeta_{co}\sqrt{1 + \left(K_p/\Omega^2\right)}\left(2.3 \mp 1.3n\sqrt{-\Delta\gamma'\Delta\gamma}\right) - \zeta_n} \tag{7.39}$$

and for $\underline{\Delta\gamma'\Delta\gamma > 0}$

$$\boxed{\delta = \frac{K_p}{2p_n^2}\,2.3 \pm 1.3n\,\frac{\Omega}{p_n}\,\zeta_{co}\sqrt{1 + \left(K_p/\Omega^2\right)}\sqrt{\Delta\gamma'\Delta\gamma}} \tag{7.40}$$

$$\boxed{\epsilon = -\left(2.3\,\frac{\Omega}{p_n}\,\zeta_{co}\sqrt{1 + \left(K_p/\Omega^2\right)} \mp 1.3n\,\frac{K_p}{2p_n^2}\sqrt{\Delta\gamma'\Delta\gamma}\right) - \zeta_n} \tag{7.41}$$

Observe from Eq. (5.10) that

$$\left(\frac{p_{n+1}}{p_n}\right) \approx \left(\frac{n+1}{n}\right)^2 \tag{7.42}$$

so that the second terms of Eqs. (7.38) - (7.41) decrease as the mode number increases, even though they contain n as a multiplying factor.

It is seen from Eqs. (7.38) - (7.41) that small departures of the sensors from their corresponding points of control have a negligible

effect on the stability of the higher modes. It is also observed that moving both sensors in the same direction from their control points is less deleterious on stability than moving them in opposite directions. This agrees (for $n = 3$) with the results of Chapter VI.

Observe from Eqs. (7.38) and (7.39) that for $K_p = 0$, as the two sensors are moved in opposite directions from their points of control, the roots depart from the equal-root case to the right and left, thus decreasing system stability. Neglecting damping, the system becomes unstable when

$$\Delta\gamma'\Delta\gamma < -\left(\frac{2.3}{1.3n}\right)^2 \tag{7.43}$$

If

$$|\Delta\gamma'| = |\Delta\gamma| \tag{7.44}$$

then, from Eq. (7.43), at the point of instability we have that

$$|\gamma| = \frac{2.3}{1.3n} \text{ radians} \tag{7.45}$$

For $n = 3$, this corresponds to

$$|\Delta\gamma| = 34^\circ \tag{7.46}$$

This compares well with the 28° figure of Section F.1 of Chapter VI considering the simplifying approximations we have made.

From Eqs. (7.38) - (7.41) we observe that δ and $\epsilon + \zeta_n$ decrease with mode number. Therefore, for locations of the sensors near their points of control, if we compute the stability bounds on the basis of the third mode without damping, then, given reasonable structural damping these stability bounds should hold for the higher modes as well. This point may be illustrated as follows: Use the value of $|\Delta\gamma|$ of Eq. (7.46) in Eq. (7.39) for $K_p = 0$ to obtain

$$\epsilon = - \frac{\Omega}{p_n} \zeta_{co}(2.3 \mp 0.77n) - \zeta_n \qquad (7.47)$$

Use Eqs. (5.10) and (5.11) for Ω/p_n and ζ_n in Eq. (7.47) to obtain, for $n \geq 3$,

$$\epsilon = - \frac{\zeta_{co}}{n^2} (2.3 \mp 0.77n) - 0.2 \qquad \begin{matrix}(\text{low-stiffness} \\ \text{structural material})\end{matrix} \qquad (7.48)$$

$$\epsilon = - \frac{\zeta_{co}}{7n^2} (2.3 \mp 0.77n) - 0.02 \qquad \begin{matrix}(\text{high-stiffness} \\ \text{structural material})\end{matrix} \qquad (7.49)$$

Observe, for $\zeta_{co} < 1$, that in both cases $\epsilon < 0$, so that we have stability for all modes for the choice of sensor locations based on the third mode without damping. Therefore the sensor-location stability bounds of $\pm 28^\circ$ from the control points, determined in Chapter VI for the third mode $(K_p = 0)$, should hold for the higher modes as well. Figure 25 presents the computer results for these sensor locations. In the figure, the fifth and seventh modes go unstable at $\zeta_{co} \approx 0.9$, which is in good agreement with the above results considering the small-angle assumptions made, and in excellent agreement with Eq. (4.24), again indicating the efficacy of the simple root formulas as a design tool.

C. EFFECT OF UNBALANCED CONTROL FORCES OR MOMENTS USING THE GENERAL METHOD: SENSORS AT ONE OF THEIR POINTS OF CONTROL

Using Eqs. (5.20) - (5.23) in Eqs. (4.15) - (4.18), we find for unbalanced actuators that for n odd we obtain Eqs. (6.1) - (6.4), which are the same equations we had for balanced control forces. However, for n even we obtain

$$\alpha_{xx} = \frac{R}{2} \Delta F_x (-1)^{n/2} \, a_{xy_n} \qquad (7.50)$$

$$\alpha_{xy} = - \frac{R}{2} \Delta F_y \, a_{xy_n} \qquad (7.51)$$

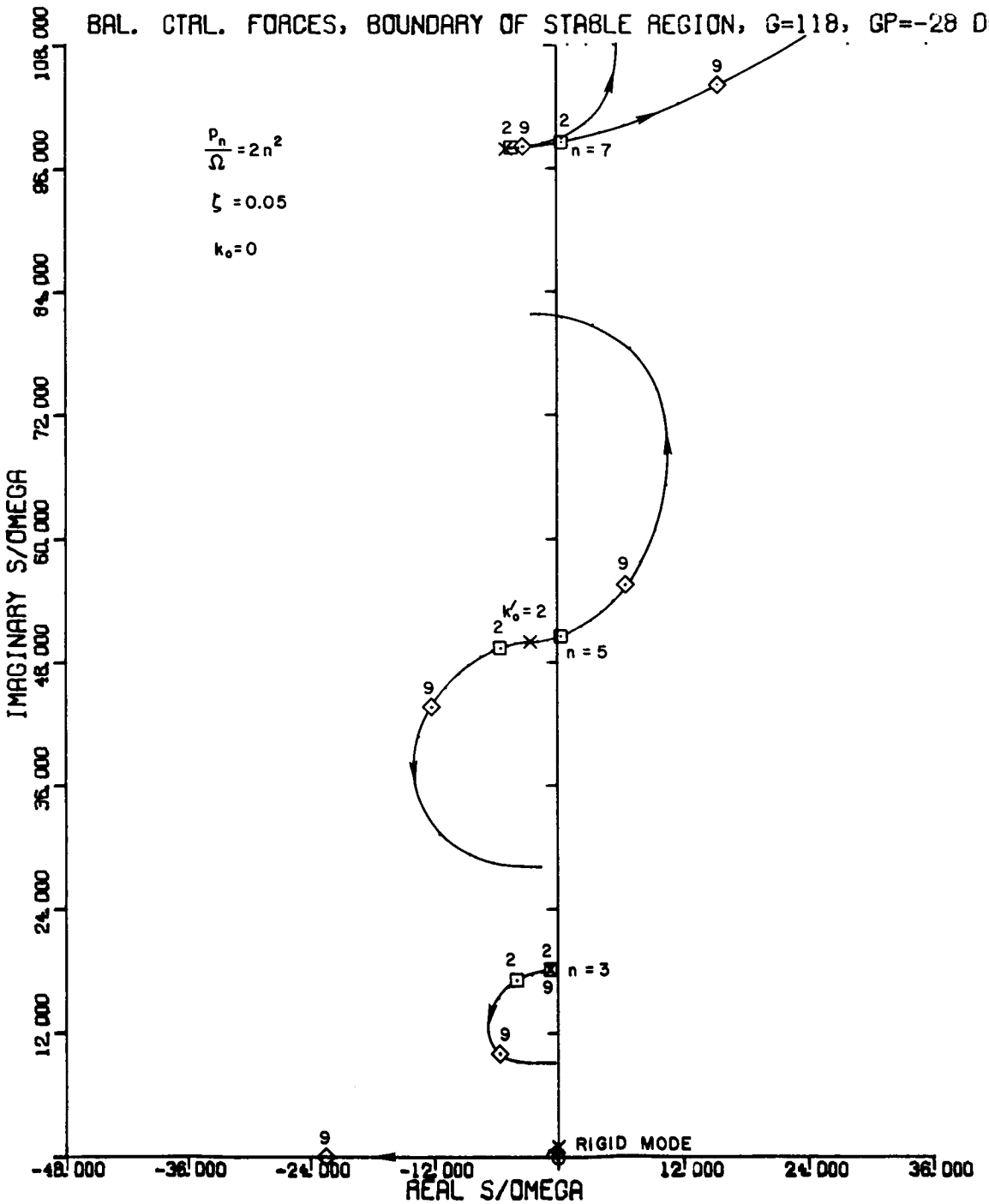

FIG. 25. ROOT LOCUS FOR BALANCED CONTROL FORCES, BOUNDARY OF STABLE REGION, $\gamma = 118°$, $\gamma' = -28°$.

$$\alpha_{yx} = \frac{R}{2} \Delta F_x (-1)^{n/2} \; a_{yy_n} \tag{7.52}$$

$$\alpha_{yy} = -\frac{R}{2} \Delta F_y \; a_{yy_n} \tag{7.53}$$

For each of the sensors at one of its points of control, that is, the

$$\mu_x \text{ sensor at } \gamma_1 = 90° \tag{7.54}$$

$$\text{or } \gamma_2 = -90° \tag{7.55}$$

and the

$$\mu_y \text{ sensor at } \gamma_1' = 0° \tag{7.56}$$

$$\text{or } \gamma_2' = 180° \tag{7.57}$$

Eqs. (5.16) - (5.19) become, for <u>n even</u>,

$$a_{xx_n} = 0 \tag{7.58}$$

$$a_{xy_n} = (-1)^x B_n (-1)^{n/2} \tag{7.59}$$

$$a_{yx_n} = 0 \tag{7.60}$$

$$a_{yy_n} = -B_n (-1)^y \tag{7.61}$$

where the x and y powers are either 1 or 2 depending on the appropriate sensor-location index as defined in Eqs. (7.54) - (7.57).

Substituting Eqs. (7.58) - (7.61) into Eqs. (7.50) - (7.53), we have, for the n^{th} even mode, that

$$\alpha_{xx} = \frac{RB_n(-1)^x}{2} \Delta F_x \tag{7.62}$$

$$\alpha_{xy} = -\frac{R}{2} B_n(-1)^{n/2} (-1)^x \Delta F_y \tag{7.63}$$

$$\alpha_{yx} = -\frac{R}{2} B_n(-1)^{n/2} (-1)^y \Delta F_x \tag{7.64}$$

$$\alpha_{yy} = \frac{R}{2} B_n(-1)^y \Delta F_y \tag{7.65}$$

Substituting Eqs. (7.62) - (7.65) into Eqs. (4.20) and (4.21), for small k's and h = 1 we obtain for the n^{th} even mode

$$\delta = \begin{cases} \frac{k}{2} RB_n \left[\Delta F_x(-1)^x + \Delta F_y(-1)^y\right] \\ 0 \end{cases} \tag{7.66}$$

$$\epsilon = \begin{cases} -\frac{k'}{2} RB_n \left[\Delta F_x(-1)^x + \Delta F_y(-1)^y\right] - \zeta_n \\ -\zeta_n \end{cases} \tag{7.67}$$

Thus as could have been ascertained from the u_n's and a_n's and from Fig. 4, for small gains only the y (or cosine) axis modes are excited by unbalanced control forces.

Substituting for k' in Eq. (7.67) from Eq. (6.45), we find that the condition for stability of the n^{th} even cosine mode is

$$\left[\Delta F_x(-1)^x + \Delta F_y(-1)^y\right] < -\frac{\zeta_n}{RB_n} \left[\frac{\Omega}{p_n} \zeta_{co} \sqrt{1 + \left(K_p/\Omega^2\right)}\right]^{-1} \tag{7.68}$$

If we desire that the allowable force imbalance be equal for both axes, then the criterion is that

$$|\Delta F_2|_{max} = |\Delta F_1|_{max} < - \frac{\zeta_n}{2RB_n} \left[\frac{\Omega}{p_n} \zeta_{co} \sqrt{1 + \left(K_p/\Omega^2 \right)} \right]^{-1} \qquad (7.69)$$

For $K_p = 0$ and $\zeta_{co} = 0.7$, this becomes

$$|\Delta F_2|_{max} = |\Delta F_1|_{max} < - \frac{\zeta_n}{1.4RB_n} \left(\frac{p_n}{\Omega} \right) \qquad (7.70)$$

Obviously the first even mode $(n = 2)$ is most critical.

From Eqs. (B4.8) and (B4.9) in Appendix B, we have, for a symmetrical cross section with isotropic structural material and $\sigma = 0.3$, that

$$n^2 \left[1 + \frac{(n^2 - 1)^2}{(n^2 + 1.3)} \right] \leqq \frac{p_n^2}{\Omega^2} \leqq n^2 \left[1 + \frac{50(n^2 - 1)^2}{(n^2 + 1.3)} \right] \qquad (7.71)$$

Thus for $\underline{n = 2}$,

$$3.3 < \frac{p_2}{\Omega} < 19 \qquad (7.72)$$

As indicated by Eq. (5.11), the damping ratio corresponding to the more rigid (higher frequency) materials is in the order of $\zeta_n = 0.02$, while the damping ratio corresponding to the less rigid materials may be in the order of $\zeta_n = 0.2$. Thus using Eq. (7.2) for RB_n and

$$0.4 \leqq \left(\frac{p_2}{\Omega} \right) \zeta_2 \leqq 0.7 \qquad (7.73)$$

we find from Eq. (7.70) that

$$0.16 \leq |\Delta F_x|_{max} = |\Delta F_y|_{max} \leq 0.30 \tag{7.74}$$

Therefore we are allowed on the order of 15 to 30 percent imbalance of forces about each axis (depending upon structural stiffness and damping) without destabilizing the even modes. A typical computer solution for 10 percent imbalance is shown in Fig. 26, where we have considered the first three excited flexible modes (n = 2, 3, 4). Observe that there is a slight effect on the third mode at the higher gains due to modal coupling.

If we use only a single unbalanced force (or moment) for control about each axis, we find that all the modes (both even and odd) will be stable if we place the sensor and the control force at the same point for each axis. This follows from the earlier observation that for small gains the odd modes are unaffected by force imbalance, and that, from Eqs. (5.24) and (5.25),

$$\Delta F_y(-1)^y = \frac{F_{y1} - F_{y2}}{F_{y1} + F_{y2}} (-1)^y \tag{7.75}$$

$$\Delta F_x(-1)^x = \frac{F_{x1} - F_{x2}}{F_{x1} + F_{x2}} (-1)^x \tag{7.76}$$

so that Eqs. (7.75) and (7.76) will be negative for the sensor and the single control force located together for each axis. For this case, Eqs. (7.66) and (7.67) become

$$\delta = \begin{cases} -kRB_n & (n^{th} \text{ even mode}) \\ 0 \end{cases} \tag{7.77}$$

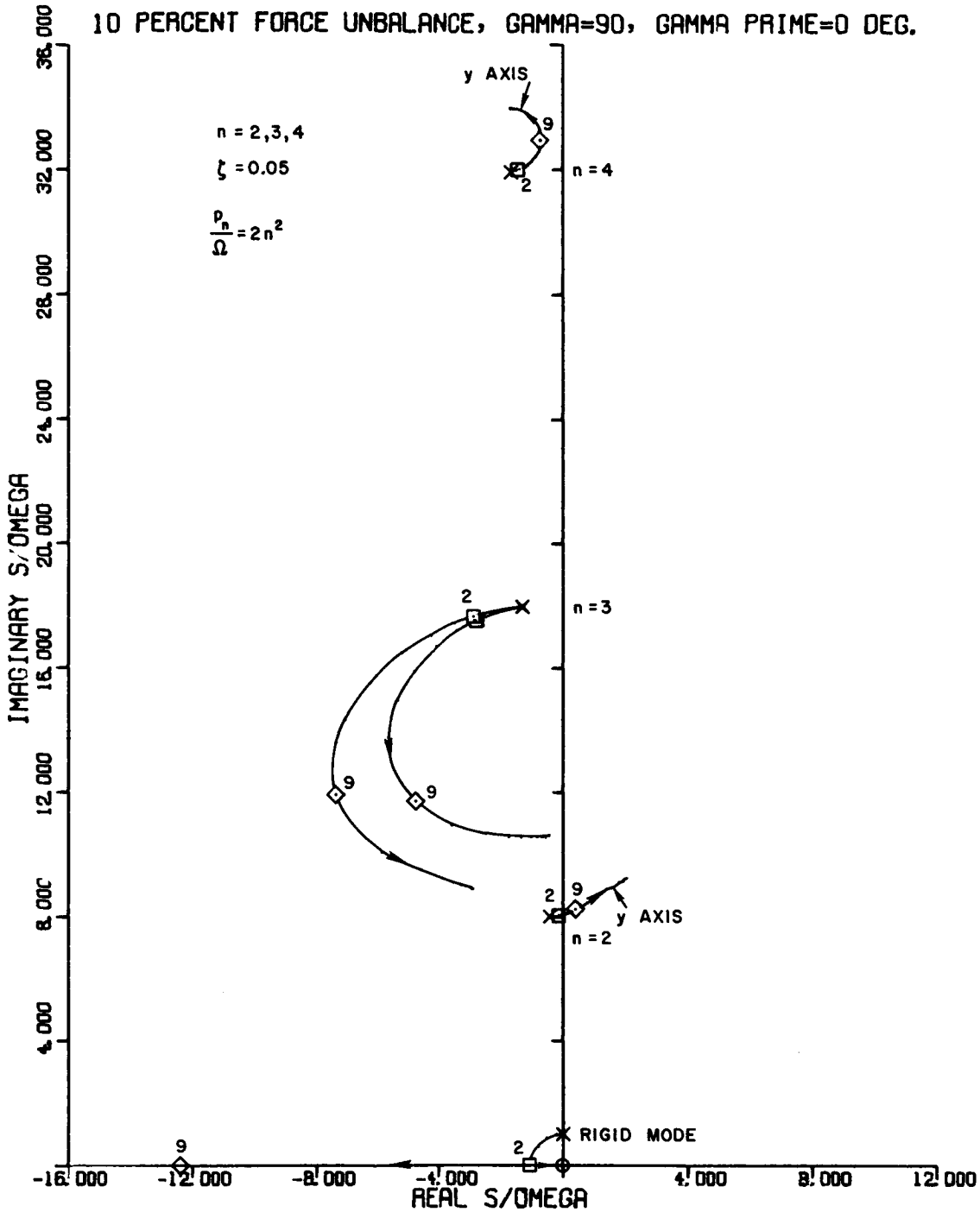

FIG. 26. ROOT LOCUS FOR 10-PERCENT FORCE IMBALANCE, $\gamma = 90°$, $\gamma' = 0°$, $k_o = 0$.

$$\epsilon = \begin{cases} k'RB_n - \zeta_n \\ \\ -\zeta_n \end{cases} \qquad (n^{th} \text{ even mode}) \tag{7.78}$$

Substituting for k' and k from Eqs. (6.45) and (3.5), Eqs. (7.77) and (7.78) become (for the n^{th} even cosine mode)

$$\delta = -\frac{K_p}{p_n^2} RB_n \tag{7.79}$$

$$\epsilon = 2\zeta_{co} RB_n \frac{\Omega}{p_n} \sqrt{1 + \left(K_p/\Omega^2\right)} - \zeta_n \tag{7.80}$$

Thus using Eq. (7.2) for RB_n, and Eq. (7.72) for Ω/p_2, we observe that the second mode is highly excited by the control system (though being well damped by it) and all the even modes are stable for the sensor and control force coincident for each axis. Comparing Eqs. (7.79) and (7.80) with Eqs. (7.4) and (7.5), we observe that for small gains the relative departure of the cosine mode roots from their poles is approximately twice as great for the even modes as it is for the odd modes. Figure 27 is the corresponding computer root locus. Observe that for large gains the third-mode x- and y-axis roots are strongly coupled.

D. USE OF A SINGLE COMMON MOMENT LOCATION FOR CONTROL OF BOTH AXES

If we use a single control moment for each control axis and if we locate the control moments for the two axes at the same point (which we designate as $\gamma = 0$, e.g., place M_{x1} at M_{y1} in Fig. 8 and dispense with M_{x2} and M_{y2}), then all modes (both odd and even) are excited, and we have, from Eqs. (5.28) - (5.31),

$$u_{xx_n} = nR \tag{7.81}$$

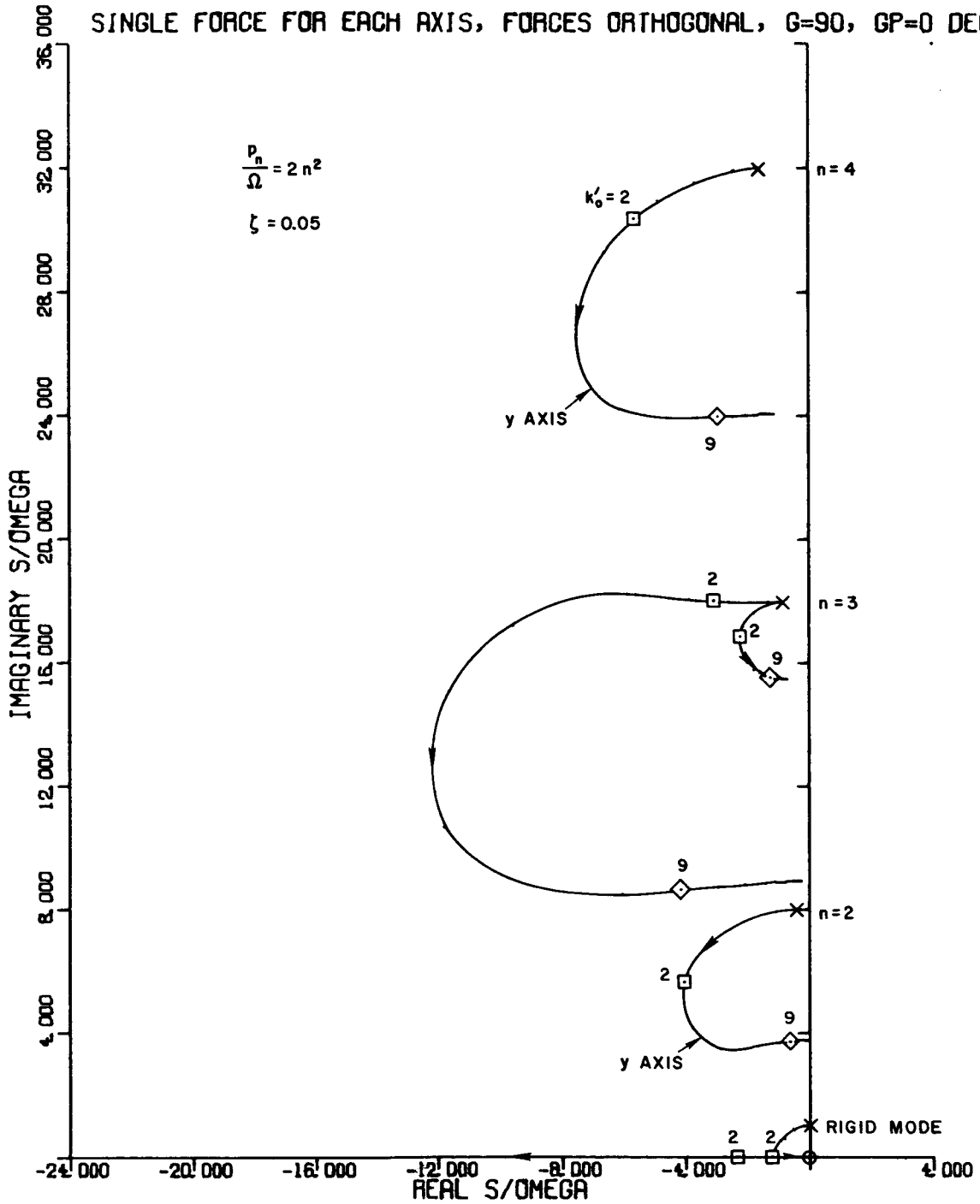

FIG. 27. ROOT LOCUS FOR SINGLE FORCE FOR EACH AXIS, FORCES ORTHOGONAL, $\gamma = 90°$, $\gamma' = 0°$, $k_o = 0$.

$$u_{xy_n} = 0 \tag{7.82}$$

$$u_{yx_n} = 0 \tag{7.83}$$

$$u_{yy_n} = -R \tag{7.84}$$

where the sine mode corresponds to the x axis and the cosine mode to the y axis.

As the location of the y-axis control is unchanged from the preceding section, it is reasonable to place the y sensor at its y moment $(\gamma' = 0)$ as before, and to explore the effect of various locations for the x sensor. For this y-sensor location, from Eqs. (5.18) and (5.19) we have

$$a_{yx_n}(\gamma') = 0 \tag{7.85}$$

$$a_{yy_n}(\gamma') = B_n \tag{7.86}$$

so that the axes are decoupled.

Using Eqs. (7.81) - (7.86) in Eqs. (3.12) and (3.13) yields

$$\epsilon = \begin{cases} \frac{k'}{2} RB_n - \zeta_{yi} \\ -\frac{k'}{2} Rn\ a_{xx_n} - \zeta_{xi} \end{cases} \tag{7.87}$$

$$\delta = \begin{cases} -\frac{k}{2} RB_n \\ \frac{k}{2} Rn\ a_{xx_n} \end{cases} \tag{7.88}$$

where from Eq. (5.16)

$$a_{xx_n}(\gamma) = \frac{n}{R} \cos n\gamma \cos \gamma - B_n \sin n\gamma \sin \gamma \qquad (7.89)$$

By comparing Eqs. (7.87) and (7.88) with Eqs. (7.4) and (7.5), it is observed that the first set of roots, corresponding to the y-axis control, are (for the odd modes) the same as before and show stability. The second set of roots, corresponding to the control of the x axis, yields stability for all modes if [as can be observed from Eq. (7.89)] the x sensor is placed at $\gamma = 0$, so that

$$a_{xx_n} = \frac{n}{R} \qquad (7.90)$$

yielding

$$\epsilon = -\frac{k'}{2} n^2 - \zeta_{xi} \qquad (7.91)$$

$$\delta = \frac{k}{2} n^2 \qquad (7.92)$$

Noting from Eq. (7.2), that

$$\frac{n^2}{RB_n} = -\frac{n^2}{2.3[1 + (1.3/n^2)]^{-1}} \qquad (7.93)$$

and comparing Eqs. (7.91) and (7.92) with the first set of roots of Eqs. (7.87) and (7.88), we find that the sine modes are much more excited than the cosine modes, as can be observed by the greatly increased damping due to control.

Using Eqs. (7.36), (7.37), and (7.42) in Eqs. (7.91) and (7.92), and neglecting structural damping yields

$$\frac{\epsilon_{n+1}}{\epsilon_n} \approx 1 \tag{7.94}$$

$$\frac{\delta_{n+1}}{\delta_n} \approx \left(\frac{n}{n+1}\right)^2 \tag{7.95}$$

Thus, for these locations the damping due to control is approximately constant (for sufficiently small gains) for all the sine modes.

For $\underline{K_p = 0}$, using Eqs. (7.36) and (5.10) in Eq. (7.91) yields

$$\frac{\zeta_{co}}{7} \leq |\epsilon| \leq \zeta_{co} \tag{7.96}$$

so that the excitation of the sine modes is so strong that we are out of the linear range for the larger values of ζ_{co}.

Therefore, due to the strong excitation of all the flexible sine modes, a single location for the control moments and sensors, though stable, cannot be recommended, although considerable improvement can be achieved by use of a rate network, rather than rate.

Figures 28 and 29 present computer results for the x and y mode roots, respectively. Observe the extreme departures of the x-axis roots from their poles compared to those of the y axis for the same gains.

Table 4 compares the computer results with those obtained by the formulas. Observe that for $k_o' \geq 1$, the conditions under which the formulas were derived (that the relative root departures from the poles are small compared to the modal frequency separation) are violated, so that the formulas only serve to indicate that large root departures have occurred.

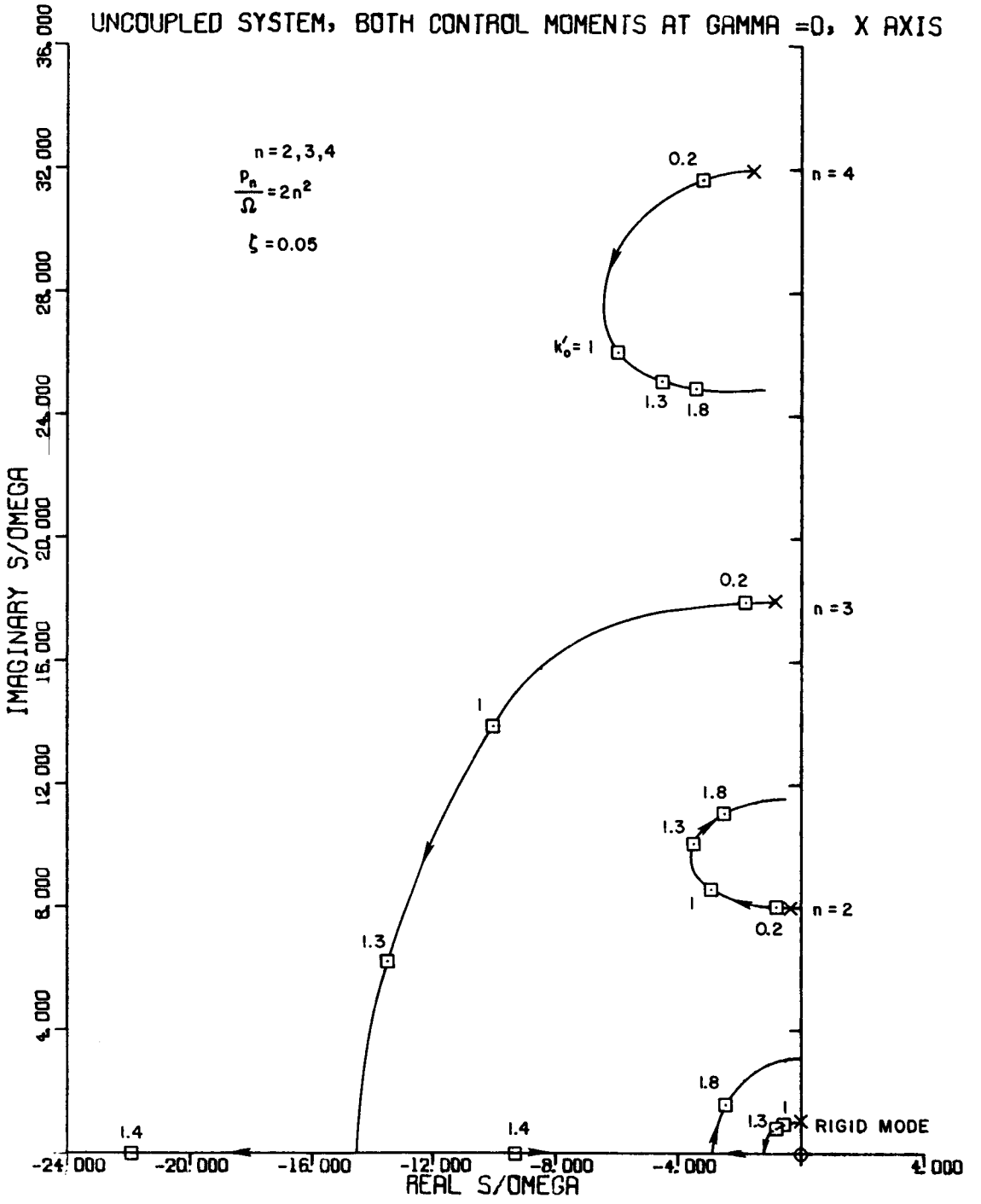

FIG. 28. ROOT LOCUS FOR UNCOUPLED SYSTEM, BOTH CONTROL MOMENTS AT $\gamma = 0°$, x AXIS, $k_o = 0$.

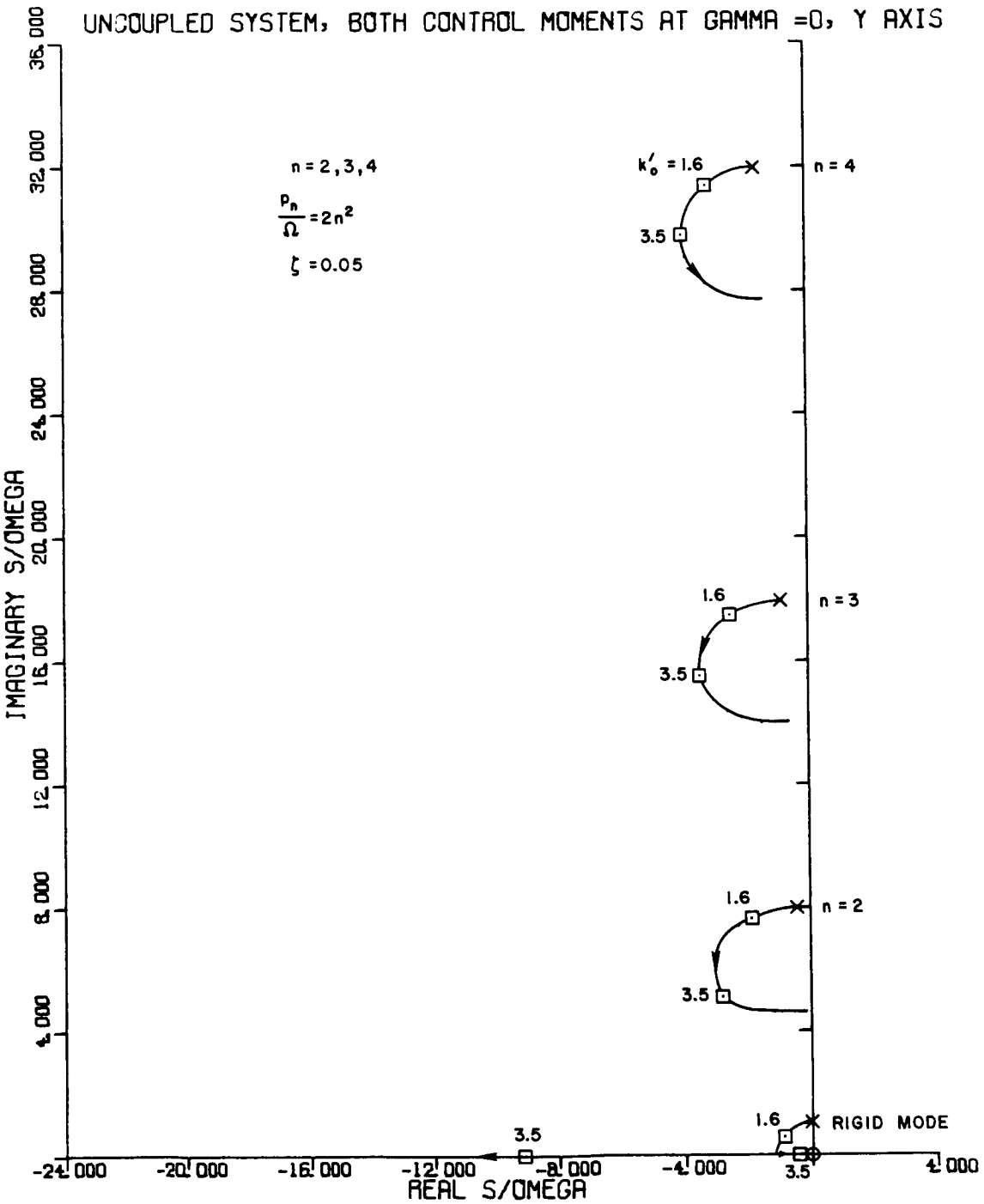

FIG. 29. ROOT LOCUS FOR UNCOUPLED SYSTEM, BOTH CONTROL MOMENTS AT $\gamma = 0°$, y AXIS, $k_o = 0$.

TABLE 4. COMPARISON OF METHODS OF FINDING ROOTS FOR BOTH CONTROL MOMENTS TOGETHER FOR THE x AXIS AND $k_o = 0$

k'_o	Rigid Mode	Second Mode			Third Mode			Fourth Mode		
		Computer	Small k'	Large k'	Computer	Small k'	Large k'	Computer	Small k'	Large k'
0.6	-0.31* 0.97	-1.71 8.07	-1.60 8.00	-1.60 7.96	-4.04 17.69	-3.60 18.00	-3.56 17.59	-5.84 29.60	-6.40 32.00	-5.36 29.90
1.00	-0.56 0.91	-2.94 8.55	-2.40 8.00	-2.40 7.97	-8.46 15.78	-5.40 18.00	-5.23 17.03	-5.94 26.05	-9.60 32.00	-6.16 27.83
1.10	-0.63 0.87	-3.31 8.90	-2.60 8.00	-2.60 7.97	-11.69 10.89	-5.85 18.00	-5.63 16.86	-4.93 25.26	-10.40 32.00	-6.20 27.37
1.30	-0.81 0.79	-3.48 10.07	-3.00 8.00	-3.00 7.98	-13.57 6.20	-6.75 18.00	-6.41 16.48	-4.54 25.11	-12.00 32.00	-6.17 26.57

*Upper number represents the real part of the root in the upper half plane. The lower number represents the imaginary part of the root.

E. SUMMARY

In this chapter, using the general method for coupled axes, we have explored the stability of the higher modes for sensor locations in the vicinity of their nominal positions at their points of control, and the effects of unbalanced control forces or moments. It was found for balanced control forces that the stability boundaries of $\pm 28^\circ$ for the sensor locations about their points of control, obtained for the third mode neglecting structural damping, will insure the stability of the higher modes as well, provided reasonable damping is included.

For small gains, unbalanced control forces do not affect the odd modes but do tend to excite the even modes. For the sensors at one of their control points, we are allowed on the order of a 15 to 30 percent imbalance of forces (or moments) about each axis (depending on structural stiffness and damping) without destabilizing the second and higher even modes. The lower values of allowable imbalance correspond to the higher stiffness-to-weight-ratio structural materials.

If only a single unbalanced force (or moment) is used for control about each axis, we find that the second mode is well damped and all the modes (both even and odd) will be stable if we place the sensor and the control force at the same point for each axis (for the forces or moments for the two axes 90° apart).

If the control moments for the two axes are placed at the same point (one-control-moment package), so that the output axis of one control moment is tangential to the centroidal line and the output axis of the other is radial, then all modes are excited; but if both sensors are also located at the same point, these modes will be stable. For small gains the axis corresponding to the excitation of the cosine modes has the same roots (except for a factor of 1/2 for the even modes) as for the preceding case of orthogonal moment locations. However, the radial control axis, exciting the sine modes, produces much greater excitation than in the previous case, yielding (for sufficiently small values of ζ_{co}) approximately equal control damping of all modes. This strong excitation of the flexible modes is undesirable from moment, power, and response considerations affecting the crewmen, so that placing the control moments in one location is inadvisable.

We demonstrated, for the nominal case, the attenuation of the root departures at the flexible modal poles due to the use of a rate network, rather than rate, making it advisable to use a rate network provided a sufficiently high ratio of lead-lag-network time constants is used so that the desirable damping ratio of $\zeta_{co} = 0.7$ can be realized for the rigid mode.

The validity of the use of the simple root formulas as a "first step" design tool was also demonstrated by comparison with computer solutions. It was shown that when the relative root departures from their modal poles were small compared to the separation of the modal poles, excellent agreement was obtained.

VIII. SUMMARY AND CONCLUSIONS

In this study we first explored the basic character of flexible vehicles employing linear-feedback control systems. The results of that work were then applied to a flexible, spinning, toroidal manned space station employing a continuous-attitude-control system for controlling the direction of the spin axis. Desirable locations were found for the control forces and sensors such that the rigid modes and all the flexible modes of motion are stable.

A. RESULTS FOR A GENERAL FLEXIBLE VEHICLE

1. Vehicles with Uncoupled Control Axes*

It was shown that the controlled-system dynamics for flexible vehicles can usually be represented by Fig. 1 for vehicles with uncoupled axes and by Fig. 4 for vehicles whose control axes are coupled. From these figures it is evident that the basic parameters that couple the flexible motion to the rigid-body motion to be controlled are the u_n's and a_n's. These flexibility control coupling parameters are given by

$$u_n = \frac{Q_n}{Q_c}, \quad \text{the factor converting the rigid-body control, } Q_c, \text{ to the } n^{th} \text{ mode forcing function, } Q_n \tag{8.1}$$

$$a_n = \frac{\mu_{ns}}{q_n}, \quad \text{the factor converting the } n^{th} \text{ mode generalized coordinate, } q_n, \text{ to the quantity, } \mu_{ns}, \text{ sensed by the feedback instrument} \tag{8.2}$$

The u_n and a_n parameters are determined in sign and magnitude by the positions of the control force (or moment) and control sensor with respect to the n^{th} mode shape, respectively.

*e.g., beamlike vehicles.

We then indicated how the characteristic roots of such systems might be found by root locus methods. However, a much simpler approach to determining system stability and estimating the system characteristic roots and real-time response was to employ a linearized expansion of the modal roots about the normalized modal frequency poles. For small root departures from the modal poles, we can write the n^{th}- mode root in the upper half plane as

$$s_n = p_n[j(1 + \delta_n) + \epsilon_n] \tag{8.3}$$

where

$$\delta_n^2, \epsilon_n^2 \ll 1 \tag{8.4}$$

Thus stability of the n^{th} mode is determined by the sign of ϵ_n.

By substituting Eq. (8.3) into the characteristic equation of the uncoupled system, assuming the equivalent structural damping ratio, ζ_n, small and using Eq. (8.4), we obtain, for small gains and the modal frequencies well separated:

$$\epsilon_n = -\frac{k'}{2} u_n a_n - \zeta_n \tag{8.5}$$

$$\delta_n = k \frac{u_n a_n}{2} \tag{8.6}$$

where

$$k' \triangleq \frac{K_v}{p_n} = 2 \frac{p_o}{p_n} \zeta_{co} \sqrt{1 + \left(K_p/p_o^2\right)} \tag{8.7}$$

$$k \triangleq \frac{K_p}{p_n^2} \tag{8.8}$$

p_o = rigid-body natural frequency (Ω in our case)

ζ_{co} = rigid-body damping ratio with control

Thus, as the root loci of the uncoupled system never cross the imaginary axis (neglecting structural damping), the n^{th} mode is stable if

$$\text{sgn } u_n = \text{sgn } a_n \tag{8.9}$$

From Eqs. (8.7) and (8.8) we observe that the equivalent gains, k' and k, rapidly diminish with mode number, so that for the cases where any increase with mode number of $|u_n a_n|$ is less than the increase of p_n, the relative departures of the roots of the higher modes from their poles are small. Because of this effect, Eqs. (8.5) and (8.6) also yield a good approximation to the higher mode roots.

In a similar fashion, we developed an indication of the real time and frequency response of the system.

If we have additional poles and zeros in series with the controller transfer function, we can estimate stability quickly, as K_v is varied, simply by using Eq. (8.5) to determine the basic angle of departure and then adding the angle change produced at the n^{th} modal pole by the additional poles and zeros. Another approach is to use Eqs. (8.3) and (8.4) in the new characteristic equation and determine the new ϵ and δ. In this way it was found that use of a rate circuit rather than rate feedback changes the phase at the poles and reduces the relative departure of the higher frequency roots but does not destabilize the system.

For the case where the departure of the roots from their flexible mode poles is small relative to the separation of the modal poles, equations were also developed for determining the system roots for large gains.

2. Vehicles with Control Axes Coupled by Flexure (e.g., Platelike Vehicles)

For a system with the control axes coupled by flexure, using Eqs. (8.3) and (8.4) in the coupled characteristic equation, for small gains we obtained a quadratic expression for ϵ_n and δ_n, given by Eq. (4.14).

As for the uncoupled case, equations for finding the coupled roots associated with the first excited flexible mode were developed for large gains, for the case where the two control axes were the same and the departure of the roots from the flexible-mode poles is small compared to the separation of the modal poles. From these equations we found that the stability criteria for the first excited flexible mode could be expressed in terms of two parameters, c and d, which are just functions of the u_n's and a_n's. Thus for pure rate feedback, the stability criteria, neglecting structural damping, are:

$$c < -d \qquad (d \text{ real}) \tag{8.10}$$

$$c < -\frac{k' |d|}{1 - (p_o/p_1)^2} \qquad (d \text{ imaginary}) \tag{8.11}$$

Thus for d real, stability is independent of gain, just as in Eq. (8.9) for the uncoupled case. However, for d imaginary, we no longer have 0° or 180° root loci, and the stability is gain dependent.

The adequacy of the small-gain and large-gain formulas as design tools, for the conditions for which they were derived, was verified by comparison with "exact" computer solutions for a space station example.

3. Conclusions

From consideration of the general root expansion approach, we can reach some general conclusions for any flexible vehicle employing a similar control system:

1. The gain associated with the rigid mode usually has very little effect on the roots of the higher modes, so that the extent of their stability is primarily determined by their own structural damping ratio.

2. The stability of the n^{th} mode is dependent on the sign of $u_n a_n$.
3. For vehicles which can be characterized as beams, it is unlikely that all flexible modes can be stabilized without structural damping, unless the sensor and the control force for each axis are placed where the signs of the slope and deflection are the same for all modes, such as the beginnings or ends of the mode shapes.
4. For beamlike vehicles, simply placing the sensor and the control force together at an arbitrary location is insufficient to insure that $u_n a_n$ will be either positive or negative or that the system will be stable. However, for the uncoupled case, when u_n varies in the same fashion as a_n along the mode shape, such as when we apply a moment and measure the resulting angle in a torsion or bending problem, then placing the moment and sensor together is sufficient to insure that $u_n a_n$ will be positive.
5. The uncoupling of the roots of one mode from those of the other modes, for small gains, can be attributed physically to the resonance phenomenon (for small damping) of the n^{th} mode at its own loop frequency, and the relatively low response of the other modes to this frequency due to the separation of modal frequencies.

B. EQUATIONS OF THE SPACE STATION

1. Vibration

Consideration of the effect of including man on the system design led to the study of a rotating manned space station shaped like a toroid having a large ratio of station radius to cross-section diameter very much like a uniform spinning ring.

Though the analysis is general, for the purpose of numerical examples we chose a spin speed of 3 rpm, a station radius of 85 ft, and a symmetrical cross section having a diameter of about 10 ft and using isotropic structural material with a Poisson's ratio of 0.3.

The dynamic response of such a rotating uniform toroid, with a large centroidal-radius to cross-sectional-radius ratio, was found to be divided into two uncoupled motions: motion in the plane of the centroidal line of the cross sections, and motion perpendicular to the plane.

The inextensible motion in the plane consists of radial motion and rotational motion about axes parallel to the spin axis. The natural

modes of vibration are sines and cosines of $n\gamma$, where n is an integer for continuity. The natural frequency was found to be

$$p_n = \frac{n}{(n^2 + 1)^{1/2}} \left[\frac{(n^2 - 1)^2}{m(\gamma)R^3/EI_{y_b}} + \Omega^2(n^2 - 3) \right]^{1/2} \qquad (n \geq 2) \qquad (8.12)$$

where

Ω = angular velocity of spin

$m(\gamma)$ = cross-sectional mass per unit central angle γ

R = radius of the centroidal line of the station

EI_{y_b} = flexural rigidity of the cross section about an axis parallel to the spin axis.

However due to Coriolis forces, the in-plane vibration was not stationary with respect to the station but precessed about the ring with a frequency

$$\Delta p_n = \frac{2\Omega n}{n^2 + 1} \qquad (8.13)$$

Since the in-plane motion is uncoupled from the motion to be controlled, it was unnecessary to consider it further.

The motion perpendicular to the plane consists of deflection parallel to the spin vector coupled with twist about the centroidal line, proportional to the deflection. As before, the natural modes of vibration are sines and cosines of $n\gamma$. For the n^{th} natural mode of vibration, the ratio of twist to deflection is given by

$$B_n = -\frac{n^2}{R} \frac{1 + \frac{\mu I_p}{EI}}{1 + \frac{\mu I_p}{EI} n^2} \qquad (8.14)$$

where

μI_p = torsional stiffness of the cross section about the centroidal axis of the cross sections

EI = flexural rigidity of the cross section about the radial axis.

The natural frequency squared of vibration for the n^{th} mode is given by

$$p_n^2 = \frac{1}{\breve{m}} \left[(n^2 - 1) \left(RB_n + n^2 \right) \right] + n^2 \Omega^2 \tag{8.15}$$

where

$$\breve{m} = \frac{m(\gamma) R^3}{EI} \tag{8.16}$$

For a symmetric cross section of isotropic structural material, the above expressions reduce to

$$B_n = - \frac{n^2}{R} \frac{2 + \sigma}{1 + \sigma + n^2} \tag{8.17}$$

$$p_n^2 = \frac{n^2 (n^2 - 1)^2}{\breve{m}(n^2 + 1 + \sigma)} + n^2 \Omega^2 \tag{8.18}$$

where σ represents Poisson's ratio. For our example, the values of these quantities are

$$RB_n = -2.3 \left(1 + \frac{1.3}{n^2} \right)^{-1} \tag{8.19}$$

$$n^4 \leqq \frac{p_n^2}{\Omega^2} \leqq 50 n^4 \qquad (n \geqq 3) \tag{8.20}$$

where the range of frequencies corresponds to the range of stiffness-to-weight ratios of the structural material.

For the high-stiffness materials we used an equivalent structural damping ratio ζ_n of 0.02 for each mode, while for the low-stiffness materials we used a value of 0.2 in our numerical calculations.

2. The Rigid-Body Equations

Following the approach of Lange [Ref. 39], the rigid-body equations of angular motion about axes in the plane, were transformed into a single vector equation in the body axis system. The resultant equation is

$$\ddot{\mu} + \Omega^2 \mu = Q \tag{8.21}$$

where

μ = the vector angle in body-fixed coordinates of the spin axis to an inertial frame

Q = the vector moment in body coordinates divided by the station moment of inertia about a diameter.

It should be observed that for our case, where the station moment of inertia about the spin axis is approximately twice that of the moment of inertia about a diameter, the natural frequency of the rigid station is once per revolution. Thus from an inertial reference frame, the axis of the spinning station may take up any fixed angle, which would appear as a once-per-revolution angle modulation as seen in a body-fixed reference frame.

3. The Control System

Equation (8.21) is the vector equation for two uncoupled oscillators. For these simple systems, it is conventional to employ position and rate feedback to design a continuous position servo. The desired quantities μ and $\dot{\mu}$ can readily be obtained from a star tracker, sun sensor, inertial platform, or similar device. If we obtain $\dot{\mu}$ by using

body-fixed rate gyros, we must also add μ according to the following relation:

$$\dot{\mu} = q - \Omega \times \mu \tag{8.22}$$

where q is the in-plane angular velocity vector.

Since the various methods of obtaining $\dot{\mu}$ are equivalent--insofar as the analysis is concerned--if the sensors are placed at the same location, we postulated that $\dot{\mu}$ is derived from the star-tracker signal as pure rate. (We indicated earlier the modifications induced by using a rate circuit.)

As seen from Eq. (8.22), μ inherently is related to $\dot{\mu}$, and the analysis shows that it is only necessary to employ $\dot{\mu}$ in the feedback path. The employment of μ feedback simply serves to raise the rigid-body frequency of oscillation above Ω. Thus the remainder of the analysis was concentrated on velocity feedback.

Note that a portion of the velocity feedback (that proportional to q) could be supplied by a body-fixed rate damper. If the rate damper is operated alone, angular rates of the spin axis would decay with a twice-per-revolution oscillation. In this case any fixed direction of the spin axis would suffice, since a rate damper does not control the orientation of the spin vector.

4. Control Forces and Moments

Two basic arrangements were considered for the control force (or moments): (1) orthogonal pairs as shown in Fig. 8 (for which control forces and moments give identical results), and (2) a single control moment for each axis with the moments applied at the same location (e.g., use of a single control moment device).

C. RESULTS FOR THE SPINNING SPACE STATION

1. Balanced Control Forces or Moments

a. Lowest Excited Mode (n = 3)

Considering just the first excited flexible mode (n = 3), the following results were obtained for $K_p = 0$:

(1) Single-Sensor Package. Without structural damping it is impossible to find a position that will stabilize the third flexible mode using a single-sensor package. The minimum third-mode structural damping ratio ζ_3 for marginal stability is roughly in the range

$$0.03\zeta_{co} < \zeta_3 < 0.3\zeta_{co} \tag{8.23}$$

where the low portion of the range is for materials of high structural stiffness. As Eq. (8.23) requires for $\zeta_{co} \geq 0.7$, higher values of ζ_3 than can reasonably be expected, it appears that ζ_{co} would have to be lower than the desirable range of 0.7 to 0.8 to achieve even marginal stability with a single-sensor package. Therefore separate sensor locations for each control axis were investigated.

(2) Two Sensors without Structural Damping. If the μ_x sensor (sensor that controls motion about the body-fixed x axis) is placed at $\gamma = 90°$ or $270°$, and the μ_y sensor is placed at $\gamma = 0°$ or $180°$, the system is uncoupled and stable for all values of gain.

If the sensors are symmetrically placed about the diagonals ($\gamma = \pm 45°$), the regions of stability extend, for any value of gain, approximately $28°$ to each side of the above locations for a space station with a symmetric cross section and isotropic structural material.

If the sensors are kept $90°$ apart, the stable region may extend nearly $50°$ to either side of the above locations, depending on the values of the gain.

If the sensors are placed symmetrically about $\gamma = 0°$ or $90°$, there is a stable region of about $\pm 20°$ width about the locations where the sensors are $90°$ apart, for rate gains of

$$K_v = 2\Omega\zeta_{co} < 0.15p_3 \qquad (8.24)$$

However, this region is poorly damped for all stable values of gain as shown by the root locus plot (at the center of this region) of Fig. 15.

Therefore, it is recommended that the μ_x sensor be placed in the vicinity of $\gamma = \pm 90^\circ$ and the μ_y sensor in the vicinity of $\gamma = 0^\circ, 180^\circ$. These locations, for which the control axes decouple, are equivalent to placing each of the sensors at one of its corresponding control forces.

b. Stability of the Higher Modes

Using the general method, stability of the higher modes ($n \geq 5$) was investigated for the μ sensors placed at the points where the two axes of control uncouple, which is the most desirable position for the third mode. It was found that without structural damping, all of the higher modes were stable for these positions of the μ sensors. In fact it was found that because the effective gain k' is proportional to Ω/p_n, the application of control had little effect on the higher modes.

2. Effect of Unbalanced Control Forces or Moments

Using the general method, it was found that, for the preferred locations of the sensors at one of their points of control, the system can tolerate up to a 15 to 30 percent imbalance of forces or moments about each axis (depending upon structural stiffness and damping) without destabilizing the even modes.

For small gains the imbalance had no effect on the odd modes. Based on results of this study, a composite diagram of allowable actuator imbalances and discrepancies in sensor locations from their corresponding points of control may be assumed to be as shown in the adjacent sketch.

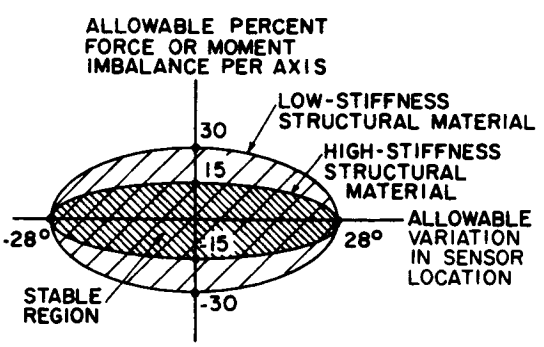

If only a single unbalanced force or moment is used for control about each axis, so that the forces or moments for the two axes are orthogonal, we find that all the modes (both even and odd) are excited, but that they will be stable and reasonably damped if for each axis we place the sensor and the control force or moment at the same point.

If we locate the moments for the two axes at the same point, we find that the system is stable provided we put the sensors there as well. However, all the flexible sine modes are highly excited by the control, and therefore we cannot consider it a satisfactory solution.

D. RECOMMENDED LOCATIONS FOR THE FORCES AND SENSORS FOR THE SPINNING SPACE STATION

Based on the preceding considerations, the recommended configuration for the control forces and sensors is as follows:

1. For each control axis a balanced pair of control forces or moments, located on opposite sides of a station diameter, should be employed. The controls for the two axes should be orthogonal.
2. The sensor for each axis should be located at one of its corresponding control forces or moments.
3. A rate network or filtered rate should be employed in place of pure rate, in order to further reduce the flexible-mode response for the higher modes.

With this arrangement, the system is stable and only the odd flexible modes $(n = 3, 5, 7, \ldots)$ are excited. The excitation of these modes is small and diminishes rapidly as the mode number is increased.

IX. CONTRIBUTIONS OF THIS STUDY AND SUGGESTED FUTURE WORK

A. CONTRIBUTIONS

As set forth in the introductory chapter, the principal contributions resulting from this investigation are as follows:

1. Development of the basic form of the equations of motion of flexible vehicles, from which the equations of forced motion of spinning pressurized toroids and the determination of their natural frequencies can be deduced.
2. Indication of a general method of approach, and derivation of simple formulas, for quickly estimating the stability, roots, and real-time response of flexible vehicles employing multiaxis linear control systems.
3. A general solution to the problem of where to place the sensors, control forces, and moments for stability of a flexible, spinning, toroidal manned space station.
4. Physical interpretation of the effect of flexibility on a control system, to provide a guide to the design or study of the control of flexible vehicles.
5. Discovery that the Coriolis forces induce precession, relative to the spinning toroid, of the natural in-plane inextensible vibrations.

B. SUGGESTED FUTURE WORK

The following areas are suggested for further exploration:

1. Study of the response of the system to internal and external disturbance forces.
2. The detailed effects of gyroscopic coupling associated with control moment devices.
3. Application of the root perturbation approach to different space station configurations and other vehicles such as boosters, missiles, and rockets.
4. The effects of discontinuous and nonlinear control on flexible vehicles.
5. The possibility of obtaining a general approach (similar to that derived here for force and sensor coupling) for structural coupling between control axes, as might occur if we include the effects of the hub on the space station but retain the toroidal mode shapes.
6. The effects of rotary inertia as applied to the space station.

7. The general problem of the effect of Coriolis forces on the free vibration of an arbitrary spinning vehicle.

C. FURTHER COMMENTS

Some further comments on the assumptions employed in this study are in order here.

1. Rotary Inertia

By neglecting rotary inertia (i.e., assuming that the moment of inertia of a cross-sectional element is zero), a number of phenomena were bypassed. One of the results of neglecting rotary inertia was that the ratio of the station moments of inertia about the spin and in-plane axes is $C/A = 2$. If rotary inertia is included, then for our space station example, this ratio would be approximately 1.997. If the hub is included, the ratio would be even somewhat less.

For a more general C/A, Eq. (C.4) of Appendix C would be

$$\ddot{\alpha} - \frac{C}{A} j\dot{\psi}\dot{\alpha} = Q\, e^{j\psi} \tag{9.1}$$

yielding the following vector equation for the star-tracker angle μ:

$$\ddot{\mu} + j\dot{\mu}\Omega\left(2 - \frac{C}{A}\right) + \left(\frac{C}{A} - 1\right)\Omega^2\mu = Q \tag{9.2}$$

Writing this in component form, we have

$$\ddot{\mu}_x - \dot{\mu}_y\left(2 - \frac{C}{A}\right)\Omega + \left(\frac{C}{A} - 1\right)\Omega^2\mu_x = Q_x \tag{9.3}$$

$$\ddot{\mu}_y + \dot{\mu}_x\left(2 - \frac{C}{A}\right)\Omega + \left(\frac{C}{A} - 1\right)\Omega^2\mu_y = Q_y \tag{9.4}$$

Applying rate and position feedback control, as previously, we obtain (for zero reference input)

$$\ddot{\mu}_x - \dot{\mu}_y\left(2 - \frac{C}{A}\right)\Omega + \dot{\mu}_x K_v + \left[\left(\frac{C}{A} - 1\right)\Omega^2 + K_p\right]\mu_x = 0 \tag{9.5}$$

$$\ddot{\mu}_y + \dot{\mu}_x\left(2 - \frac{C}{A}\right)\Omega + \dot{\mu}_y K_v + \left[\left(\frac{C}{A} - 1\right)\Omega^2 + K_p\right]\mu_y = 0 \tag{9.6}$$

Thus the characteristic equation is given by

$$\begin{vmatrix} \left(s^2 + K_v s + p_{co}^2\right) & -gs \\ gs & \left(s^2 + K_v s + p_{co}^2\right) \end{vmatrix} = 0 \tag{9.7}$$

where

$$g \triangleq \left(2 - \frac{C}{A}\right)\Omega \tag{9.8}$$

Equation (9.7) yields

$$\left(s^2 + K_v s + p_{co}^2\right)^2 + g^2 s^2 = 0 \tag{9.9}$$

For $K_v = 0$ and g small

$$s \approx \pm j p_{co}\left(1 \pm \frac{g}{2p_{co}}\right) \tag{9.10}$$

so that the natural frequencies of the rigid mode are slightly removed from the uncoupled $(C/A = 2)$ case.

Equation (9.9) can be factored into

$$\left(s^2 + K_v s + p_{co}^2 + jgs\right)\left(s^2 + K_v s + p_{co}^2 - jgs\right) = 0 \qquad (9.11)$$

or

$$\left(1 + \frac{K_v s}{s^2 + p_{co}^2 + jgs}\right)\left(1 + \frac{K_v s}{s^2 + p_{co}^2 - jgs}\right) = 0 \qquad (9.12)$$

which can be approximately rewritten with the denominators factored as

$$\left\{1 + \frac{K_v s}{\left[s + j\left(p_{co} + \frac{g}{2}\right)\right]\left[s - j\left(p_{co} - \frac{g}{2}\right)\right]}\right\}$$

$$\times \left\{1 + \frac{K_v s}{\left[s + j\left(p_{co} - \frac{g}{2}\right)\right]\left[s - j\left(p_{co} + \frac{g}{2}\right)\right]}\right\} = 0 \qquad (9.13)$$

For g small, these factored characteristic equations yield only slightly different roots than the case where the rotary inertia was neglected. As we have seen earlier, the flexible-mode roots are very little affected by the rigid-mode conditions, so that these small changes in the rigid-mode roots will have a negligible effect on the roots associated with the flexible modes.

For g large, as might occur if we had a very large hub, it might be worthwhile to modify the control equations to take the rigid-body axis coupling into consideration as was done by Lange [Ref. 39]. For such a modified control system, it would be necessary to modify our perturbation analysis, as was done for the lead-lag network, to obtain the new flexible-mode roots. If we follow our previous approach, new mode shapes based upon the new configuration would be required for this case. A way to circumvent this is to (1) employ the toroidal mode shapes,

(2) consider the hub rigid and the spokes represented by weightless beams, and (3) match forces, moments, and deflections where the spokes join the toroid. In such an analysis, we would have structural coupling between the mode shapes for the two axes, as well as coupling due to control, and again a new perturbation analysis would be necessary.

2. Response of the System to Large Star-Tracker Angles

As can be determined from Appendix A, the form of the vibration equations is unaffected by large reference angles. Similarly, the sensor feedback of the flexible motion is independent of the reference angles of the rigid body. Thus the character of the flexible motion is unchanged by large angular motions of the rigid body.

If the vibratory motion were to exceed the linear range, we would be in the structural yield region so that the response would be unsatisfactory. Thus for the purposes of analysis, use of the linear equations for the flexible motion is satisfactory, and the problem of large angular motions of the body is primarily a rigid-body rather than a flexible one, as long as the applied forces or moments are sufficiently small such that the flexible motion is in the linear range.

APPENDIX A. BASIC FORM OF THE EQUATIONS OF MOTION OF FLEXIBLE VEHICLES

In this appendix we indicate the basic form of the equations of motion of flexible vehicles. Specifically, we show that for a wide range of conditions, the rigid-body motion and the flexural motion are uncoupled, except for the coupling that might occur through the applied forces.

1. Free Vibration about Equilibrium

If we consider a generic mass particle, $\rho\, dV$, then from Newton's law of motion we have

$$\rho\bar{a}\, dV \equiv \rho\left\{\bar{a}_{c.m.} + \bar{\omega} \times \left[\bar{\omega} \times \left(\bar{r}_o + \hat{\bar{\Delta r}}\right)\right] + \dot{\bar{\omega}} \times \left(\bar{r}_o + \hat{\bar{\Delta r}}\right) + \hat{\dot{\bar{\Delta r}}} + 2\bar{\omega} \times \dot{\bar{\Delta r}}\right\} dV$$

$$= \overline{dF}_{el} + \overline{dF}_o + \overline{dF} \qquad (A.1)$$

where

ρ = mass density

V = volume

$\bar{a}_{c.m.}$ = acceleration of the center of mass (c.m.) of the vehicle

$\bar{r}_o$ = the undeflected vector position of the mass particle with respect to the vehicle, measured from the vehicle center of mass

$\hat{\bar{\Delta r}}$ = total elastic deflection

$\overline{dF}_{el}$ = the elastic force acting on the particle

$\overline{dF}_o$ = the steady state force acting on the particle, such as internal pressure

$\overline{dF}$ = variable portion of the forces acting on the particle

For the equilibrium condition at a constant spin velocity, $\bar{\Omega}$, Eq. (A.1) can be written as

$$\rho\left\{\bar{\Omega} \times \left[\bar{\Omega} \times \left(\bar{r}_o + \overline{\Delta r}_o\right)\right]\right\} = \bar{L}_{el}(\Delta r_o) + \frac{\overline{dF}_o}{dV} \tag{A.2}$$

where $\overline{\Delta r}_o$ is the equilibrium deflection and $\bar{L}_{el}$ is a linear vector operator involving $\overline{\Delta r}$ and its partial derivatives with respect to $\bar{r}$.

If we consider small perturbations about the equilibrium condition, by letting

$$\hat{\overline{\Delta r}} \triangleq \overline{\Delta r}_o + \overline{\Delta r} \tag{A.3}$$

$$\bar{r} \triangleq \bar{r}_o + \overline{\Delta r}_o \tag{A.4}$$

$$\bar{\omega} \triangleq \bar{\Omega} + \overline{\Delta\omega} \tag{A.5}$$

then Eq. (A.1) reduces to

$$\rho\Big[\bar{a}_{c.m.} + \bar{\omega} \times (\bar{\omega} \times \bar{r}) + \bar{\omega} \times (\bar{\omega} \times \overline{\Delta r}) - \bar{\Omega} \times (\bar{\Omega} \times \bar{r}) + \cancel{\bar{\Omega} \times (\bar{\Omega} \times \bar{r})} + \dot{\bar{\omega}} \times \bar{r} + \dot{\bar{\omega}} \times \overline{\Delta r} + \ddot{\overline{\Delta r}} + 2\bar{\omega} \times \dot{\overline{\Delta r}}\Big] = \cancel{\bar{L}_{el}(\overline{\Delta r}_o)} + \bar{L}_{el}(\overline{\Delta r}) + \cancel{\frac{\overline{dF}_o}{dV}} + \frac{\overline{dF}}{dV} \tag{A.6}$$

or

$$\rho\Big[\bar{a}_{c.m.} + \bar{\omega} \times (\bar{\omega} \times \bar{r}) - \bar{\Omega} \times (\bar{\Omega} \times \bar{r}) + \dot{\bar{\omega}} \times \bar{r} + \dot{\bar{\omega}} \times \overline{\Delta r} + \ddot{\overline{\Delta r}}\Big] = \bar{L}(\overline{\Delta r}) + \frac{\overline{dF}}{dV} - \rho(2\bar{\omega} \times \dot{\overline{\Delta r}})^{\dagger} \tag{A.7}$$

where we have defined

$$\bar{L}(\overline{\Delta r}) = \bar{L}_{el}(\overline{\Delta r}) - \bar{\omega} \times (\bar{\omega} \times \overline{\Delta r}) \tag{A.8}$$

For free vibration about equilibrium, we have

$$\rho \frac{\partial^2 \overline{\Delta r}(\bar{r},t)}{\partial t^2} = \bar{L}(\overline{\Delta r}) \tag{A.9}$$

If we let

$$\overline{\Delta r} = T(t)\ \bar{w}(\bar{r}) \tag{A.10}$$

Eq. (A.9) takes the form

$$\bar{\rho}\ \bar{w}(\bar{r})\ \ddot{T}(t) = \bar{L}[\bar{w}(\bar{r})]\ T(t) \tag{A.11}$$

---

†We will assume in the remainder of this appendix that this Coriolis term is insignificant. When the Coriolis term is significant, we no longer have the equation of free vibration in the simple form of Eq. (A.9) and special approaches must then be employed in its solution. One such approach will be illustrated later by the treatment of the in-plane motion of the space station. Of course the Coriolis term could be retained as a forcing term and $\dot{\overline{\Delta r}}$ expanded in terms of the mode shapes which were obtained by neglecting the Coriolis forces, as in Eq. (A.25). However, lack of suitable orthogonality conditions causes the equations for the modal generalized coordinates $q_n(t)$ to appear in coupled form rather than in the desirable uncoupled form of Eq. (A.41).

Equation (A.11) is satisfied for T's of the form

$$T(t) = T_o \, e^{ipt} \tag{A.12}$$

yielding the equation for $\bar{w}$

$$\bar{L}[\bar{w}(\bar{r})] + p^2 \rho \bar{w}(\bar{r}) = 0 \tag{A.13}$$

If we take two values of the eigenvalue p^2, and their corresponding eigenfunctions $\bar{w}$, that satisfy Eq. (A.13) for the boundary conditions appropriate to the particular flexible vehicle, we have the equations

$$\bar{L}\left[\bar{w}_n(\bar{r})\right] + p_n^2 \, \bar{w}_n(\bar{r}) \, \rho = 0 \tag{A.14}$$

$$\bar{L}\left[w_m(r)\right] + p_m^2 \, \bar{w}(\bar{r}) \, \rho = 0 \tag{A.15}$$

Taking the dot products of Eq. (A.14) with $\bar{w}_m(\bar{r})$, and Eq. (A.15) with $\bar{w}_n(\bar{r})$, and integrating over the volume yields

$$\int_V \bar{w}_m(\bar{r}) \cdot \bar{L}\left[\bar{w}_n(\bar{r})\right] \, dV + p_n^2 \int_V \rho \, \bar{w}_m(\bar{r}) \cdot \bar{w}_n(\bar{r}) \, dV = 0 \tag{A.16}$$

$$\int_V \bar{w}_n(\bar{r}) \cdot \bar{L}\left[\bar{w}_m(\bar{r})\right] \, dV + p_m^2 \int_V \rho \, \bar{w}_n(\bar{r}) \cdot \bar{w}_m(\bar{r}) \, dV = 0 \tag{A.17}$$

Subtracting Eq. (A.17) from Eq. (A.16) gives

$$\left(p_n^2 - p_m^2\right) \int_V \rho \, \bar{w}_n(\bar{r}) \cdot \bar{w}_m(\bar{r}) \, dV = \int_V \left[\bar{w}_n(\bar{r}) \cdot \bar{L}\left(\bar{w}_m\right) - \bar{w}_m(\bar{r}) \cdot \bar{L}\left(\bar{w}_n\right)\right] dV \tag{A.18}$$

If we integrate the right-hand side by parts, we usually find that (since the eigenfunctions satisfy the boundary conditions) the right-hand side is equal to zero. Thus we have the modal orthogonality conditions

$$\int_V \rho\, \bar{w}_n(\bar{r}) \cdot \bar{w}_m(\bar{r})\, dV = 0 \qquad m \neq n \tag{A.19}$$

Using Eq. (A.19) in Eq. (A.16), we also obtain

$$\int_V \bar{w}_m(\bar{r}) \cdot \bar{L}\left[\bar{w}_n(\bar{r})\right] dV = 0 \qquad m \neq n \tag{A.20}$$

In addition, because there are no external forces or moments induced by the free vibrations of a flexible vehicle, the linear momentum and the angular momentum are unaffected, thus yielding the relationships

$$\int_V \rho\, \bar{w}_n(\bar{r})\, dV = 0 \tag{A.21}$$

$$\int_V \bar{r} \times \rho \bar{w}_n(\bar{r})\, dV = 0 \tag{A.22}$$

where we have measured $\bar{r}$ from the center of mass of the vehicle.

From Eq. (A.13), it is apparent that Eqs. (A.21) and (A.22) also imply that

$$\int_V \bar{L}\left[\bar{w}_n(\bar{r})\right] dV = 0 \tag{A.23}$$

$$\int_V \bar{r} \times \bar{L}\left[\bar{w}_n(\bar{r})\right] dV = 0 \tag{A.24}$$

For forced vibration problems we can employ a modal expansion for the deflection

$$\overline{\Delta r} = \sum_{m=1}^{N} q_m(t)\ \overline{w}_m(\overline{r}) \tag{A.25}$$

and solve for the generalized coordinates $q_m(t)$.

2. Forced Vibration

For forced vibration we may employ Eq. (A.25) in Eq. (A.7) and discard products of small quantities to obtain

$$\rho\Bigg[\overline{a}_{c.m.} + \overline{\omega} \times (\overline{\omega} \times \overline{r}) - \overline{\Omega} \times (\overline{\Omega} \times \overline{r}) + \dot{\overline{\omega}} \times \overline{r} + \sum_{m=1}^{N} \ddot{q}_m(t)\ \overline{w}_m(\overline{r})\Bigg] = \sum_{m=1}^{N} q_m(t)\ \overline{L}\left[\overline{w}_m(\overline{r})\right] + \frac{\overline{\partial F}}{\partial V} \tag{A.26}$$

Integrating Eq. (A.26) over the volume and using Eqs. (A.21) and (A.23), we obtain the rigid-body equation of translation

$$M_o\ \overline{a}_{c.m.} = \overline{F} \tag{A.27}$$

where

$$M_o \triangleq \int_V \rho\ dV, \quad \text{the mass of the vehicle} \tag{A.28}$$

Similarly, taking the cross product with $\bar{r}$ and using Eqs. (A.22) and (A.24), and the center-of-mass condition, Eq. (A.26) yields the rigid-body equation of angular motion about the center of mass

$$\bar{\bar{I}} \cdot \dot{\bar{\omega}} + \bar{\omega} \times (\bar{\bar{I}} \cdot \bar{\omega}) = \bar{M}_{c.m.} \tag{A.29}$$

where $\bar{M}_{c.m.}$ is the external moment about the center of mass and $\bar{\bar{I}}$ is the inertia dyadic about the center of mass.

Taking the dot product of Eq. (A.26) with $\bar{w}_n(\bar{r})$, integrating over V, and utilizing Eqs. (A.19) and (A.20), we obtain the vibration equations

$$M_n \ddot{q}_n + K_n q_n = F_n - \int_V \rho[\bar{\omega} \times (\bar{\omega} \times \bar{r}) - \bar{\Omega} \times (\bar{\Omega} \times \bar{r})] \cdot \bar{w}_n(\bar{r})\, dV$$

$$- \int_V \rho[\dot{\bar{\omega}} \times \bar{r}] \cdot \bar{w}_n(\bar{r})\, dV \tag{A.30}$$

where

$$M_n = \int_V \rho\, \bar{w}_n(\bar{r}) \cdot \bar{w}_n(\bar{r})\, dV = \begin{bmatrix} n^{th}\text{-mode} \\ \text{generalized} \\ \text{mass} \end{bmatrix} \tag{A.31}$$

$$K_n = - \int_V \bar{w}_n(\bar{r}) \cdot \bar{L}[\bar{w}_n(\bar{r})]\, dV = \begin{bmatrix} n^{th}\text{-mode} \\ \text{generalized} \\ \text{spring constant} \end{bmatrix} \tag{A.32}$$

$$F_n = \int_V \frac{\partial \bar{F}}{\partial V} \cdot \bar{w}_n(\bar{r})\, dV = \begin{bmatrix} n^{th}\text{-mode} \\ \text{generalized} \\ \text{force} \end{bmatrix} \tag{A.33}$$

Equation (A.30) can be rewritten as

$$\ddot{q}_n + p_n^2 q_n = Q_n - \frac{1}{M_n} \int_V \rho[\bar{\omega} \times (\bar{\omega} \times \bar{r}) - \bar{\Omega} \times (\bar{\Omega} \times \bar{r})] \cdot \bar{w}_n(\bar{r})\, dV$$

$$- \frac{1}{M_n} \int_V \rho[\dot{\bar{\omega}} \times \bar{r}] \cdot \bar{w}_n(\bar{r})\, dV \qquad (A.34)$$

where

$$p_n^2 = \frac{K_n}{M_n} = \text{square of } n^{th}\text{-mode natural frequency of vibration} \qquad (A.35)$$

$$Q_n = \frac{F_n}{M_n} = n^{th}\text{-mode forcing function} \qquad (A.36)$$

A simple approach to determine the n^{th}-mode natural frequency is to equate the maximum potential energy to the maximum kinetic energy of the n^{th} mode to obtain a version of the Rayleigh equation

$$p_n^2 = \frac{2V_n}{q_n^2 M_n} \qquad (A.37)$$

where V_n is the potential energy of the n^{th} mode.

If we call the spin axis z, expand the integrals in Eq. (A.34) and make use of Eqs. (A.5) and (A.22), we obtain

$$\ddot{q}_n + p_n^2 q_n = Q_n + \Omega\Delta\omega_x (W_{zx} + W_{xz}) + \Omega\Delta\omega_y (W_{zy} + W_{yz}) - 2\Omega\Delta\omega_z (W_{xx} + W_{yy}) \qquad (A.38)$$

where we have defined

$$W_{ij} = -\frac{1}{M_n}\int_V \rho r_i w_j(\bar{r})\, dV \tag{A.39}$$

Observe that if the vehicle is not spinning ($\Omega = 0$), or if the deflection is (1) only in the direction of the spin vector or (2) due to pure torsion about the spin axis, then Eq. (A.38) reduces to

$$\ddot{q}_n + p_n^2 q_n = Q_n \tag{A.40}$$

where we employed Eq. (A.22) in the last two cases.

If we include equivalent viscous structural damping forces proportional to the modal deflection, Eq. (A.40) takes the form

$$\boxed{\ddot{q}_n + 2\zeta_n p_n \dot{q}_n + p_n^2 q_n = Q_n} \tag{A.41}$$

where ζ_n is the equivalent viscous damping ratio.

In this study we only deal with systems whose modal equations are of the form of Eq. (A.40) or (A.41). However, it is interesting to note that for those systems for which the Coriolis forces are negligible, the resulting general equation, Eq. (A.38), can also be put in the form of Eq. (A.40), except that the new n^{th}-mode forcing function contains terms proportional to the rigid-body forcing function and its derivative. This may be demonstrated as follows.

Expanding Eq. (A.29) and making use of Eq. (A.5), we have (for x, y, z the principal axes)

$$\Delta\dot{\omega}_x + \Delta\omega_y a = \frac{M_x}{I_x} \triangleq Q_x \tag{A.42}$$

$$\Delta\dot{\omega}_y - \Delta\omega_x b = \frac{M_y}{I_y} \triangleq Q_y \tag{A.43}$$

$$\Delta\dot{\omega}_z = \frac{M_z}{I_z} \triangleq Q_z \tag{A.44}$$

where

$$a \triangleq \frac{I_z - I_y}{I_x}\,\Omega \tag{A.45}$$

$$b \triangleq \frac{I_z - I_x}{I_y}\,\Omega \tag{A.46}$$

Substituting for $\dot{\omega}_y$ in Eq. (A.43) from Eq. (A.42), and for $\dot{\omega}_x$ in Eq. (A.42) from Eq. (A.43), we obtain

$$\Delta\ddot{\omega}_x + ab\Delta\omega_x = -aQ_y + \dot{Q}_x \tag{A.47}$$

$$\Delta\ddot{\omega}_y + ab\Delta\omega_y = bQ_x + \dot{Q}_y \tag{A.48}$$

Multiplying Eq. (A.47) by λ, Eq. (A.48) by μ, and the derivative of Eq. (A.44) by ν, adding them to Eq. (A.38), and defining

$$\tilde{q}_n = q_n + 2\lambda\omega_x + \mu\Delta\omega_y + \nu\Delta\omega_z \tag{A.49}$$

we obtain

$$\begin{aligned}\ddot{\tilde{q}}_n + p_n^2\tilde{q}_n = Q_n &+ \Delta\omega_x\left[(W_{zx} + W_{xz})\Omega - \lambda\left(ab - p_n^2\right)\right] - a\lambda Q_y + \lambda\dot{Q}_x \\ &+ \Delta\omega_y\left[(W_{zy} + W_{yz})\Omega - \mu\left(ab - p_n^2\right)\right] + b\mu Q_x + \mu\dot{Q}_y \\ &+ \Delta\omega_y\left[-2\Omega(W_{xx} + W_{yy}) + \nu p_n^2\right] + \nu\dot{Q}_z\end{aligned} \tag{A.50}$$

If we let

$$\lambda = \frac{(W_{zx} + W_{xz})\Omega}{ab - p_n^2} \tag{A.51}$$

$$\mu = \frac{(W_{zy} + W_{yz})\Omega}{ab - p_n^2} \tag{A.52}$$

$$\nu = \frac{2(W_{xx} + W_{yy})\Omega}{p_n^2} \tag{A.53}$$

then Eq. (A.50) reduces to

$$\ddot{\tilde{q}}_n + p_n^2 \tilde{q}_n = Q_n + b\mu Q_x - a\lambda Q_y + 2\lambda \dot{Q}_x + \mu\lambda \dot{Q}_y + \nu\lambda \dot{Q}_z$$

$$\triangleq \tilde{Q}_n(t) \tag{A.54}$$

APPENDIX B. EQUATIONS OF MOTION OF THE SPACE STATION

In this appendix we derive the equations of motion of a spinning, pressurized, toroidal space station. In the first section we discuss the mathematical model and the assumptions, we indicate how the required coordinate transformations are obtained, and we derive the total linear acceleration of the origin of the local body-fixed axes. Then in Section 2 we derive the equations of motion of an element of the toroid, using the equations of equilibrium approach, and observe the the motion divides itself into uncoupled in-plane and out-of-plane motions even when spin and pressurization are included. In Section 3, employing the techniques of Appendix A, we obtain the solutions to the free vibration equations, and present the equations of forced motion in terms of the mode shapes for the out-of-plane motion. And in the last section we determine the range of values of the natural frequencies of vibration for our example space station.

1. Fundamentals

a. Mathematical Model and Assumptions

(1) The mathematical model of the space station chosen for analysis is a uniform, flexible, circular toroid, whose overall diameter is large in comparison with the diameter of its cross section. The principal axes of the cross section are considered to be (for the undeflected case) in the radial and spin axis directions.

(2) Since the cross-sectional diameter of the toroid is small in relation to the overall diameter, the inertial forces associated with the motion of a cross section can be considered to be due to the motion of the center of mass of the cross section. Thus, as is common in beam vibration theory [see for example Tong, Ref. 42, p. 247] when the diameter of the cross section is small compared to the length of the beam or the wavelength of vibration, the dynamic effects of the rotary inertia of the cross section will be neglected.

(3) All vibrational motions, changes in spin speed, or departure of the spin axis from an inertially fixed direction will be assumed small, so that higher order terms consisting of powers or products of these motions and their derivatives may be neglected as having only second and higher order effects.

(4) The stresses due to deflection will be assumed to be approximately proportional to the additional curvature or twist due to strain. This is consistent with simple beam theory, which is good when the cross-sectional diameter of the beam is small compared to the length or radius of curvature of the beam and when the distortion of the cross section is small compared to the rotation of the cross section.

(5) As the frequencies associated with gravity gradient effects are much smaller than the spin velocity or flexural frequencies, we will neglect gravity gradient effects for this study and will consider our vehicle to be effectively in inertial space.

Based on these assumptions, we have the mathematical model shown in Fig. 30. The axes x, y, z are fixed to the rigid vehicle and act as a point of departure for the flexural motion. These axes (x, y, z) are referenced to the inertially fixed axes X, Y, Z by the Euler angles ϕ, θ, ψ. The vehicle spin axis is z.

Following the notation of Love [Ref. 34], the local undeflected axes fixed to the rigid body are x_o, y_o, z_o. The corresponding deflected body-fixed axes are x_b, y_b, z_b.

b. Coordinate Transformations

Using the flow diagram method of Curtis [Ref. 43], Fig. 31 presents the Euler-angle flow diagram from the inertially fixed axes to the deflected local body axes. The coordinate transformations required in this study can be read by inspection from this diagram.

The next to the last three rotations shown in Fig. 31 are the components of the small vector angle $\bar{\Psi}$, which specifies the rotation of the deflected local body-fixed axes b to the undeflected local axes o. For small deflections, $\bar{\Psi}$ can be written in terms of the direction cosines as

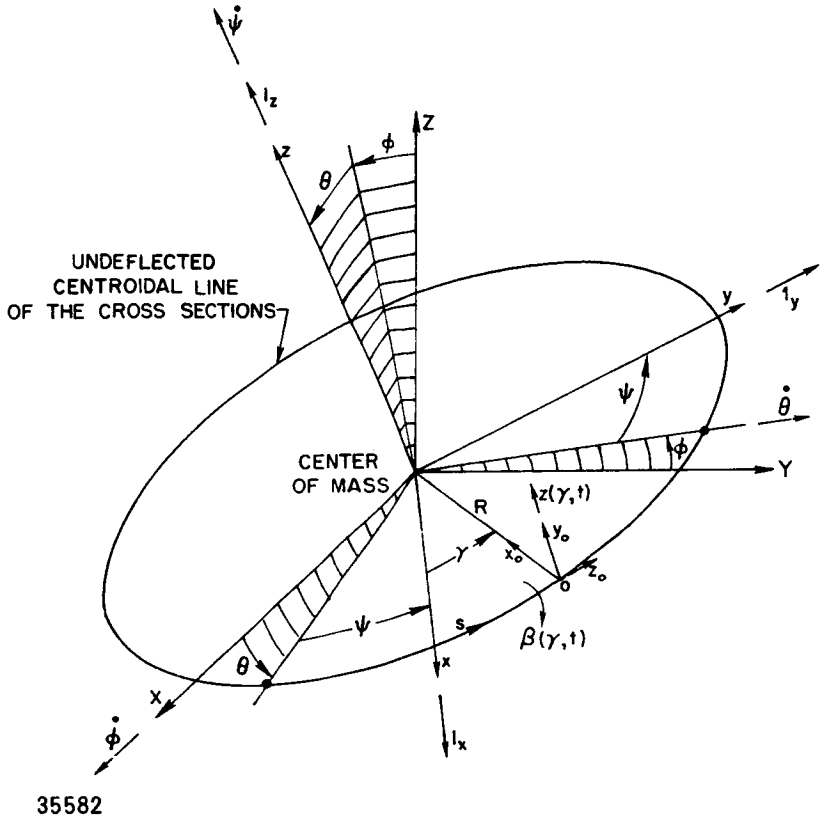

FIG. 30. MATHEMATICAL MODEL OF A SPINNING TOROID.

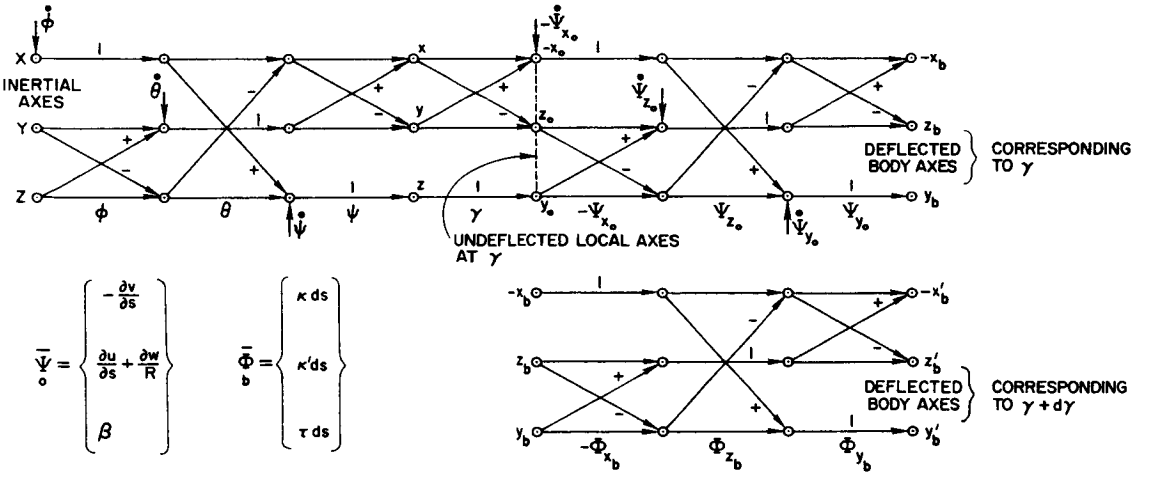

HORIZONTAL LINES ARE COSINES OF THE INDICATED ROTATIONS, EXCEPT FOR 1's SHOWN FOR THE AXES ABOUT WHICH ROTATION TAKES PLACE.

SLANT LINES ARE SINES OF THE INDICATED ROTATIONS, THEIR APPROPRIATE SIGNS BEING SHOWN.

FIG. 31. COORDINATE TRANSFORMATION FLOW DIAGRAM.

$$\underset{o}{\overline{\Psi}} = \begin{Bmatrix} \cos\ (y_b, z_o) \\ \cos\ (z_b, x_o) \\ \cos\ (x_b, y_o) \end{Bmatrix}^{\dagger} \tag{B1.1}$$

Substituting for the direction cosines from Eqs. (6), page 447 of Love [Ref. 34], we obtain $\overline{\Psi}$ in terms of the deflections (u, v, w) along the o axes and the twist, β, about the z_o axis, as

$$\underset{o}{\overline{\Psi}} = \begin{Bmatrix} -\dfrac{\partial v}{\partial s} \\ \dfrac{\partial u}{\partial s} + \dfrac{w}{R} \\ \beta \end{Bmatrix} \tag{B1.2}$$

Since the angle is small, the components can be considered to be in either the o or b coordinate systems.

The last three rotations shown in Fig. 31 are the components of $\overline{\Phi}$--the small vector rotation of the body axes over the arc length ds--due to the components of curvature and twist, κ, κ', τ. Thus

$$\underset{b}{\overline{\frac{d\Phi}{ds}}} = \begin{Bmatrix} \kappa \\ \kappa' \\ \tau \end{Bmatrix} \tag{B1.3}$$

For an originally untwisted ring of radius R, we have

$$\underset{b}{\begin{Bmatrix} \kappa_o \\ \kappa'_o \\ \tau_o \end{Bmatrix}} = \begin{Bmatrix} 0 \\ \dfrac{1}{R} \\ 0 \end{Bmatrix} \tag{B1.4}$$

---

†A letter under a vector denotes the coordinate system in which the components are expressed.

Thus from Eqs. (6), page 447 of Love [Ref. 34], we have

$$\begin{Bmatrix} \kappa \\ \kappa' \\ \tau \end{Bmatrix}_b = \begin{Bmatrix} \frac{\beta}{R} - \frac{d^2 v}{ds^2} \\ \frac{1}{R} + \frac{d^2 u}{ds^2} + \frac{dw}{R\,ds} \\ \frac{d\beta}{ds} + \frac{1}{R}\frac{dv}{ds} \end{Bmatrix} \tag{B1.5}$$

c. The Total Linear Acceleration of the Origin of the Local Body-Fixed Axes

In addition to using the notation that a letter under a vector denotes the coordinate system in which the components are expressed, we will now use the notation that a letter above a vector indicates time differentiation with respect to that coordinate system. Thus I above a vector indicates its time rate of change with respect to inertial space.

The total linear acceleration of the body-fixed axes b in the o coordinate system is thus expressed as

$$\underset{o}{\overline{a_b}} = \underset{o}{\overline{a_c}} + \underset{o}{\overline{\overline{\omega}^I}} \times (\underset{o}{\overline{R}} + \underset{o}{\overline{r}}) + \underset{o}{\overline{\omega}} \times [\underset{o}{\overline{\omega}} \times (\underset{o}{\overline{R}} + \underset{o}{\overline{r}})] + 2\underset{o}{\overline{\omega}} \times \underset{o}{\overline{v}}_{rel} + \underset{o}{\overline{a}}_{rel} \tag{B1.6}$$

where (using Fig. 31):

$\underset{o}{\overline{\omega}}$ = the angular velocity of the rigid body in o coordinates

$$= \begin{Bmatrix} -(\omega_x \cos\gamma + \omega_y \sin\gamma) \\ \omega_z \\ \omega_y \cos\gamma - \omega_x \sin\gamma \end{Bmatrix} \tag{B1.7}$$

$$\overline{r}_o = \begin{Bmatrix} u \\ v \\ w \end{Bmatrix} \tag{B1.8}$$

$\overline{a_c}_o$ = acceleration of the origin of the rigid-body axes: x, y, z

$$= \begin{Bmatrix} -\left(a_{c_x} \cos\gamma + a_{c_y} \sin\gamma\right) \\ a_{c_z} \\ \left(a_{c_y} \cos\gamma - a_{c_x} \sin\gamma\right) \end{Bmatrix} \tag{B1.9}$$

$$\overline{v}_{rel_o} = \begin{Bmatrix} \dot{u} \\ \dot{v} \\ \dot{w} \end{Bmatrix} = \dot{\overline{r}}_o \tag{B1.10}$$

$$\overline{a}_{rel_o} = \begin{Bmatrix} \ddot{u} \\ \ddot{v} \\ \ddot{w} \end{Bmatrix} = \ddot{\overline{r}}_o \tag{B1.11}$$

Considering all quantities small except ω_z and R, Eq. (B1.5) can thus be written in component form as

$$\overline{a_b}_o = \begin{Bmatrix} -\left(a_{c_x} \cos\gamma + a_{c_y} \sin\gamma\right) + \omega_z^2 R - \omega_z^2 u + 2\omega_z \dot{w} + \ddot{u} \\ a_{c_z} - R(\dot{\omega}_y \cos\gamma - \dot{\omega}_x \sin\gamma) + \omega_z R(\omega_x \cos\gamma + \omega_y \sin\gamma) + 0 + \ddot{v} \\ \left(a_{c_y} \cos\gamma - a_{c_x} \sin\gamma\right) + \dot{\omega}_z R - \omega_z^2 w - 2\omega_z \dot{u} + \ddot{w} \end{Bmatrix} \tag{B1.12}$$

The total acceleration of the body axes in the x_b, y_b, z_b coordinates is given by

$$\overline{a_b}_b = \overline{a_b}_o - \overline{\Psi}_o \times \overline{a_b}_o \tag{B1.13}$$

Using Eq. (B.1.2) for $\overline{\Psi}$ and noting that all quantities are small except $R\omega_z^2$ so that their products may be discarded, we obtain

$$\overline{a}_b = \begin{Bmatrix} -\left(a_{c_x} \cos\gamma + a_{c_y} \sin\gamma\right) + \omega_z^2 R - \omega_z^2 u + 2\omega_z \dot{w} + \ddot{u} \\ -\beta R\omega_z^2 + a_{c_z} - R(\dot{\omega}_y \cos\gamma - \dot{\omega}_x \sin\gamma) + \omega_z R(\omega_x \cos\gamma + \omega_y \sin\gamma) + \ddot{v} \\ \left(\frac{\partial u}{\partial s} + \frac{v}{R}\right) R\omega_z^2 + \left(a_{c_y} \cos\gamma - a_{c_x} \sin\gamma\right) + \dot{\omega}_z R - \omega_z^2 w - 2\omega_z \dot{u} + \ddot{w} \end{Bmatrix}_b$$

(B1.14)

2. Derivation of the Equations of Motion of an Element of the Toroid

As indicated by Lang [Ref. 33], "forced-motion solutions of vibrating rings have been given little consideration." Therefore, we will return to Love and extend his basic derivation in a somewhat modified form to fit our problem. Because of the dimensions of the toroid we are considering, it behaves essentially as a ring and therefore has often been referred to as such in this report. In the following derivation we consider the principal axes of the cross section to be, in the undeflected case, in the radial and spin-axis directions. First we derive the linearized equations of equilibrium for an element of the ring. Then we substitute for the stress couples in these equations in terms of the curvature and twist due to deflection. In the third subsection we perturb the equations about a constant spin velocity and internal pressure, and obtain the equations of motion of the element as uncoupled sets of inplane and out-of-plane motions. For convenience we make a change of variable from the distance s around the rim to the nondimensional central angle, γ.

a. Derivation of the Equations of Equilibrium of an Element

Following the nomenclature of Love, we will consider an element of the ring of length ds, as shown in Fig. 32, where x_b, y_b, z_b are body-fixed orthogonal axes. Assuming that a cross section rotates without appreciable distortion:

z_b is the axis along the deflected centroidal line of the ring

x_b is the axis originally along the radius (directed inward)

y_b is the axis originally perpendicular to the plane of the undeflected ring.

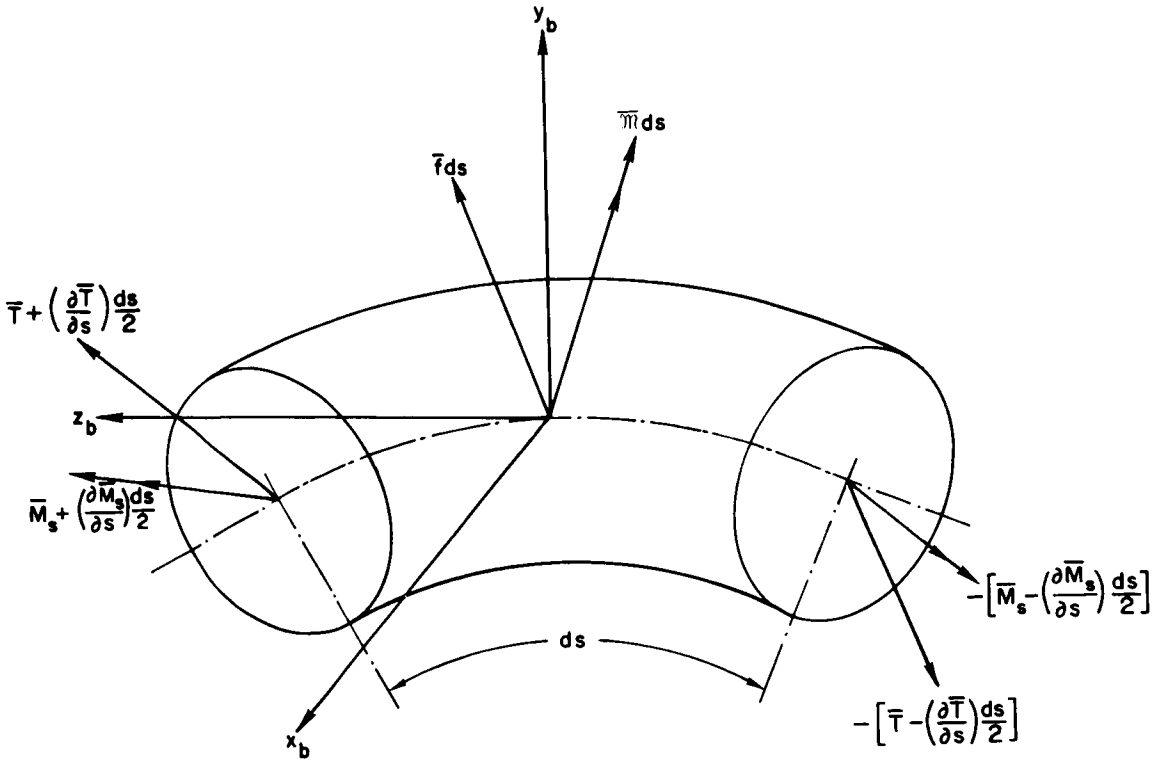

FIG. 32. FORCES AND MOMENTS ACTING ON AN ELEMENT OF THE RING OF LENGTH ds.

The force equation for the element can be written using Newton's law as

$$\overline{\text{force}} = (\text{mass}) \times \overline{\text{acceleration}}$$

$$= \left(\frac{\overline{\partial F}}{\partial s}\right) ds = (mds)\ \overline{a} \qquad \text{(B2.1)}$$

or

$$\overline{f}\ ds + \left[1 + \left(\frac{\overline{\partial\Phi}}{\partial s}\frac{ds}{2}\right)\times\right]\left(\overline{T} + \frac{\overline{\partial T}}{\partial s}\frac{ds}{2}\right) - \left[1 - \left(\frac{\overline{\partial\Phi}}{\partial s}\frac{ds}{2}\right)\times\right]\left(\overline{T} - \frac{\overline{\partial T}}{\partial s}\frac{ds}{2}\right) = (m\ ds)\ \overline{a} \qquad \text{(B2.2)}$$

where

m = mass per unit arc length s along the centroidal line

$\overline{f}$ ds = external force vector acting on the element

$\overline{T}$ = (N, N', T) = traction on the cross section.

Discarding terms in $(ds)^2$ and dividing through by ds yields

$$\bar{f} + \frac{\partial \bar{\Phi}}{\partial s} \times \bar{T} + \frac{\partial \bar{T}}{\partial s} = m\,\bar{a} \tag{B2.3}$$

Writing Eq. (B2.3) in component form, we have

$$\begin{aligned} f_{x_b} + \frac{\partial N}{\partial s} - N'\tau + T\kappa' &= ma_{x_b} \\ f_{y_b} + \frac{\partial N'}{\partial s} - T\kappa + N\tau &= ma_{y_b} \\ f_{z_b} + \frac{\partial T}{\partial s} - N\kappa' + N'\kappa &= ma_{z_b} \end{aligned} \tag{B2.4}$$

Using the D'Alembert principle, the moment equation for the element can be written as

$$\frac{\partial \bar{M}}{\partial s}\, ds = 0 \tag{B2.5}$$

or for ds small, we have from Fig. 32:

$$\bar{\mathfrak{M}}\, ds + \left(1 + \frac{\bar{\Phi}}{2} \times\right)\left(\bar{M}_s + \frac{\partial \bar{M}_s}{\partial s}\frac{ds}{2}\right) - \left(1 - \frac{\bar{\Phi}}{2} \times\right)\left(\bar{M}_s - \frac{\partial \bar{M}_s}{\partial s}\frac{ds}{2}\right)$$

$$+ \frac{d\bar{s}}{2} \times \left(\bar{T} + \frac{\partial \bar{T}}{\partial s}\frac{ds}{2}\right) + \frac{d\bar{s}}{2} \times \left(\bar{T} - \frac{\partial \bar{T}}{\partial s}\frac{ds}{2}\right) + \frac{\partial \bar{M}_{DAL}}{\partial s}\, ds = 0 \tag{B2.6}$$

where

$\bar{\mathfrak{M}}\, ds$ = external moment vector acting on the element

$\bar{M}_s$ = (G, G', H) = stress moment vector acting on the cross section

$\frac{\partial \bar{M}_{DAL}}{\partial s}\, ds$ = D'Alembert moment vector acting on the element due to rotary inertia.

Discarding terms in $(ds)^2$, and dividing through by ds and noting that in the limit

$$\frac{\overline{ds}}{ds} = \bar{1}_{z_b} = \text{unit vector along } z_b \tag{B2.7}$$

we have

$$\bar{\mathfrak{M}} + \frac{\overline{\partial M_s}}{\partial s} + \bar{\Phi} \times \bar{M}_s + \bar{1}_{z_b} \times \bar{T} + \frac{\overline{\partial M_{DAL}}}{\partial s} = 0 \tag{B2.8}$$

Neglecting rotary inertia we can write Eq. (B2.8) in component form as

$$\mathfrak{M}_{x_b} + \frac{\partial G}{\partial s} - G'\tau + H\kappa' - N' = 0$$

$$\mathfrak{M}_{y_b} + \frac{\partial G'}{\partial s} - H\kappa + G\tau + N = 0 \tag{B2.9}$$

$$\mathfrak{M}_{z_b} + \frac{\partial H}{\partial s} - G\kappa' + G'\kappa = 0$$

b. Substitution for the Stress Couples

Using the ordinary approximate theory used by Love, the stress couples are related to the curvature and twist by the following equations for isotropic material

$$G = EI_x(\kappa - \kappa_o)$$

$$G' = EI_y(\kappa' - \kappa'_o) \tag{B2.10}$$

$$H = \mu I_p(\tau - \tau_o)$$

where

E = Young's modulus of elasticity

μ = the shear modulus of elasticity

I_x = area moment of inertia about x_b

I_y = area moment of inertia about y_b

I_p = area moment of inertia about z_b.

Noting from Eqs. (B1.4) and (B1.5) that $(\kappa - \kappa_o)$, $(\kappa' - \kappa_o)$, and $(\tau - \tau_o)$ are small and that κ_o and τ_o are zero, we can substitute Eq. (B2.10) into (B2.9) which reduces it to

$$\mathfrak{M}_{x_b} + EI_x \frac{\partial \kappa}{\partial s} + \mu I_p \tau \kappa_o' - N' = 0$$

$$\mathfrak{M}_{y_b} + EI_y \frac{\partial(\kappa' - \kappa_o')}{\partial s} + N = 0 \qquad \text{(B2.11)}$$

$$\mathfrak{M}_{z_b} + \mu I_p \frac{\partial \tau}{\partial s} - EI_x \kappa \kappa_o' = 0$$

From the first two of these equations we have

$$N' = \mathfrak{M}_{x_b} + EI_x \frac{\partial \kappa}{\partial s} + \mu I_p \tau \kappa_o'$$

$$N = -\mathfrak{M}_{y_b} - EI_y \frac{\partial(\kappa' - \kappa_o')}{\partial s} \qquad \text{(B2.12)}$$

Substituting Eqs. (B2.12) into (B2.4) and again noting that the curvature and twist due to deflection and their derivatives are small, and assuming that $\mathfrak{M}_{x_b}$ and $\mathfrak{M}_{y_b}$ are on the average small, we obtain

$$f_{x_b} - \frac{\partial \mathcal{M}_{y_b}}{\partial s} - EI_y \frac{\partial^2(\kappa' - \kappa_o')}{\partial s^2} + T\kappa' = ma_{x_b}$$

$$f_{y_b} + \frac{\partial \mathcal{M}_{x_b}}{\partial s} + EI_x \frac{\partial^2 \kappa}{\partial s^2} + \mu I_p \kappa_o' \frac{\partial \tau}{\partial s} - T\kappa = ma_{y_b} \qquad \text{(B2.13)}$$

$$f_{z_b} + \kappa_o' \mathcal{M}_{y_b} + \kappa_o' EI_y \frac{\partial(\kappa' - \kappa_o')}{\partial s} + \frac{\partial T}{\partial s} = ma_{z_b}$$

Using the last of Eqs. (B2.11) in the second of Eqs. (B2.13) yields

$$\hat{f}_{x_b} - EI_y \frac{\partial^2(\kappa' - \kappa_o')}{\partial s^2} + T\kappa' = ma_{x_b}$$

$$\hat{f}_{y_b} + EI_x \left[\frac{\partial^2 \kappa}{\partial s^2} + \kappa(\kappa_o')^2 \right] - T\kappa = ma_{y_b} \qquad \text{(B2.14)}$$

$$\hat{f}_{z_b} + \kappa_o' EI_y \frac{\partial(\kappa' - \kappa_o')}{\partial s} + \frac{\partial T}{\partial s} = ma_{z_b}$$

where we have defined

$$\hat{f}_{x_b} \triangleq f_{x_b} - \frac{\partial \mathcal{M}_{y_b}}{\partial s}$$

$$\hat{f}_{y_b} \triangleq f_{y_b} + \frac{\partial \mathcal{M}_{x_b}}{\partial s} - \kappa_o' \mathcal{M}_{z_b} \qquad \text{(B2.15)}$$

$$\hat{f}_{z_b} \triangleq f_{z_b} + \kappa_o' \mathcal{M}_{y_b}$$

Substituting for κ, κ', and τ from Eqs. (B1.4) and (B1.5) in Eqs. (B2.11) and (B2.14) we finally have

$$\boxed{\begin{aligned}
&\hat{f}_{x_b} - EI_y\left(\frac{\partial^4 u}{\partial s^4} + \frac{1}{R}\frac{\partial^3 w}{\partial s^3}\right) + T\left(\frac{1}{R} + \frac{\partial^2 u}{\partial s^2} + \frac{1}{R}\frac{\partial w}{\partial s}\right) = ma_{x_b} \\
&\hat{f}_{y_b} + EI_x\left(\frac{1}{R}\frac{\partial^2 \beta}{\partial s^2} - \frac{\partial^4 v}{\partial s^4} + \frac{\beta}{R^3} - \frac{1}{R^2}\frac{\partial^2 v}{\partial s^2}\right) - T\left(\frac{\beta}{R} - \frac{\partial^2 v}{\partial s^2}\right) = ma_{y_b} \\
&\hat{f}_{z_b} + \frac{EI_y}{R}\left(\frac{\partial^3 u}{\partial s^3} + \frac{1}{R}\frac{\partial^2 w}{\partial s^2}\right) + \frac{\partial T}{\partial s} = ma_{z_b}
\end{aligned}} \qquad \text{(B2.16)}$$

and

$$\boxed{\begin{aligned}
&\mathcal{M}_{x_b} + EI_x\left(\frac{1}{R}\frac{\partial \beta}{\partial s} - \frac{\partial^3 v}{\partial s^3}\right) + \mu I_p\left(\frac{1}{R}\frac{\partial \beta}{\partial s} + \frac{1}{R^2}\frac{\partial v}{\partial s}\right) - N' = 0 \\
&\mathcal{M}_{y_b} + EI_y\left(\frac{\partial^3 u}{\partial s^3} + \frac{1}{R}\frac{\partial^2 w}{\partial s^2}\right) + N = 0 \\
&\mathcal{M}_{z_b} - EI_x\left(\frac{\beta}{R^2} - \frac{1}{R}\frac{\partial^2 v}{\partial s^2}\right) + \mu I_p\left(\frac{\partial^2 \beta}{\partial s^2} + \frac{1}{R}\frac{\partial^2 v}{\partial s^2}\right) = 0
\end{aligned}} \qquad \text{(B2.17)}$$

c. Equations Perturbed about a Constant Spin Velocity and Internal Pressure

If the ring is not vibrating, has no external forces, and is spinning at constant angular velocity $\omega_z \triangleq \Omega$ about an axis at right angles to the plane of the ring, then the conditions at every element are the same. Thus all derivatives with respect to s are zero. Employing this condition in the first of Eqs. (B2.16) and using the accelerations due to spin from Eq. (B1.14), we obtain

$$\frac{T}{R} = m(R - u)\Omega^2 - f_{x_b} \tag{B2.18}$$

where

$$f_{x_b} = -\kappa' SP \tag{B2.19}$$

S = cross-sectional area

P = internal pressure.

Thus if we (1) consider R as the equilibrium radius under constant spin speed Ω and tension SP due to internal pressure, (2) define new u, v, w, f_{x_b} and f_{y_b}, which are equal to zero at equilibrium, (3) let

$$T \triangleq mR^2\Omega^2 + SP + \Delta T \tag{B2.20}$$

and

$$\omega_z \triangleq \Omega + \Delta\omega_z \tag{B2.21}$$

where ΔT and $\Delta\omega_z$ are small (e.g., external tangential forces are small), and (4) dispense with the equations for N and N', then Eqs. (B2.16) and (B2.17) reduce to the two uncoupled sets:

Out-of-Plane Equations

$$\frac{\check{f}_{y_b}(\gamma)}{m(\gamma)}\check{m}_x + R\left(\frac{\partial^2\beta}{\partial\gamma^2} + \beta\right) - \frac{\partial^4 v}{\partial\gamma^4} - \frac{\partial^2 v}{\partial\gamma^2} - \check{m}_x\Omega^2\left(\beta R - \frac{\partial^2 v}{\partial\gamma^2}\right) = \check{m}_x a_{y_b} \tag{B2.22}$$

$$\frac{R^2 \mathcal{M}_{z_b}(\gamma)}{EI_x} + \frac{\partial^2 v}{\partial\gamma^2}\left(1 + \frac{\mu I_p}{EI_x}\right) + R\left(\frac{\mu I_p}{EI_x}\frac{\partial^2\beta}{\partial\gamma^2} - \beta\right) = 0 \tag{B2.23}$$

In-Plane Equations

$$\frac{\breve{m}_y}{m(\gamma)} \breve{f}_{x_b}(\gamma) - \frac{\partial^4 u}{\partial \gamma^4} - \frac{\partial^3 w}{\partial \gamma^3} + \Omega^2 \breve{m}_y \left(R + \frac{\partial^2 u}{\partial \gamma^2} + \frac{\partial w}{\partial \gamma} \right) + \frac{\Delta T}{m(\gamma)} \breve{m}_y = \breve{m}_y a_{x_b} \tag{B2.24}$$

$$\frac{\breve{m}_y}{m(\gamma)} \breve{f}_{z_b}(\gamma) + \frac{\partial^3 u}{\partial \gamma^3} + \frac{\partial^2 w}{\partial \gamma^2} + \frac{\breve{m}_y}{m(\gamma)} \frac{\partial(\Delta T)}{\partial \gamma} = \breve{m}_y a_{z_b} \tag{B2.25}$$

In the above equations we have used the definitions

$$\breve{m}_y = \frac{m(\gamma) R^3}{EI_y} \tag{B2.26}$$

$$\breve{m}_x = \frac{m(\gamma) R^3}{EI_x} \tag{B2.27}$$

where $m(\gamma)$ is the mass per unit angle, γ, and from Eqs. (B2.15), using Eq. (B1.5), we have defined

$$\breve{f}_{y_b}(\gamma) \triangleq f_{y_b}(\gamma) + \frac{1}{R} \left[\frac{\partial \mathcal{M}_{x_b}(\gamma)}{\partial \gamma} - \mathcal{M}_{z_b}(\gamma) \right] \tag{B2.28}$$

$$\breve{f}_{x_b}(\gamma) \triangleq f_{x_b}(\gamma) - \frac{1}{R} \frac{\partial \mathcal{M}_{y_b}(\gamma)}{\partial \gamma} \tag{B2.29}$$

$$\breve{f}_{z_b}(\gamma) \triangleq f_{z_b}(\gamma) + \frac{1}{R} \mathcal{M}_{y_b}(\gamma) \tag{B2.30}$$

where $f(\gamma)$, $\mathcal{M}(\gamma)$ are the force and moment, respectively, per unit angle γ, and we have employed

$$s = R\gamma \tag{B2.31}$$

3. Equations of Motion

From Section 2, we observe that the in-plane and out-of-plane equations are decoupled.* However, coupling might be introduced by the control system. To examine this possibility we make the following observations: To control the angular motions of the spin axis, we apply moments parallel to the plane of the ring, or, equivalently, forces parallel to the spin axis. To first order, these moments or forces have no effect on the in-plane motion. Similarly, to sense the angular motion of the spin axis, we use attitude or rate sensors having input axes parallel to the plane of the ring. Again to first order, these do not sense in-plane motions. Therefore the only portion of the flexural motion directly excited or sensed by the control system is the out-of-plane motion and thus for the rest of this study we need only consider the out-of-plane motion due to flexure. This flexure can be represented by the linear deflection $z(\gamma,t)$ and the twist $\beta(\gamma,t)$ of the centroidal line of the ring, as shown in Fig. 30.

Using the approach of Appendix A, we may solve the unforced equations of motion for their natural frequencies and mode shapes of free vibration, and obtain the equations of forced motion in terms of their mode shapes. Though we only present complete results for the out-of-plane motion, it is interesting to examine the in-plane vibration because of the Coriolis forces discussed in Appendix A.

a. Solution of the Unforced Equations of In-Plane Motion

The free vibration equations of in-plane motion are obtained from Eqs. (B2.24) and (B2.25), by employing Eq. (B1.14) for the acceleration (considering the base plane fixed and rotating at constant angular velocity Ω), as

$$\breve{m}_y \frac{\partial^2 u}{\partial t^2} = \left\{\left[\Delta T \frac{\breve{m}_y}{m(\gamma)} - \frac{\partial^4 u}{\partial \gamma^4} - \frac{\partial^3 w}{\partial \gamma^3}\right] + \Omega^2 \breve{m}_y \left(\frac{\partial^2 u}{\partial \gamma^2} + \frac{\partial w}{\partial \gamma} + u\right)\right\} - \breve{m}_y \left(2\Omega \frac{\partial w}{\partial t}\right) \tag{B3.1}$$

*This effect may be illustrated easily for the nonrotating case by taking an inflated English bicycle tube and shaking it appropriately to produce both rigid-body and flexural motions in each of the two regimes and observing that the in-plane and out-of-plane motions are uncoupled.

$$\breve{m}_y \frac{\partial^2 w}{\partial t^2} = \left\{\left[\frac{\partial \Delta T}{\partial \gamma} \frac{\breve{m}_y}{m(\gamma)} + \frac{\partial^3 u}{\partial \gamma^3} + \frac{\partial^2 w}{\partial \gamma^2}\right] - \Omega^2 \breve{m}_y \left(\frac{\partial u}{\partial \gamma}\right)\right\} + \breve{m}_y \left(2\Omega \frac{\partial u}{\partial t}\right) \qquad \text{(B3.2)}$$

Observe that Eqs. (B3.1) and (B3.2) are simply the in-plane components of Eq. (A.9), with the Coriolis term of Eq. (A.7) included.

Love indicates that for the nonrotating case, the solutions to these equations are separable into modes in which the centroidal line is unextended and much higher frequency modes involving extension of the centroidal line. As we do not intend to directly apply forces in the in-plane direction for attitude control, excitation of in-plane motions should be small, so we will only concern ourselves with the inextensible modes.

The conditions for nonextension of the centroidal line is given by Eq. (8), page 448 of Love, as

$$\frac{\partial w}{\partial \gamma} = u \qquad \text{(B3.3)}$$

Eliminating $\partial \Delta T/\partial \gamma$ between Eqs. (B3.1) and (B3.2) and making use of Eq. (B3.3), we obtain

$$- \frac{\partial^6 w}{\partial \gamma^6} - 2 \frac{\partial^4 w}{\partial \gamma^4} - \frac{\partial^2 w}{\partial \gamma^2} + \Omega^2 \breve{m}_y \left(\frac{\partial^4 w}{\partial \gamma^4} + 3 \frac{\partial^2 w}{\partial \gamma^2}\right)$$

$$- 4\Omega \breve{m}_y \frac{\partial^2 w}{\partial \gamma \partial t} + \breve{m}_y \left(\frac{-\partial^4 w}{\partial t^2 \partial \gamma^2} + \frac{\partial^2 w}{\partial t^2}\right) = 0 \qquad \text{(B3.4)}$$

Equation (B3.4) is not separable, but noting from Love that the eigenfunctions for the nonrotating case are sines and cosines of $n\gamma$, we shall seek solutions of the form

$$w(\gamma, t) = T_1(t) \sin n\gamma + T_2(t) \cos n\gamma \qquad \text{(B3.5)}$$

Substituting Eq. (B3.5) in Eq. (B3.4) yields

$$[T_1(t)\sin n\gamma + T_2(t)\cos n\gamma]\left[n^6 - 2n^4 + n^2 + \Omega^2\breve{m}_y(n^4 - 3n^2)\right]$$

$$- 4\Omega\breve{m}_y n\left[\frac{\partial T_1(t)}{\partial t}\cos n\gamma - \frac{\partial T_2(t)}{\partial t}\sin n\gamma\right]$$

$$+ \breve{m}_y\left[\frac{\partial^2 T_1(t)}{\partial t^2}\sin n\gamma + \frac{\partial^2 T_2(t)}{\partial t^2}\cos n\gamma\right][n^2 + 1] = 0 \qquad \text{(B3.6)}$$

If we define the square of the natural frequency, neglecting the Coriolis forces, as

$$p_n^2 \triangleq \frac{n^2(n^2 - 1)^2}{\breve{m}_y(n^2 + 1)} + \Omega^2\,\frac{n^2(n^2 - 3)}{(n^2 + 1)}\ ^{\dagger} \qquad \text{(B3.7)}$$

and

$$\Delta p_n \triangleq \frac{2\Omega n}{(n^2 + 1)} \qquad \text{(B3.8)}$$

we may write Eq. (B3.6) as

$$\left[\frac{\partial^2 T_1(t)}{\partial t^2}\sin n\gamma + \frac{\partial^2 T_2(t)}{\partial t^2}\cos n\gamma\right] - 2\Delta p_n\left[\frac{\partial T_1(t)}{\partial t}\cos n\gamma - \frac{\partial T_2(t)}{\partial t}\sin n\gamma\right]$$

$$+ p_n^2[T_1(t)\sin n\gamma + T_2(t)\cos n\gamma] = 0 \qquad \text{(B3.9)}$$

---

†Observe that the negative frequency (or instability) for the rigid mode (n = 1) arises because we have assumed the base plane (and center of rotation) fixed. The rigid-mode instability disappears if we consider the coupling with the rigid base plane accelerations, $\bar{a}_c$. The first two modes (n = 0 and 1) have zero bending frequency contributions and are large and small rigid-body translations respectively. As this is incorporated in the motion of the plane xy, we need not consider them.

Since Eq. (B3.9) must hold for all γ, the coefficients of $\sin n\gamma$ and $\cos n\gamma$ must each be individually zero, so that we obtain

$$\left[\frac{\partial^2 T_1(t)}{\partial t^2} + p_n^2 T_1(t)\right] + 2\Delta p_n \frac{\partial T_2(t)}{\partial t} = 0 \qquad \text{(B3.10)}$$

$$\left[\frac{\partial^2 T_2(t)}{\partial t^2} + p_n^2 T_2(t)\right] - 2\Delta p_n \frac{\partial T_1(t)}{\partial t} = 0 \qquad \text{(B3.11)}$$

Defining

$$T(t) \triangleq T_1(t) + jT_2(t) \qquad \text{(B3.12)}$$

we may write Eqs. (B3.10) and (B3.11) as

$$\frac{\partial^2 T(t)}{\partial t^2} + p_n^2 T(t) - j2\Delta p_n T(t) = 0 \qquad \text{(B3.13)}$$

Taking the Laplace transform of Eq. (B3.13) yields

$$\left[s^2 - 2j\Delta p_n s + p_n^2\right]T(s) = [s - 2j\Delta p_n]T(0) + \dot{T}(0) \qquad \text{(B3.14)}$$

The roots of the associated characteristic equation are

$$s = j\left[\Delta p_n \pm p_n\sqrt{1 - (\Delta p_n/p_n)^2}\,\right] \qquad \text{(B3.15)}$$

By defining

$$p_n' \triangleq p_n\sqrt{1 - (\Delta p_n/p_n)^2} \qquad \text{(B3.16)}$$

these reduce to:†

$$s = j(p_n' + \Delta p_n),\ j(-p_n' + \Delta p_n) \tag{B3.17}$$

Thus we can write Eq. (B3.14) as

$$T(s) = \frac{[s - 2j\Delta p_n]T(0) + \dot{T}(0)}{[s - j(p_n' + \Delta p_n)][s - j(-p_n' + \Delta p_n)]} \tag{B3.18}$$

Taking the inverse Laplace transform, we have

$$T(t) = \left[T(0)\left(\cos p_n' t - j\,\frac{\Delta p_n}{p_n'}\sin p_n' t\right) + \frac{\dot{T}(0)}{p_n'}\sin p_n' t\right]\exp(j\Delta p_n t) \tag{B3.19}$$

Substituting from Eq. (B3.19) into Eq. (B3.5), we obtain

$$w_n(\gamma,t) = \left\{T_1(0)\cos p_n' t + \left[\frac{\dot{T}_1(0)}{p_n'} + T_2(0)\,\frac{\Delta p_n}{p_n'}\right]\sin p_n' t\right\}\sin(n\gamma + \Delta p_n t)$$

$$+ \left\{T_2(0)\cos p_n' t + \left[\frac{\dot{T}_2(0)}{p_n'} - T_1(0)\,\frac{\Delta p_n}{p_n'}\right]\sin p_n' t\right\}\cos(n\gamma + \Delta p_n t) \tag{B3.20}$$

Observe that the presence of the Coriolis terms causes the following:

1. A reduction of the natural in-plane frequency p_n.
2. Coupling of the in-plane sine and cosine modes.
3. Precession of the in-plane vibration around the ring with the frequency Δp_n.

---

†Reference 36 shows that for the case of a rotating disk, the Coriolis forces produce coupling between the radial and tangential types of vibration and that the radial vibration frequencies are increased, whereas the tangential vibration frequencies are decreased.

b. Summary of the Differential Equations of Motion Considering Out-of-Plane Vibration

We may conveniently summarize the differential equations of motion as follows:†

(1) Translation

$$M\ddot{X}_c = \int_0^{2\pi} \breve{f}_x(\gamma)\, d\gamma \cos\psi - \int_0^{2\pi} \breve{f}_y(\gamma)\, d\gamma \sin\psi \qquad \text{(B3.21)}$$

$$M\ddot{Y}_c = \int_0^{2\pi} \breve{f}_x(\gamma)\, d\gamma \sin\psi + \int_0^{2\pi} \breve{f}_y(\gamma)\, d\gamma \cos\psi \qquad \text{(B3.22)}$$

$$M\ddot{Z}_c = \int_0^{2\pi} \breve{f}_z(\gamma)\, d\gamma \qquad \text{(B3.23)}$$

(2) Rotation

$$\ddot{\phi} + 2\dot{\theta}\dot{\psi} = \frac{R}{A} \int_0^{2\pi} \breve{f}_z(\gamma)\, (\sin\gamma \cos\psi + \cos\gamma \sin\psi)\, d\gamma \qquad \text{(B3.24)}$$

$$\ddot{\theta} - 2\dot{\phi}\dot{\psi} = \frac{R}{A} \int_0^{2\pi} \breve{f}_z(\gamma)\, (\sin\gamma \sin\psi - \cos\gamma \cos\psi)\, d\gamma \qquad \text{(B3.25)}$$

$$\ddot{\psi} = \frac{-R}{2A} \int_0^{2\pi} \breve{f}_x(\gamma) \sin\gamma\, d\gamma + \frac{R}{2A} \int_0^{2\pi} \breve{f}_y(\gamma) \cos\gamma\, d\gamma \qquad \text{(B3.26)}$$

(3) Out-of-Plane Vibration

$$\ddot{q}_{ns} + 2\zeta_n p_n \dot{q}_{ns} + p_n^2 q_{ns} = \frac{2}{M} \int_0^{2\pi} \breve{f}_z(\gamma) \sin n\gamma\, d\gamma \triangleq Q_{ns} \qquad (n \geq 2)$$

(B3.27)

†The symbols are defined in Section b.(4).

$$\ddot{q}_{nc} + 2\zeta_n p_n \dot{q}_{nc} + p_n^2 q_{ns} = \frac{2}{M} \int_0^{2\pi} \check{f}_z(\gamma) \cos n\gamma \, d\gamma \triangleq Q_{nc} \qquad (n \geq 2)$$

(B3.28)

where

$$\int_0^{2\pi} \check{f}_z \sin n\gamma \, d\gamma = \int_0^{2\pi} f_z \sin n\gamma \, d\gamma$$

$$+ \int_0^{2\pi} \frac{M'_x}{R} (n \cos n\gamma \cos \gamma + \sin n\gamma \sin \gamma) \, d\gamma$$

$$+ \int_0^{2\pi} \frac{M'_y}{R} (n \cos n\gamma \sin \gamma - \sin n\gamma \cos \gamma) \, d\gamma$$

(B3.29)

$$\int_0^{2\pi} \check{f}_z \cos n\gamma \, d\gamma = \int_0^{2\pi} f_z \cos n\gamma \, d\gamma$$

$$+ \int_0^{2\pi} \frac{M'_x}{R} (-n \sin n\gamma \cos \gamma + \cos n\gamma \sin \gamma) \, d\gamma$$

$$+ \int_0^{2\pi} \frac{M'_y}{R} (-n \sin n\gamma \sin \gamma - \cos n\gamma \cos \gamma) \, d\gamma$$

(B3.30)

and where we have used the following modal expansions for flexure:

$$z(\gamma,t) = \sum_{n=2}^{N} q_{ns}(t) \sin n\gamma + \sum_{n=2}^{N} q_{nc}(t) \cos n\gamma \triangleq \sum_{n=2}^{N} z_n \qquad (B3.31)$$

$$\beta(\gamma,t) = \sum_{n=2}^{N} B_n q_{ns}(t) \sin n\gamma + \sum_{n=2}^{N} B_n q_{nc}(t) \cos n\gamma \triangleq \sum_{n=2}^{N} \beta_n \qquad (B3.32)$$

For isotropic structural material and a symmetric cross section

$$p_n^2 = \frac{n^2(n^2 - 1)^2}{\check{m}(n^2 + 1 + \sigma)} + n^2\Omega^2 \qquad \text{(B3.33)}$$

$$B_n = -\frac{1}{R}\frac{(2 + \sigma)}{[1 + (1+\sigma)/n^2]} \qquad \text{(B3.34)}$$

(4) Notation

The symbols used in these equations are either defined by Fig. 30 or are given below:

$$M = 2\pi\, m(\gamma) = \text{mass of the station} \qquad \text{(B3.35)}$$

$$A = \frac{MR^2}{2} = \text{mass moment of inertia of the station about a diameter} \qquad \text{(B3.36)}$$

$$\check{m} = \frac{m(\gamma)R^3}{EI} \qquad \text{(B3.37)}$$

$m(\gamma)$ = mass per unit angle of the station rim

$\check{f}_i(\gamma)$ = equivalent force per unit angle in the i^{th} direction (includes the actual force and the apparent force per unit angle due to the position rate of change of the moment distribution)

$M_i'(\gamma)$ = rate of change with respect to γ of the moments in the i^{th} direction

$f_i(\gamma)$ = force per unit angle in the i^{th} direction

ζ_n = structural damping ratio of the n^{th} mode of vibration

p_n = natural frequency of the n^{th} mode of vibration

σ = Poisson's ratio

E = Young's modulus for the structural material

I = area moment of inertia of the cross section about the radial axis

$z_n(\gamma,t)$ = deflection of the n^{th} out-of-plane mode of vibration

$B_n = (\beta_n/Z_n)$ = ratio of twist to deflection for the n^{th} out-of-plane mode of vibration

Ω = spin speed, equilibrium value of $\dot{\psi}$.

Observe that the natural frequency may also be obtained by employing Eq. (A.37) as follows:

For our problem, the potential energy of the n^{th} mode can be written for free out-of-plane vibration as

$$V_n = \frac{1}{2}\int_0^{2\pi} EI(\kappa - \kappa_o)_n^2 R\, d\gamma + \frac{1}{2}\int_0^{2\pi} \mu I_p(\tau - \tau_o)_n^2 R\, d\gamma - \frac{1}{2}\int_0^{2\pi}\left[m(\gamma)\Omega^2 \frac{\partial^2 z_n}{\partial\gamma^2}\right] z_n\, d\gamma \quad (B3.38)$$

where μ is the torsional rigidity of the structural material and I_p is the polar area moment of inertia of the cross-sectional structure.

Using Eqs. (B3.31), (B3.38), (B1.4), (B1.5) and (A.31) in Eq. (A.37) and noting that

$$|\bar{w}| \equiv z(\gamma) \quad (B3.39)$$

we obtain

$$p_n^2 = \frac{n^2(n^2-1)^2}{\breve{m}[(EI/\mu I_p) + n^2]} + n^2\Omega^2 \quad (B3.40)$$

in which we have employed

$$B_n = -\frac{n^2}{R}\,\frac{[1 + (\mu I_p/EI)]}{\left[1 + (\mu I_p/EI)n^2\right]} \tag{B3.41}$$

For isotropic structural material

$$E = 2\mu(1 + \sigma) \tag{B3.42}$$

and for a symmetric cross section

$$I = \frac{I_p}{2} \tag{B3.43}$$

so that Eq. (B3.40) reduces to Eq. (B3.33) as required.

4. Values of Parameters

An indication of the values of the parameters may be obtained as follows:

a. Natural Frequencies of the Station

We will relate the natural frequencies of the station to the spin speed Ω which is the rigid-body frequency.

From Eq. (B3.33) we can write the ratio of the square of the n^{th} natural frequency to spin speed as

$$\frac{p_n^2}{\Omega^2} = n^2\left[1 + \frac{(n^2 - 1)^2}{n^2 + 1 + \sigma}\left(\frac{1}{m(\gamma)\,\Omega^2 R}\right)\frac{EI}{R^2}\right] \tag{B4.1}$$

For an artificial g level of one-third of an earth g, we have that

$$m(\gamma)\,\Omega^2 R = m(\gamma)\,\frac{g}{3} = \frac{W(\gamma)}{3} \tag{B4.2}$$

where $W(\gamma)$ is the earth weight of the station cross section per unit angle.

The structural area moment of inertia of the cross section for a monocoque shell is given by

$$I = \frac{A}{2}\left(\frac{d}{2}\right)^2 \equiv \frac{A}{2}\left(\frac{d}{2R}\right)^2 R^2 \qquad \text{(B4.3)}$$

where

$d \triangleq$ diameter of the cross section

$A \triangleq$ structural area of the cross section.

However we may express A as

$$A = \frac{W_s(s)}{\rho_s} \triangleq \frac{W_s(\gamma)}{\rho_s R} \qquad \text{(B4.4)}$$

where

$W_s(s)$ = weight of the structure per unit length of perimeter

ρ_s = weight density of the structural material.

Substituting Eqs. (B4.2) - (B4.4) in Eq. (B2.1), we have

$$\frac{p_n^2}{\Omega^2} = n^2 \left\{ 1 + \frac{3(n^2 - 1)^2 (d/2R)^2}{n^2 + 1 + \sigma} \left[\left(\frac{E}{\rho_s}\right) \left(\frac{W_s(\gamma)}{W(\gamma)}\right) \frac{1}{2R} \right] \right\} \qquad \text{(B4.5)}$$

If we use nominal values of

$$\frac{W_s(\gamma)}{W(\gamma)} = 0.1$$

$$R = 85 \text{ ft} \times 12 \cong 1000 \text{ in.}$$

$$\sigma = 0.3$$

$$d = 10 \text{ ft} \times 12 = 120 \text{ in.}$$

then Eq. (B4.5) becomes

$$\frac{p_n^2}{\Omega^2} \cong n^2 \left[1 + 0.5 \, \frac{10^{-6}(n^2 - 1)^2}{n^2 + 1.3} \, \frac{E}{\rho_s} \right] \tag{B4.6}$$

For materials like aluminum, which have a high stiffness-to-weight ratio

$$\frac{E}{\rho_s} \approx \frac{10^7 \text{ psi}}{0.1 \text{ lb/in.}^3} = 10^8 \text{ in.} \tag{B4.7}$$

Thus using Eq. (B4.7) in Eq. (B4.6) to obtain an upper limit on the frequency ratio, we have

$$\left(\frac{p_n}{\Omega} \right)^2 \leqq n^2 \left\{ 1 + 50 \left[\frac{(n^2 - 1)^2}{n^2 + 1.3} \right] \right\} \tag{B4.8}$$

A lower limit might be established by considering an E/ρ_s of $1/50$ in Eq. (B4.7) to obtain

$$\frac{p_n^2}{\Omega^2} \geqq n^2 \left[1 + \frac{(n^2 - 1)^2}{n^2 + 1.3} \right] \tag{B4.9}$$

Thus for $n \geqq 3$, we may roughly approximate the limits of p_n^2/Ω^2 as

$$\boxed{n^4 \leqq \frac{p_n^2}{\Omega^2} \leqq 50 \, n^4} \qquad n \geqq 3 \tag{B4.10}$$

As a check on this range of p_n^2/Ω^2, we may proceed as follows. We may write the equilibrium tension along the centroidal line of the cross section as

$$T = m(\gamma)\, R\Omega^2 + SP \tag{B4.11}$$

where

S = area of station cross section

P = internal pressure of station.

The elongation per unit length along the centroidal line is given by

$$e = \frac{T}{AE} \tag{B4.12}$$

Thus using Eqs. (B4.2) and (B4.12) in (B4.11), we have

$$AE = \frac{T}{e} = \frac{W(\gamma)/3 + SP}{e} \tag{B4.13}$$

Using Eqs. (B4.2), (B4.3) and (B4.13) in Eq. (B4.1), we obtain

$$\frac{p_n^2}{\Omega^2} = n^2 \left\{ 1 + \frac{(n^2 - 1)^2}{n^2 + 1 + \sigma} \left[\frac{1 + \frac{3SP}{W(\gamma)}}{2e} \left(\frac{d}{2R} \right)^2 \right] \right\} \tag{B4.14}$$

The station cross-sectional area and weight can be expressed as

$$S = \pi\left(\frac{d}{2}\right)^2 \equiv \pi R^2 \left(\frac{d}{2R}\right)^2 \tag{B4.15}$$

$$W(\gamma) = \frac{W}{2\pi} \tag{B4.16}$$

where W is the earth weight of the station.

Using Eqs. (B4.5) and (B4.6) yields

$$\frac{3SP}{W(\gamma)} = \frac{6\pi^2 R^2 (d/2R)^2 P}{W} \tag{B4.17}$$

If we use Eq. (B4.17) in Eq. (B4.14), and let

W = 150,000 lb

P = 7.5 psi (an enriched atmosphere of lower pressure being used to retard leakage)

and then use the other nominal values for the parameters, we obtain:

$$\frac{p_n^2}{\Omega^2} = n^2 \left\{ 1 + \left[\frac{(n^2 - 1)^2}{n^2 + 1 + \sigma} \right] \frac{0.02}{e} \right\} \tag{B4.18}$$

If we allow an e, due to equilibrium tension, of 0.0005 for the stiffer materials and 0.02 for the softer materials, we find the upper and lower bounds for p_n^2/Ω^2 as

$$\frac{p_n^2}{\Omega^2} \leqq n^2 \left[1 + \frac{40(n^2 - 1)^2}{n^2 + 1 + \sigma} \right] \tag{B4.19}$$

$$\frac{p_n^2}{\Omega^2} \geqq n^2 \left[1 + \frac{(n^2 - 1)^2}{n^2 + 1 + \sigma} \right] \tag{B4.20}$$

Thus the expression of Eq. (B4.10) appears to be a reasonable approximation and therefore has been used throughout this study.

b. Structural Damping

Though the equivalent viscous structural damping ratio ζ_n is usually considered to increase with frequency, we shall consider it to be the same for all frequencies.

We shall assume that

$$0.02 \leq \zeta_n \leq 0.2 \qquad \text{(B4.21)}$$

with the lower values corresponding to materials with a high stiffness-to-weight ratio, and the higher values corresponding to materials with a low stiffness-to-weight ratio.

APPENDIX C. SYNTHESIS OF A LINEAR CONTROL SYSTEM AND THE EFFECTS OF FLEXIBILITY ON THE OUTPUT OF THE FEEDBACK SENSOR

In synthesizing the control of flexible missiles and similar vehicles, it is common to first formulate the control system assuming the vehicle rigid. Then the effects of flexibility on the system are determined, and suitable modifications to the control are made to obtain the desired performance in the presence of flexibility. We follow a similar approach.

Though many systems have been conceived for the control of the spin axis of a rigid spinning satellite [Refs. 45-58], the one suggested by Lange [Ref. 39]* appears to be among the most straightforward and useful approaches to the problem when we consider a continuous linear control system. We therefore essentially follow that derivation with the modifications necessary to apply it to our system.

Having determined a suitable control system for the rigid vehicle, we then determine the quantities actually sensed by the feedback instruments when flexibility is included.

In Section 1 below we employ complex variable theory to simplify the equations of the angular motion of the spin axis. In Section 2 we incorporate a control law. Section 3 contains a discussion of the mechanization of the control system. In Section 4 we determine the quantities actually sensed by the feedback instruments.

1. Transformation of the Equations of Angular Motion

Equations (B3.24) and (B3.25) for the angular motion of the spin axis can be written as

$$\ddot{\phi} + 2\dot{\theta}\dot{\psi} = \left[\frac{R}{A}\int_0^{2\pi} \breve{f}_z(\gamma)\,\sin\gamma\,d\gamma\right]\cos\psi + \left[\frac{R}{A}\int_0^{2\pi} \breve{f}_z(\gamma)\,\cos\gamma\,d\gamma\right]\sin\psi \tag{C.1}$$

$$\ddot{\theta} - 2\dot{\phi}\dot{\psi} = \left[\frac{R}{A}\int_0^{2\pi} \breve{f}_z(\gamma)\,\sin\gamma\,d\gamma\right]\sin\psi - \left[\frac{R}{A}\int_0^{2\pi} \breve{f}_z(\gamma)\,\cos\gamma\,d\gamma\right]\cos\psi \tag{C.2}$$

*Lobel [Ref. 44] uses a similar control law but his presentation lacks the excellent analytical justification of Lange.

Defining the small vector angle of the spin axis as

$$\alpha = \phi + j\theta \tag{C.3}$$

then multiplying Eq. (C.2) by j and adding it to Eq. (C.1), we have

$$\ddot{\alpha} - 2j\dot{\psi}\dot{\alpha} = (Q_x + jQ_y)\, e^{j\psi} \triangleq Q\, e^{j\psi} \tag{C.4}$$

where Q is the vector moment expressed in the body-fixed coordinates divided by the moment of inertia. Its components are

$$Q_x = \frac{R}{A} \int_0^{2\pi} \check{f}_z(\gamma) \sin\gamma \, d\gamma \tag{C.5}$$

$$Q_y = -\frac{R}{A} \int_0^{2\pi} \check{f}_z(\gamma) \cos\gamma \, d\gamma \tag{C.6}$$

Equation (C.4) is the vector equation for the motion of the spin axis written in inertial coordinates. However, it is difficult to work with because of the presence of j.

For our problem, we can obtain a single vector equation without the j if we write α in the body frame. Thus, as indicated in Fig. 33, we define the small vector angle of the spin vector in body coordinates as

$$\mu \triangleq \alpha\, e^{-j\psi} \tag{C.7}$$

Using Eq. (C.7), we can rewrite Eq. (C.4) as*

$$\ddot{\mu} + \dot{\psi}^2 \mu = Q \tag{C.8}$$

*Lange indicates that a somewhat more complex equation results when the moment-of-inertia ratios of the station are other than 2.

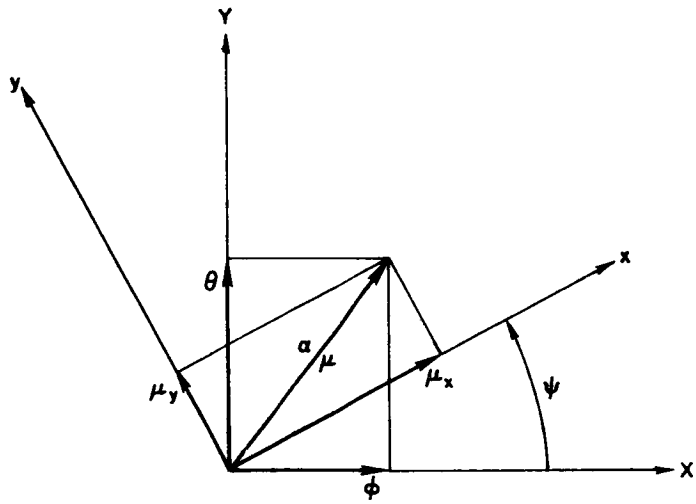

NOTE THAT IN THE ROTATING SYSTEM α APPEARS TO BE ROTATING CLOCKWISE WITH VELOCITY $\dot{\psi}$, OR

$$\mu = \alpha\, e^{-j\dot{\psi}t} = \alpha\, e^{-j\psi}$$

FIG. 33. RELATIONSHIP OF THE SMALL VECTOR ANGLE OF THE SPIN AXIS POSITION IN NONROTATING AND ROTATING FRAMES.

which is the simple vector equation for the angle of the spin axis as written in body coordinates. Thus as seen from the rotating system the vector angle μ (the angle of the spin axis referenced to inertial space) oscillates at $\dot{\psi}$ with a natural period of once per revolution.

2. Incorporation of a Control Law

The forcing function Q may be broken up into a control moment and a disturbance moment

$$Q = Q_c + Q_D \tag{C.9}$$

For a simple system such as Eq. (C.8), it is natural to assume the standard control law

$$Q_c = -K_v\dot{\mu} - K_p\mu \tag{C.10}$$

where K_v is the velocity gain and K_p is the position gain.

Thus Eq. (C.8) becomes

$$\ddot{\mu} + K_v\dot{\mu} + \left(\Omega^2 + K_p\right)\mu = Q_D \qquad (C.11)$$

where, for the variation in $\dot{\psi}$ small, $\dot{\psi}$ has been replaced by the nominal spin speed Ω.

The characteristic equation of Eq. (C.11) is

$$s^2 + K_v s + \left(\Omega^2 + K_p\right) = 0 \qquad (C.12)$$

where s is the Laplace operator for equations in rotating coordinates.

Equation (C.12) can be written in the form

$$1 + K_v \frac{s}{s^2 + \left(\Omega^2 + K_p\right)} = 0 \qquad (C.13)$$

for which the root locus is given in Fig. 34 as a function of K_v. It is observed that μ (and equivalently, its real and imaginary parts, μ_x and μ_y) is stable for all positive values of K_p and K_v.

Note that μ is asymptotically stable for $K_v = 2\left(K_p + \Omega^2\right)^{1/2}$ so that to an observer on the station (for this value of K_v) a spin-axis-angle error would be decreasing exponentially in a nonoscillatory fashion. However in inertial space, at this value of K_v, the spin axis would be spiraling in with a rotational frequency equal to spin rate. To observe this let us turn our attention back to α. From Eq. (C.7)

$$\alpha = \mu\, e^{j\Omega t} \qquad (C.14)$$

so that

$$\mathcal{L}\{\alpha\}(s) = \mathcal{L}\{\mu\}(s - j\Omega) \qquad (C.15)$$

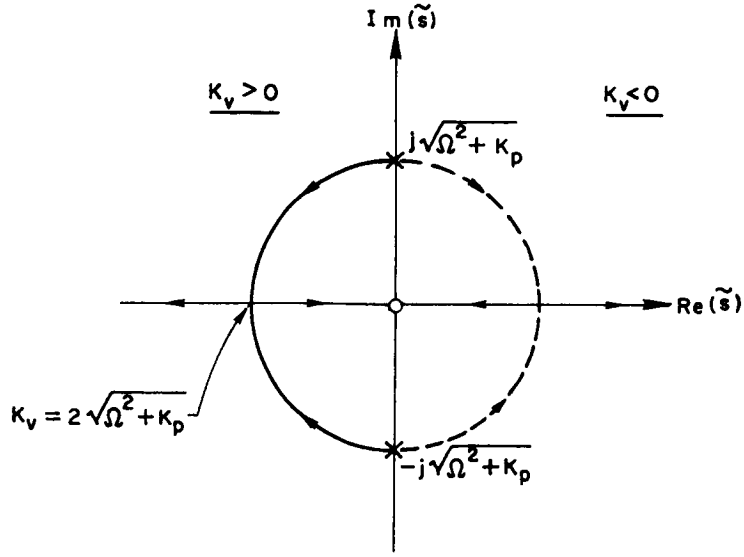

CHARACTERISTIC EQUATION: $1 + K_v \dfrac{s}{s^2 + (\Omega^2 + K_p)} = 0$

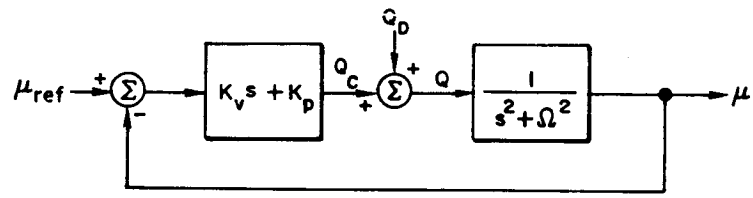

35586

FIG. 34. CHARACTERISTIC ROOTS OF μ (THE ANGLE OF THE SPIN VECTOR IN BODY COORDINATES).

Therefore the root locus for α is simply the root locus for μ (given in Fig. 34) shifted upward by Ω, as indicated in Fig. 35.

3. Mechanization

The control given in Eq. (C.10) could be mechanized using a body-fixed star tracker to measure μ directly, with $\dot{\mu}$ being derived from it. The star-tracker angle rate $\dot{\mu}$ may also be obtained by observing from the Coriolis law that

$$\dot{\mu} = q - \Omega \times \mu = q - j\Omega\mu \qquad \text{(C.16)}$$

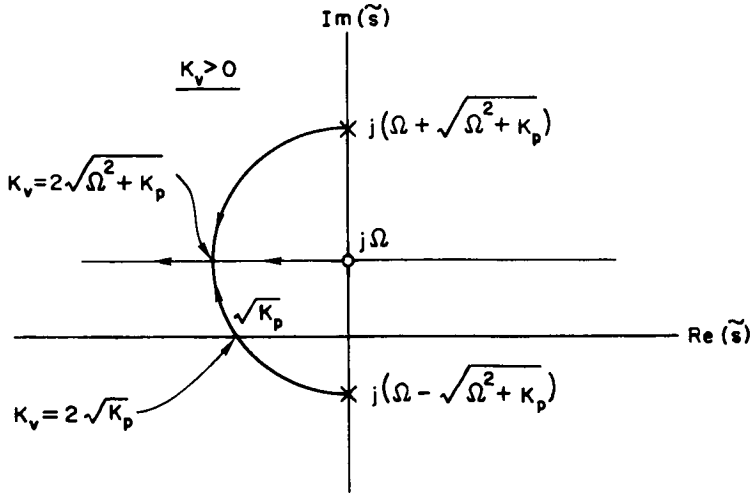

CHARACTERISTIC EQUATION: $1 + K_v \frac{s - j\Omega}{s^2 - 2j\Omega s + K_p} = 0$

35587

FIG. 35. CHARACTERISTIC ROOTS OF α (THE ANGLE OF THE SPIN VECTOR IN INERTIAL COORDINATES).

where the in-plane angular velocity vector q is given by

$$q = \omega_x + j\omega_y \tag{C.17}$$

Thus Eq. (C.10) could be written as

$$Q_c = -K_v\dot{\mu} - K_p\mu$$

$$= -K_v q - (K_p - jK_v\Omega)\mu \tag{C.18}$$

The components of q could be obtained directly by body-mounted rate gyros with input axes along x and y, thus no differentiation of μ need be required: however, a knowledge of Ω is necessary and a complication of the control system results due to the crossproduct term. However $-K_v q$ could be provided by a rate damper, so that a reduction of

the active control force could be realized, and the system could be passive, except when we desire to control μ.

If we just have a passive control system, then

$$Q_c = -K_v q = -K_v(\dot{\mu} + j\Omega\mu) \tag{C.19}$$

and Eq. (C.8) becomes

$$\ddot{\mu} + K_v\dot{\mu} + \left(\Omega^2 + j\Omega K_v\right)\mu = Q_D \tag{C.20}$$

The characteristic equation of (C.20) is

$$s^2 + K_v s + \left(\Omega^2 + j\Omega K_v\right) = 0 \tag{C.21}$$

or

$$1 + K_v \frac{s + j\Omega}{s^2 + \Omega^2} = 0 \tag{C.22}$$

The root loci of Eq. (C.22) is given in Fig. 36. It is observed that the system is stable for all values of K_v, and in the rotating system the vector μ rotates at once per revolution and approaches a limit cycle which corresponds to a fixed vector α in inertial space.

4. Quantities Actually Sensed by the Attitude and Rate Instruments When Flexibility Is Considered

In Section 2 we found that the control law could be expressed by

$$Q_c = -K_v\dot{\mu} - K_p\mu \tag{C.23}$$

or

$$Q_c = -K_v q - (K_p - K_v\dot{\psi}\times)\mu \tag{C.24}$$

which were written for zero reference conditions.

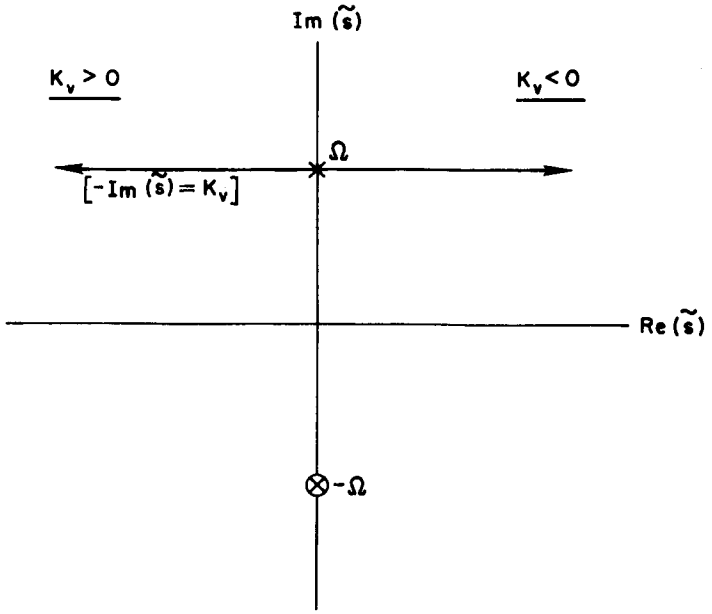

$$\mu \text{ CHARACTERISTIC EQUATION} = 1 + K_v \frac{s+j\Omega}{s+j\Omega)(s-j\Omega} = 0$$

35588

FIG. 36. ROOT LOCI FOR A RATE-DAMPED SYSTEM CONSIDERED IN A ROTATING FRAME.

From Fig. 31 we note that

$$\check{f}_{yb} \cong \check{f}_z \tag{C.25}$$

so that the effect of deflection on the magnitude of the body-fixed control force is negligible. Thus the effect of deflection on the values of the control system quantities must be only through the sensors which read μ and q.

For small deflections the sensed μ and q are given by

$$\mu_s = \mu_R + \mu_F \tag{C.26}$$

$$q_s = q_R + q_F \tag{C.27}$$

where the subscripts R and F refer to the rigid and flexible portions respectively.

We note that

$$\mu_F(\gamma) = \mu_{F_x} + j\mu_{F_y} = \Psi_x + j\Psi_y \tag{C.28}$$

where the small vector angle $\overline{\Psi}$ for the angle due to flexure is obtained from Eq. (B1.2) and Fig. 30 as

$$\begin{Bmatrix} \Psi_x \\ \Psi_y \\ \Psi_z \end{Bmatrix} = \begin{Bmatrix} \frac{1}{R}\frac{\partial z}{\partial \gamma}\cos\gamma - \beta\sin\gamma \\ \frac{1}{R}\frac{\partial z}{\partial \gamma}\cos\gamma + \beta\sin\gamma \\ \frac{1}{R}\left(\frac{\partial u}{\partial \gamma} + w\right) \end{Bmatrix} \tag{C.29}$$

Thus Eq. (C.26) becomes

$$\begin{aligned} \mu_s &= \mu_R + \mu_F \\ &= \mu_{R_x} + j\mu_{R_y} + \left(\frac{1}{R}\frac{\partial z}{\partial \gamma}\cos\gamma - \beta\sin\gamma\right) \\ &\quad + j\left(\frac{1}{R}\frac{\partial z}{\partial \gamma}\sin\gamma + \beta\cos\gamma\right) \end{aligned} \tag{C.30}$$

From Fig. 31 the angular velocity measured in body-fixed coordinates x_b, y_b, z_b is given by

$$\overline{\omega}_b^b = \begin{Bmatrix} \beta\omega_z - \left(\omega_x\cos\gamma + \omega_y\sin\gamma + \frac{1}{R}\frac{\partial^2 z}{\partial\gamma\,\partial t}\right) \\ \omega_z + \frac{\partial}{\partial t}\left(\frac{\partial u}{R\,\partial\gamma} + \frac{w}{R}\right) \\ \frac{\partial z}{R\,\partial y}\omega_z + \omega_y\cos\gamma - \omega_x\sin\gamma + \frac{\partial\beta}{\partial t} \end{Bmatrix} \tag{C.31}$$

Again referring to Fig. 30 we observe that body-mounted gyros located at γ, positioned in the x, y, z directions when undeflected, will actually sense in the deflected case:

$$\begin{Bmatrix} \omega_{R_x} + \omega_{F_x} \\ \omega_{R_y} + \omega_{F_y} \\ \omega_{R_z} + \omega_{F_z} \end{Bmatrix} = \begin{bmatrix} -\cos\gamma & 0 & -\sin\gamma \\ -\sin\gamma & 0 & \cos\gamma \\ 0 & 1 & 0 \end{bmatrix} \begin{Bmatrix} \omega_{x_b} \\ \omega_{y_b} \\ \omega_{z_b} \end{Bmatrix}$$

$$= \begin{Bmatrix} \omega_x - \left(\beta\omega_z - \frac{1}{R}\frac{\partial^2 z}{\partial\gamma\,\partial t}\right)\cos\gamma - \left(\frac{\partial\beta}{\partial t} + \frac{\partial z}{R\,\partial\gamma}\omega_z\right)\sin\gamma \\ \omega_y - \left(\beta\omega_z - \frac{1}{R}\frac{\partial^2 z}{\partial\gamma\,\partial t}\right)\sin\gamma + \left(\frac{\partial\beta}{\partial t} + \frac{\partial z}{R\,\partial\gamma}\omega_z\right)\cos\gamma \\ \omega_z + \frac{\partial}{\partial t}\left(\frac{\partial u}{R\,\partial\gamma} + \frac{w}{R}\right) \end{Bmatrix} \qquad (C.32)$$

Using

$$z(\gamma,t) = \sum_{n=2}^{N} q_{ns}(t)\sin n\gamma + \sum_{n=2}^{N} q_{nc}(t)\cos n\gamma \qquad (C.33)$$

and

$$\beta(\gamma,t) = \sum_{n=2}^{N} B_n z_n = \sum_{n=2}^{N} B_n[q_{ns}(t) \sin n\gamma + q_{nc}(t) \cos n\gamma] \qquad (C.34)$$

we find from Eq. (C.30) that

$$\mu_{F_x} = \left(\frac{1}{R}\frac{\partial z}{\partial \gamma} \cos \gamma - \beta \sin \gamma\right)$$

$$= \frac{1}{R} \sum_{n=2}^{N} n(q_{ns} \cos n\gamma - q_{nc} \sin n\gamma) \cos \gamma$$

$$- \sum_{n=2}^{N} B_n(q_{ns} \sin n\gamma + q_{nc} \cos n\gamma) \sin \gamma$$

$$\triangleq \sum_{n=2}^{N} \mu_{F_{x_n}}$$

$$= \sum_{n=2}^{N} \left[\left(\frac{n}{R} \cos n\gamma \cos \gamma - B_n \sin n\gamma \sin \gamma\right) q_{ns}\right.$$

$$\left. + \left(-\frac{n}{R} \sin n\gamma \cos \gamma - B_n \cos n\gamma \sin \gamma\right) q_{nc}\right]$$

$$= \sum_{n=2}^{N} \left(a_{xx_n} q_{x_n} + a_{xy_n} q_{y_n}\right) \qquad (C.35)$$

$$\mu_{F_y} = \left(\frac{1}{R}\frac{\partial z}{\partial \gamma}\cos\gamma + \beta\cos\gamma\right)$$

$$= \frac{1}{R}\sum_{n=2}^{N} n(q_{ns}\cos n\gamma - q_{nc}\sin n\gamma)\sin\gamma$$

$$+ \sum_{n=2}^{N} B_n(q_{ns}\sin n\gamma + q_{nc}\cos n\gamma)\cos\gamma$$

$$\triangleq \sum_{n=2}^{N} \mu_{F_{y_n}}$$

$$= \sum_{n=2}^{N}\left[\left(\frac{n}{R}\cos n\gamma\sin\gamma + B_n\sin n\gamma\cos\gamma\right)q_{ns}\right.$$

$$\left. + \left(-\frac{n}{R}\sin n\gamma\sin\gamma + B_n\cos n\gamma\cos\gamma\right)q_{nc}\right]$$

$$\triangleq \sum_{n=2}^{N}\left(a_{yx_n}q_{x_n} + a_{yy_n}q_{y_n}\right) \qquad (C.36)$$

If we used gyros to obtain rate, then from Eqs. (C.16) and (C.17)

$$\dot{\mu}_F = q_F - \omega_z \times \mu_F \qquad (C.37)$$

where

$$q_F = \omega_{F_x} + j\omega_{F_y} \qquad (C.38)$$

Substituting for the ω's from Eq. (C.32), we find that Eq. (C.37) yields the same answer for $\dot{\mu}_F$ as would be obtained from differentiating Eqs. (C.35) and (C.36).

Therefore for active control of the system, whether we mechanize the system using gyros or derive $\dot{\mu}$ from the μ sensor output, the results considering flexure are basically the same.

APPENDIX D. SUMMARY OF EQUATIONS IN STATE SPACE FORM FOR COMPUTER SOLUTION

In this appendix we summarize the system equations derived in Appendixes B and C, and write them in a form suitable for computer solution.

1. Summary of Equations

For generality it is convenient to normalize all quantities with respect to the rigid-body natural frequency p_o. Thus we define

$$\tau = p_o t \tag{D.1}$$

$$k_o = K_p/p_o^2 \tag{D.2}$$

$$k_o' = K_v/p_o \tag{D.3}$$

$$r_{on} = p_n/p_o \tag{D.4}$$

$$P = Q/p_o^2 \tag{D.5}$$

Using Eqs. (D.1) - (D.5) in the results of Appendixes B and C yields the following:

Rigid-Body Equations

$$\frac{d^2\mu_{R_x}}{d\tau^2} + \mu_{R_x} = P_{c_x} + P_{D_x} \tag{D.6}$$

$$\frac{d^2\mu_{R_y}}{d\tau^2} + \mu_{R_y} = P_{c_y} + P_{D_y} \tag{D.7}$$

Vibration Equations

$$\frac{d^2\hat{q}_{n_x}}{d\tau^2} + 2\zeta_n r_{on} \frac{d\hat{q}_{n_x}}{d\tau} + r_{on}^2 \hat{q}_{n_x} = \frac{u_{n_{xx}}}{R}\left(P_{c_x} + P_{D_x}\right) + \frac{u_{n_{xy}}}{R}\left(P_{c_y} + P_{D_y}\right) + \frac{P_{D_{nx}}}{R} \tag{D.8}$$

$$\frac{d^2\hat{q}_{n_y}}{d\tau^2} + 2\zeta_n r_{on} \frac{d\hat{q}_{n_y}}{d\tau} + r_{on}^2 \hat{q}_{n_y} = \frac{u_{n_{yx}}}{R}\left(P_{c_x} + P_{D_x}\right) + \frac{u_{n_{yy}}}{R}\left(P_{c_y} + P_{D_y}\right) + \frac{P_{D_{ny}}}{R} \tag{D.9}$$

where we have defined

$$\hat{q} = \frac{q}{R} \tag{D.10}$$

so that R has been used as a normalizing factor to give the q's the same dimensions as the μ's.

Control Equations for Position and Rate Feedback

$$P_{c_x} = -k_o' \frac{d\mu_{s_x}}{d\tau} - k_o \mu_{s_x} + k_o' \frac{d\mu_{ref_x}}{d\tau} + k_o \mu_{ref_x} \tag{D.11}$$

$$P_{c_y} = -k_o' \frac{d\mu_{s_y}}{d\tau} - k_o \mu_{s_y} + k_o' \frac{d\mu_{ref_y}}{d\tau} + k_o \mu_{ref_y} \tag{D.12}$$

Control Equations for the Use of a Rate Network in Place of Rate

$$\frac{dP_{c_x}}{d\tau} + \frac{1}{T_1} P_{c_x} = - \left(\frac{k'_o}{p_o} + k_o\right)\left(\frac{d\mu_{s_x}}{d\tau} - \frac{d\mu_{ref_y}}{d\tau}\right) - \left(\frac{k'_o}{p_o T_o} + \frac{k_o}{T_1}\right)\left(\mu_{s_x} - \mu_{ref_x}\right) \tag{D.13}$$

$$\frac{dP_{c_y}}{d\tau} + \frac{1}{T_1} P_{c_y} = - \left(\frac{k'_o}{p_o} + k_o\right)\left(\frac{d\mu_{s_y}}{d\tau} - \frac{d\mu_{ref_y}}{d\tau}\right) - \left(\frac{k'_o}{p_o T_o} + \frac{k_o}{T_1}\right)\left(\mu_{s_y} - \mu_{ref_y}\right) \tag{D.14}$$

where we have defined the normalized lead-lag-network time constants as

$$T_o \triangleq p_o \tau_o \tag{D.15}$$

$$T_1 \triangleq p_o \tau_1 \tag{D.16}$$

and where μ_s, the quantity sensed by the feedback instrumentation, is given by

$$\mu_{s_x} = \mu_{R_x} + \sum_{n=2}^{N} \left(Ra_{n_{xx}} \hat{q}_{n_x} + Ra_{n_{xy}} \hat{q}_{n_y}\right) \tag{D.17}$$

$$\mu_{s_y} = \mu_{R_y} + \sum_{n=2}^{N} \left(Ra_{n_{yx}} \hat{q}_{n_y} + Ra_{n_{yy}} \hat{q}_{n_y}\right) \tag{D.18}$$

2. Equations in State Space Form

a. Position and Rate Feedback

For the use of position and rate feedback we define the state vector for the x axis as

$$z_x = \begin{Bmatrix} \mu_{R_x} \\ d\mu_{R_x}/d\tau \\ \hat{q}_{2x} \\ d\hat{q}_{2x}/d\tau \\ \hat{q}_{3x} \\ d\hat{q}_{3x}/d\tau \\ \hat{q}_{4x} \\ d\hat{q}_{4x}/d\tau \end{Bmatrix} \tag{D.19}$$

where we interpret $\hat{q}_2$, $\hat{q}_3$, and $\hat{q}_4$ to be the normalized generalized coordinates of the first three excited flexible modes. In this appendix we will only show three flexible modes, the generalization to a greater number of modes being apparent.

Using the previous equations, we now write the equations of motion in state space form for pure rate and position feedback as

$$\frac{dz}{d\tau} \triangleq \begin{Bmatrix} \frac{dz_x}{d\tau} \\ \frac{dz_y}{d\tau} \end{Bmatrix} = Bz + C \begin{Bmatrix} \mu_{ref_x} \\ \frac{d}{d\tau}\left(\mu_{ref_x}\right) \\ \mu_{ref_y} \\ \frac{d}{d\tau}\left(\mu_{ref_y}\right) \end{Bmatrix} + D \begin{Bmatrix} P_{D_x} \\ P_{D_{2x}} \\ P_{D_{3x}} \\ P_{D_{4x}} \\ P_{D_y} \\ P_{D_{2y}} \\ P_{D_{3y}} \\ P_{D_{4y}} \end{Bmatrix} \tag{D.20}$$

where

$$B = B_1 - k_o' B_2 - k_o B_3 \tag{D.21}$$

and C and D are the appropriate matrices associated with the reference inputs and the disturbance functions, respectively. Thus

$$B_1 = \left[\begin{array}{cccccccc|cccccccc}
0 & 1 & & & & & & & & & & & & & & \\
-1 & 0 & 0 & & & & & & & & & & & & & \\
 & 0 & 0 & 1 & & & & & & & & & & & & \\
 & & -r_{o2}^2 & 2\zeta_2 r_{o2} & 0 & & & & & & & & & & & \\
 & & & 0 & 0 & 1 & & & & & & & & & & \\
 & & & & -r_{o3}^2 & -2\zeta_3 r_{o3} & 0 & & & & & & & & & \\
 & & & & & 0 & 0 & 1 & & & & & & & & \\
 & & & & & & -r_{o4}^2 & 2\zeta_4 r_{o4} & & & & & & & & \\
\hline
 & & & & & & & & 0 & 1 & & & & & & \\
 & & & & & & & & -1 & 0 & 0 & & & & & \\
 & & & & & & & & & 0 & 0 & 1 & & & & \\
 & & & & & & & & & & -r_{o2}^2 & -2\zeta_2 r_{o2} & 0 & & & \\
 & & & & & & & & & & & 0 & 0 & 1 & & \\
 & & & & & & & & & & & & -r_{o3}^2 & -2\zeta_3 r_{o3} & 0 & \\
 & & & & & & & & & & & & & 0 & 0 & 1 \\
 & & & & & & & & & & & & & & -r_{o4}^2 & 2\zeta_4 r_{o4}
\end{array}\right] \qquad \text{(D.22)}$$

$$B_2 = \left[\begin{array}{cccccccc|cccccccc}
0 & 0 & 0 & 0 & 0 & 0 & 0 & 0 & 0 & 0 & 0 & 0 & 0 & 0 & 0 & 0 \\
0 & 1 & 0 & Ra_{2xx} & 0 & Ra_{3xx} & 0 & Ra_{4xx} & 0 & 0 & 0 & Ra_{2xy} & 0 & Ra_{3xy} & 0 & Ra_{4xy} \\
0 & 0 & 0 & 0 & 0 & 0 & 0 & 0 & 0 & 0 & 0 & 0 & 0 & 0 & 0 & 0 \\
0 & \frac{u_{2xx}}{R} & 0 & A_{22xx} & 0 & A_{23xx} & 0 & A_{24xx} & 0 & \frac{u_{2xy}}{R} & 0 & A_{22xy} & 0 & A_{23xy} & 0 & A_{24xy} \\
0 & 0 & 0 & 0 & 0 & 0 & 0 & 0 & 0 & 0 & 0 & 0 & 0 & 0 & 0 & 0 \\
0 & \frac{u_{3xx}}{R} & 0 & A_{32xx} & 0 & A_{33xx} & 0 & A_{44xx} & 0 & \frac{u_{3xy}}{R} & 0 & A_{32xy} & 0 & A_{33xy} & 0 & A_{34xy} \\
0 & 0 & 0 & 0 & 0 & 0 & 0 & 0 & 0 & 0 & 0 & 0 & 0 & 0 & 0 & 0 \\
0 & \frac{u_{4xx}}{R} & 0 & A_{42xx} & 0 & A_{43xx} & 0 & A_{44xx} & 0 & \frac{u_{4xy}}{R} & 0 & A_{42xy} & 0 & A_{43xy} & 0 & A_{44xy} \\
\hline
0 & 0 & 0 & 0 & 0 & 0 & 0 & 0 & 0 & 0 & 0 & 0 & 0 & 0 & 0 & 0 \\
0 & 0 & 0 & Ra_{2yx} & 0 & Ra_{3yx} & 0 & Ra_{4yx} & 0 & 1 & 0 & Ra_{2yy} & 0 & Ra_{3yy} & 0 & Ra_{4yy} \\
0 & 0 & 0 & 0 & 0 & 0 & 0 & 0 & 0 & 0 & 0 & 0 & 0 & 0 & 0 & 0 \\
0 & \frac{u_{2yx}}{R} & 0 & A_{22yx} & 0 & A_{23yx} & 0 & A_{24yx} & 0 & \frac{u_{2yy}}{R} & 0 & A_{22yy} & 0 & A_{23yy} & 0 & A_{24yy} \\
0 & 0 & 0 & 0 & 0 & 0 & 0 & 0 & 0 & 0 & 0 & 0 & 0 & 0 & 0 & 0 \\
0 & \frac{u_{3yx}}{R} & 0 & A_{32yx} & 0 & A_{33yx} & 0 & A_{34yx} & 0 & \frac{u_{3yy}}{R} & 0 & A_{32yy} & 0 & A_{33yy} & 0 & A_{34yy} \\
0 & 0 & 0 & 0 & 0 & 0 & 0 & 0 & 0 & 0 & 0 & 0 & 0 & 0 & 0 & 0 \\
0 & \frac{u_{4yx}}{R} & 0 & A_{42yx} & 0 & A_{43yx} & 0 & A_{44yx} & 0 & \frac{u_{4yy}}{R} & 0 & A_{42yy} & 0 & A_{43yy} & 0 & A_{44yy}
\end{array}\right] \qquad \text{(D.23)}$$

where we have defined

$$A_{nmij} = u_{nii}a_{mij} + u_{nij}a_{mjj} \qquad (i,j \text{ are } x \text{ or } y) \qquad (D.24)$$

Matrix B_3 is the same as matrix B_2 except that all its columns are shifted one column to the left, i.e.,

$$B_3(i,j) = B_2(i,j+1) \qquad (D.25)$$

If we partition B into quarters, the off-diagonal matrices contain the coupling terms between the x and y axes. The presence of the A_{nmij} terms, where $n \neq m$, represents the coupling between the flexible modes that has been neglected in the derivation of the perturbation formulas for finding the roots associated with the flexible modes.

b. Use of a Rate Network

For the case where we use a rate network in place of rate, it is convenient to define an augmented state vector, including the control functions, as follows:

$$z'_x \triangleq \begin{Bmatrix} P_{c_x} \\ \mu_{R_x} \\ d\mu_{R_x}/d\tau \\ \hat{q}_{2x} \\ d\hat{q}_{2x}/d\tau \\ \hat{q}_{3x} \\ d\hat{q}_{3x}/d\tau \\ \hat{q}_{4x} \\ d\hat{q}_{4x}/d\tau \end{Bmatrix} \qquad (D.26)$$

Thus for a rate network we can write

$$\frac{dz'}{d\tau} = \begin{Bmatrix} \frac{dz'_x}{d\tau} \\ \\ \frac{dz'_y}{d\tau} \end{Bmatrix} = B'z' + C' \begin{Bmatrix} \mu_{ref_x} \\ \frac{d}{d\tau}\left(\mu_{ref_x}\right) \\ \mu_{ref_y} \\ \frac{d}{d\tau}\left(\mu_{ref_y}\right) \end{Bmatrix} + D' \begin{Bmatrix} P_{D_x} \\ P_{D_{2x}} \\ P_{D_{3x}} \\ P_{D_{4x}} \\ P_{D_y} \\ P_{D_{2y}} \\ P_{D_{3y}} \\ P_{D_{4y}} \end{Bmatrix} \qquad (D.27)$$

where C' and D' represent the new appropriate natrices and where

$$B' = B'_1 - \frac{k'_o}{p_o} B'_2 - k_o B'_3 \qquad (D.28)$$

The matrices for B'_1 and B'_2 are given in Eqs. (D.29) and (D.30) on the following page; B'_3 is the same as B'_2 except that T_o is replaced by T_1.

$$B_1' = \left[\begin{array}{cccccccccc|cccccccccc}
-\frac{1}{T} & 0 & & & & & & & & & & & & & & & & & & \\
0 & 0 & 1 & & & & & & & & & & & & & & & & & \\
1 & -1 & 0 & 0 & & & & & & & & & & & & & & & & \\
0 & 0 & 0 & 0 & 1 & & & & & & & & & & & & & & & \\
\frac{u_{2xx}}{R} & 0 & 0 & -r_{o2}^2 & -2\zeta_2 r_{o2} & 0 & & & & & \frac{u_{2xy}}{R} & & & & & & & & & \\
0 & 0 & 0 & 0 & 0 & 0 & 1 & & & & 0 & & & & & & & & & \\
\frac{u_{3xx}}{R} & 0 & 0 & 0 & 0 & -r_{o3}^2 & -2\zeta_3 r_{o3} & 0 & & & \frac{u_{3xy}}{R} & & & & & & & & & \\
0 & 0 & 0 & 0 & 0 & 0 & 0 & 0 & 1 & & 0 & & & & & & & & & \\
\frac{u_{4xx}}{R} & 0 & 0 & 0 & 0 & 0 & 0 & -r_{o4}^2 & -2\zeta_4 r_{o4} & & \frac{u_{4xy}}{R} & & & & & & & & & \\
\hline
 & & & & & & & & & & -\frac{1}{T} & 0 & & & & & & & & \\
 & & & & & & & & & & 0 & 0 & 1 & & & & & & & \\
 & & & & & & & & & & 1 & -1 & 0 & 0 & & & & & & \\
 & & & & & & & & & & 0 & 0 & 0 & 0 & 1 & & & & & \\
\frac{u_{2yx}}{R} & & & & & & & & & & \frac{u_{2yy}}{R} & 0 & 0 & -r_{o2}^2 & -2\zeta_2 r_{o2} & 0 & & & & \\
0 & & & & & & & & & & 0 & 0 & 0 & 0 & 0 & 0 & 1 & & & \\
\frac{u_{3yx}}{R} & & & & & & & & & & \frac{u_{3yy}}{R} & 0 & 0 & 0 & 0 & -r_{o3}^2 & -2\zeta_3 r_{o3} & 0 & & \\
0 & & & & & & & & & & 0 & 0 & 0 & 0 & 0 & 0 & 0 & 0 & 1 & \\
\frac{u_{4yx}}{R} & & & & & & & & & & \frac{u_{4yy}}{R} & 0 & 0 & 0 & 0 & 0 & 0 & -r_{o4}^2 & -2\zeta_4 r_{o4} &
\end{array}\right] \qquad \text{(D.29)}$$

$$B_2' = \left[\begin{array}{cccccccccc|cccccccccc}
0 & \frac{1}{T_o} & 1 & \frac{Ra_{2xx}}{T_o} & Ra_{2xx} & \frac{Ra_{3xx}}{T_o} & Ra_{3xx} & \frac{Ra_{4xx}}{T_o} & Ra_{4xx} & & 0 & 0 & 0 & \frac{Ra_{2xy}}{T_o} & Ra_{2xy} & \frac{Ra_{3xy}}{T_o} & Ra_{3xy} & \frac{Ra_{4xy}}{T_o} & Ra_{4xy} & \\
 & & & & & & & & & & & & & & & & & & & \\
 & & & & & & & & & & & & & & & & & & & \\
 & & & & & & & & & & & & & & & & & & & \\
 & & & & & & & & & & & & & & & & & & & \\
 & & & & & & & & & & & & & & & & & & & \\
 & & & & & & & & & & & & & & & & & & & \\
 & & & & & & & & & & & & & & & & & & & \\
 & & & & & & & & & & & & & & & & & & & \\
 & & & & & & & & & & & & & & & & & & & \\
\hline
0 & 0 & 0 & \frac{Ra_{2yx}}{T_o} & Ra_{2yx} & \frac{Ra_{3yx}}{T_o} & Ra_{3yx} & \frac{Ra_{4yx}}{T_o} & Ra_{4yx} & & 0 & \frac{1}{T_o} & 1 & \frac{Ra_{2yy}}{T_o} & Ra_{2yy} & \frac{Ra_{3yy}}{T_o} & Ra_{3yy} & \frac{Ra_{4yy}}{T_o} & Ra_{4yy} & \\
 & & & & & & & & & & & & & & & & & & & \\
 & & & & & & & & & & & & & & & & & & & \\
 & & & & & & & & & & & & & & & & & & & \\
 & & & & & & & & & & & & & & & & & & & \\
 & & & & & & & & & & & & & & & & & & & \\
 & & & & & & & & & & & & & & & & & & & \\
 & & & & & & & & & & & & & & & & & & & \\
 & & & & & & & & & & & & & & & & & & & \\
 & & & & & & & & & & & & & & & & & & &
\end{array}\right] \qquad \text{(D.30)}$$

REFERENCES

1. Richard E. Andeen, "Stabilizing Flexible Vehicles," Astronautics and Aeronautics, 2, Aug 1964, pp. 38-44.

2. J. F. Schaefer, "On the Bounded Control of Some Unstable Mechanical Systems," SUDAER Rept. 223, Department of Aeronautics and Astronautics, Stanford University, Stanford, Calif., Apr 1965 (Ph.D. Dissertation, Jun 1965).

3. R. L. Blisplinghoff and H. Ashley, Principles of Aeroelasticity, John Wiley & Sons, New York, 1962.

4. Y. C. Fung, An Introduction to the Theory of Aeroelasticity, John Wiley & Sons, New York, 1955.

5. J. B. Rea, "Dynamic Analysis of Aeroelastic Aircraft by the Transfer Function - Fourier Method," J. Aerospace Sci., 18, 6, Jun 1951, pp. 375-397.

6. J. L. Beharrell and H. R. Friedrich, "The Transfer Function of a Rocket-Type Guided Missile with Consideration of Its Structural Elasticity," J. Aerospace Sci., 21, 7, Jul 1954, pp. 454-458.

7. K. Kachigan, "The General Theory and Analysis of a Flexible Bodied Missile with Autopilot," Rept. ZU-7-048, Convair, San Diego, Calif., 11 Nov 1955.

8. M. V. Barton, et al, "Generalized Missile Dynamics Analysis," Repts. Nos. EM 8-7,-8,-9,-10,-15,-16 (GM TR - 00165,00438,00359, 00360,00431,00445), Space Technology Laboratories, Los Angeles, Calif., 7 Apr 1958.

9. S. Rusk, "Flexible Missile Dynamics," LMSD-6122, Lockheed Missiles and Space Division, Palo Alto, Calif., 30 Jul 1958.

10. J. J. Rodden, "Equations of Motion for Large Elastic Boosters with Fuel Slosh and Swiveling Engine," LDC 57-15-112, Lockheed Missiles and Space Co., Sunnyvale, Calif., 22 Aug 1962.

11. T. R. Beal, "Dynamic Stability of a Uniform Free-Free Beam under a Gimbaled Thrust of Periodically Varying Magnitude," SUDAER Rept. 161, Department of Aeronautics and Astronautics, Stanford University, Stanford, Calif., Jun 1963 (Ph.D. Dissertation).

12. R. H. Cannon, Jr., "Root Locus Analysis of Structural Coupling in Control Systems," ASME Paper No. 58-A-65, 1958.

13. D. R. Lukens, A. F. Schmitt, and G. T. Broucek, "Approximate Transfer Functions for Flexible-Booster-and-Autopilot Analysis," WADD TR-61-93, Apr 1961.

14. L. G. Hoffman and A. Kezer, "Simplified Analysis of Flexible Booster Flight Control Systems," M.I.T./I.L.E. 1210, Cambridge, Mass., Jun 1962.

15. P. K. C. Wang, "Stability Analysis of a Simplified Flexible Vehicle Via Lyapunov's Direct Method," AIAA J., 3, 9, Sep 1965, pp. 1764-1765.

16. J. Zaborsky, W. J. Luedde, and M. J. Wendl, "New Flight Control Techniques for a Highly Elastic Booster," ASD Tech. Rept. 61-231, Sep 1961.

17. R. E. Koop and R. J. White, "A Control Scheme for Attitude Control of Large Flexible Boosters," SAE Preprint 429C, 9-13 Oct 1961.

18. John F. L. Lee, "A Digital Adaptive Flight Control System for Flexible Missiles," Symposium on Ballistic Missile and Space Technology, 7th, Transactions, Vol. II, Colorado Springs, Colo., 13-16 Aug 1962, Los Angeles Aerospace Corp., 1962.

19. Peter Gad, "An Adaptive Autopilot Control System," TNB General Precision Aerospace, 7, 1st Quarter 1964, pp. 9-15.

20. Harold H. Burke and Alan D. Storms, "Aerodynamic Load Reduction Techniques for Large Elastic Launch Vehicles - A Comparative Study," IEEE Intern. Conv. Rec., 12, Pt. 7, 1964, pp. 92-106.

21. "Space-Station Stabilization and Control Study," Rept. No. AB-1210-0020, Sperry Gyroscope Co., Great Neck, New York, N.Y., Dec 1963.

22. Clement L. Tai and M. H. Loh, "Planar Motion of a Rotating Cable-Connected Space Station in Orbit," AIAA Paper No. 64-493, 1964.

23. Clement L. Tai and M. H. Loh, "Analysis of Free Vibration of Elastic Space Station of Y-Configuration," AIAA Annual Structures and Materials Conference, Fifth, Palm Springs, Calif., 1-3 Apr 1964.

24. Fred W. Hopper, "Dynamic Behavior of Large Flexible Rotating Space Stations during Docking Maneuvers," Advan. Astronautical Sci., 16, Part 1, Western Periodicals, North Hollywood, Calif., 1963, pp. 366-383.

25. F. J. Freuh and J. M. Miller, "The Effect of Elasticity on the Stability of Manned Rotating Space Stations," Giannini Controls Corporation Rept. 64-0991, Astromechanics Res. Div., May 1964.

26. F. J. Freuh and J. M. Miller, "An Experimental Investigation of the Elastic Structural Stability of a Manned Rotating Space Station Model," AIAA Paper 65-406, Jul 1965.

27. G. M. Andrew and J. M. Johnson, Jr., "Automatic Control of Aeroelastic Modes," IAS Paper 62-86, Jun 1962.

28. W. B. Gevarter, "Analysis of the Stability of a Flexible Space Vehicle during Powered Flight," LMSC 658720, Lockheed Missiles & Space Co., Sunnyvale, Calif., 9 Jan 1964.

29. J. T. Tou, Modern Control Theory, McGraw-Hill Book Company, New York, 1964, pp. 13-15.

30. W. Von Braun, "Crossing the Last Frontier," Colliers Magazine, 22 Mar 1952.

31. R. Berglund and E. A. Weber, "Self Erecting Manned Space Laboratory," Proc. of the National Meeting on Manned Space Flight, IAS and NASA, St. Louis, Mo., 30 Apr - 2 May 1962.

32. W. C. Hurty and M. F. Rubinstein, Dynamics of Structures, Prentice Hall, Inc., Englewood Cliffs, N.J., 1964.

33. T. E. Lang, "Vibration of Thin Circular Rings, Part 1. Solutions for Modal Characteristics and Forced Excitation," Tech. Rept. No. 32-261, Jet Propulsion Laboratory, Pasadena, Calif., 1 Jul 1962.

34. A. E. H. Love, "A Treatise on the Mathematical Theory of Elasticity," Dover, New York, 1944, pp. 381-398, 444-454.

35. W. Eversman, "The Transverse Vibrations of a Spinning Annular Elastic Membrane with Free Edges," Ph.D. Dissertation and SUDAER Rept. No. 184, Department of Aeronautics and Astronautics, Stanford University, Stanford, Calif., Apr 1964.

36. R. L. Huston, "In-Plane Vibration of Spinning Disks," AIAA J., 3, 8, Aug 1965, pp. 1519-1520.

37. J. L. Nowinski, "Nonlinear Transverse Vibrations of a Spinning Disk," Trans. ASME, J. Appl. Mech., 31, Series E, 1, Mar 1964, pp. 72-78.

38. R. A. Di Taranto and M. Lessen, "Coriolis Acceleration Effect on the Vibration of a Rotating Thin-Walled Circular Cylinder," J. Appl. Mech., 31, 1964, pp. 700-701.

39. B. O. Lange, "The Control and Use of Drag-Free Satellites," SUDAER Rept. 194, Department of Aeronautics and Astronautics, Stanford University, Stanford, Calif., Jun 1964 (Ph.D. Dissertation, May 1964) pp. 70-108.

40. R. E. Kalman, "When Is a Linear Control System Optimal," J. Basic Eng., Mar 1964, pp. 51-60.

41. B. J. Loret, "Optimization of Space Vehicle Design with Respect to Artificial Gravity," Aerospace Medicine, May 1963.

42. K. N. Tong, Theory of Mechanical Vibration, John Wiley & Sons, New York, 1960.

43. Emory C. Curtis, "Coordinate Transformation Problems Made Easy with Signal Flow," an internal Lockheed Missiles & Space Co. Document, Sunnyvale, Calif., 25 Mar 1963.

44. Mitchell Lobel, "Stabilization and Control of a Rotating Manned Space Station--A Total System Concept," AIAA Preprint 63-340, 1963.

45. A. Cormack, III and C. C. Couchman, "Consideration of Crew Comfort in Relation to the Dynamics of Rotating Space Stations," AIAA Paper No. 64-338, 1964.

46. John E. Drake, and David B. Jackson, "Concepts and Techniques for Attitude Control, Dynamic Balance, and Stabilization of a Manned, Rotating Space Station," Advanc. Astronautical Sci., 16, Part 1, Western Periodicals, North Hollywood, Calif., 1963.

47. E. I. Ergin and P. C. Wheeler, "Magnetic Attitude Control of a Spinning Satellite," AIAA Paper No. 64-235, 1964.

48. Peter R. Kurzhals, "Stability and Control for the Manned Orbital Laboratory," Presented at the SAE A-18 Committee Meeting, Houston, Tex., 11-13 Dec 1963.

49. Peter R. Kurzhals and Claude R. Keckler, "Spin Dynamics of Manned Space Stations," NASA TR R-155, Dec 1963.

50. George W. LeCompte and Jerrel G. Bland, "Simply Mechanized Attitude Control for Spinning Vehicles," AIAA Preprint No. 63-341, 1963.

51. S. I. Lieberman, and Z. Margosian, "A Class of Time-Optimal Velocity Control Laws for a Spinning Space Vehicle," IEEE Trans. on Automatic Control, AC-9, Jul 1964, pp. 286, 277.

52. NASA, "Feasibility Study and Design of Passive Dampers for a Manned Rotating Space Station," Engineering Mechanics Laboratory, NASA CR-163, Mar 1965.

53. H. Patapoff, "Bank Angle Control System for a Spinning Satellite," AIAA Preprint No. 63-339, 1963.

54. Walter K. Polstorff, "Dynamics of a Rotating Space Station," Simulation, 3, 4, Oct 1964.

55. John G. Shearin and Peter R. Kurzhals, "Stability and Control of Manned Rotating Space Stations," Advanc. Astronautical Sci., 13, Western Periodicals, North Hollywood, Calif., 1963, pp. 61-74.

56. W. T. Thomson, "Spin Stabilization of Attitude against Gravity Torque," J. Astronautical Sci., 9, 2, 1962, pp. 31-33.

57. P. C. Wheeler, "Two-Pulse Attitude Control of an Asymmetric Spinning Satellite," Progress in Astronautics and Aeronautics, Vol. 13, Academic Press, New York, 1964, pp. 261-287.

58. E. Y. Yu, "Spin Decay, Spin-Precession Damping and Spin-Axis Drift of the Telstar Satellite," Bell Sys. Tech. Jour., XLII, 5, Sep 1963.